Droplet-Based Microfluidic Systems Coupled to Mass Spectrometry for Enzyme Kinetics

The research described within this thesis was carried out in the Mesoscale Chemical Systems group and the BIOS Lab-on-a-Chip group at the MESA+ Institute for Nanotechnology at the University of Twente, Enschede, the Netherlands. The technology program of the Ministry of Economic Affairs of the Netherlands (project no. 6626) and the Technology Foundation STW, the applied science division of the NWO, financially supported this research.

Promotor:

prof. dr. J.G.E. Gardeniers, Universiteit Twente, the Netherlands

Commissie:

prof. dr. ir. A. van den Berg, Universiteit Twente, the Netherlands
prof. dr. F. Mugele, Universiteit Twente, the Netherlands
prof. dr. T. Laurel, Lund University, Sweden
dr. E.T. Carlen, Universiteit Twente, the Netherlands
prof. dr. ir. J.C.M. van Hest, Radboud Universiteit Nijmegen, the Netherlands
prof. dr. J. Lammertyn, Universiteit van Leuven, Belgium

Title: Droplet-Based Microfluidic Systems Coupled to Mass Spectrometry for Enzyme Kinetics
Author: Kevin P. Nichols
ISBN: 978-90-9023931-6

Droplet-Based Microfluidic Systems Coupled to Mass Spectrometry for Enzyme Kinetics

ter verkrijging van
de graad van doctor aan de Universiteit Twente,
op gezag van rector magnificus,
prof. dr. E. Brinksma,
volgens het besluit van het College voor Promoties
in het openbaar te verdedigen
op donderdag 9 april 2009 om 13.15 uur

door

Kevin Paul Nichols
geboren op 16 december 1981
te DuBois, Pennsylvania, Amerika

Dit proefschrift is goedgekeurd door:

Promotor: prof. dr. ir. J.G.E. Gardeniers

Table of Contents

List of Acronyms

AC	Alternating Current
BHF	Buffered Hydrofluoric Acid
BJH	Barrett–Joyner–Halenda method
CFD	Computational Fluid Dynamics
DC	Direct Current
DEP	Dielectrophoresis
DI	Deionized (water)
DIOS	Desorption/Ionization on Silicon
EDC	Enhanced Duty Cycle
EHD	Electrohydrodynamic
EWOD	Electrowetting on Dielectric
HDMS	High Definition Mass Spectrometry
HF	Hydrofluoric Acid
HPLC	High Performance Liquid Chromatography
IBE	Ion Beam Etching
IMS	Imaging Mass Spectrometry
ITO	Indium Tin Oxide
MALDI	Matrix Assisted Laser Desorption/Ionization
MATLAB	A numerical computing language
MEMS	Micro-Electro-Mechanical Systems
MS	Mass Spectrometry
PDMS	Polydimethylsiloxane
PECVD	Plasma Enhanced Chemical Vapor Deposition
PTPase	Protein Tyrosine Phosphatase
RIE	Reactive Ion Etching
SiN	Silicon Nitride
SiO	Silicon Oxide
SU-8	A photodefinable epoxy
TOF	Time of Flight

Chapter 1

Introduction

A summary of the three droplet-based microfluidic systems for analyzing enzyme kinetics discussed in this thesis is presented. In addition, notable previous devices that accomplish similar tasks are discussed. Finally, relevant background information for the field is given.

Summary of Devices Presented in This Thesis

The purpose of the devices described in this thesis is to analyze enzyme kinetics through mass spectrometry. In addition to basic science, enzyme kinetics is useful for the optimization of process conditions[1], the study of disease progression,[2-6] the understanding of drug interactions,[7-10] mechanisms,[11, 12] and metabolism,[13] and determining the stability of various enzyme containing commercial products.[1] Mass spectrometry was selected specifically because it allows the study of enzyme kinetics without the incorporation of a chromophore, which many biologically relevant substrates do not contain.[14] The majority of previously reported microfluidic systems require the use of a chromophore, such as a fluorescent substrate or product, to facilitate detection. The ability to interrogate non-fluorescent molecules using mass spectrometry alone has obvious, significant advantages. All devices described were fabricated using miniaturization techniques, due to the scaling benefits associated with lab-on-a-chip systems[15-19]. Three miniaturized systems were fully developed towards this end: a digital microfluidic system (ch. 2-3), a digital nanofluidic system (ch. 4), and a non-digital, droplet-based microfluidic system (ch. 5).

Summary of Chapters 2-3: Digital microfluidics coupled to mass spectrometry

In chapters two and three we described a digital microfluidic system that electrically combined substrate and enzyme droplets and quenched an array of such droplets at varying time intervals. This produced droplets locked at points along an enzyme progress curve. These droplets were then dried and transferred to a mass spectrometer, where they were ionized using matrix assisted laser desorption/ionization time-of-flight mass spectrometry (MALDI-TOF MS) to determine the relative concentration of reaction intermediates. This system was capable of analyzing millisecond scale pre-steady-state kinetics, and producing results equivalent to that produced using more time-consuming methods and without the

need for the incorporation of a chromophore. However, to do so it required the presence of an internal standard, a molecule that ionizes at equimolar ratios to the molecule of interest. Without an internal standard, non-uniform distribution of solutes during droplet drying prevented even relative quantitation. In an attempt to overcome this limitation, two additional systems were developed.

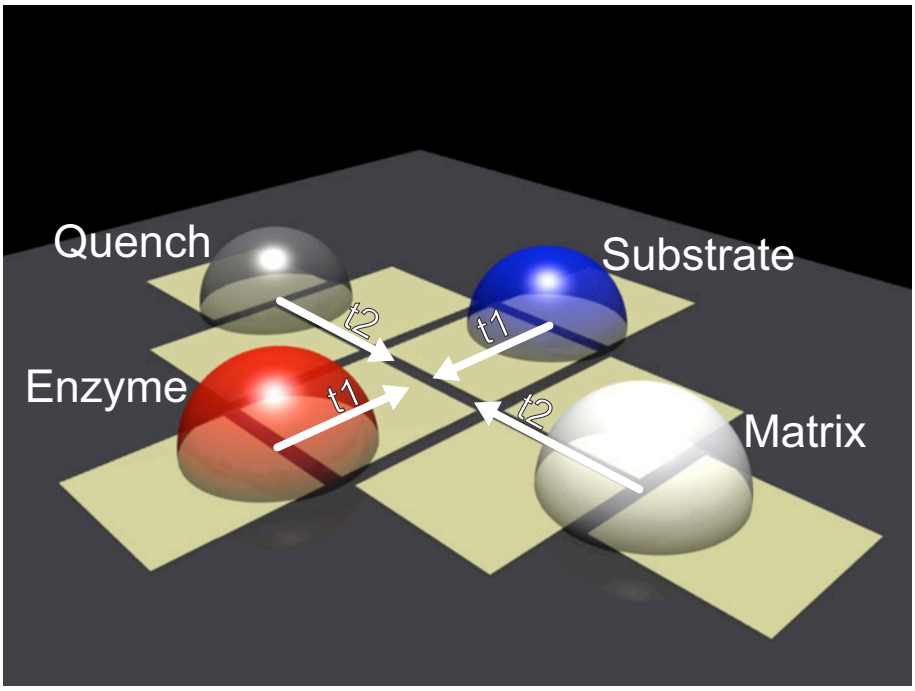

Figure 1 – Chapters two and three. In this digital microfluidic system, first, an enzyme and a substrate are combined together, and allowed to react. After a set time interval, a strong acid quenches the reaction, and a matrix is added to allow eventual mass spectrometry. This design is iterated at multiple points across the chip, and a complete kinetic curve can be obtained by taking mass spectra, which give the relative concentrations of the enzymatic reaction intermediates being studied, at such points.

Summary of Chapter 4: Digital nanofluidic analog of ch. 2-3 design

In chapter four, a nanochannel system, similar in principle to the microscale digital microfluidic system described in chapters two and three, except for the scale, was constructed in an attempt to overcome the internal standard requirement of our digital microfluidic system. It was assumed that further miniaturization would permit faster mixing and more uniform solute distribution. While we successfully fabricated our system as intended, we encountered reagent heating far above what simulations had predicted. This system was therefore abandoned and an alternative solution sought. However, the device structure may prove useful for other applications, and fabrication and characterization details are given accordingly.

Summary of Chapter 5: Porous Si, droplet microfluidics coupled to MS

As an alternative to the nanochannel system, the final device we developed was a non-digital, droplet-based system, described in chapter five. Though this system manipulated droplets, it was not a digital microfluidic system; this device manipulated nanoliter droplets in microchannels as opposed to microliter droplets on a planar electrode surface. After combining an enzyme and a substrate droplet together, this device sampled a trace amount of the reaction products and substrates, and locked them away from the enzyme on the other side of a membrane as the droplet traveled down a microchannel. A point in space on the microchannel therefore corresponds with a point in time in the reaction, and the concentration change along the length of the microchannel can be used to produce an enzyme progress curve. The particular membrane we used was porous silicon, a conductive, hydrophobic material with pores easily tunable on the nanometer scale, and that, when used in a configuration referred to as desorption/ionization on silicon mass spectrometry (DIOS MS), is also a suitable replacement for the matrix in MALDI-TOF MS.

a.)

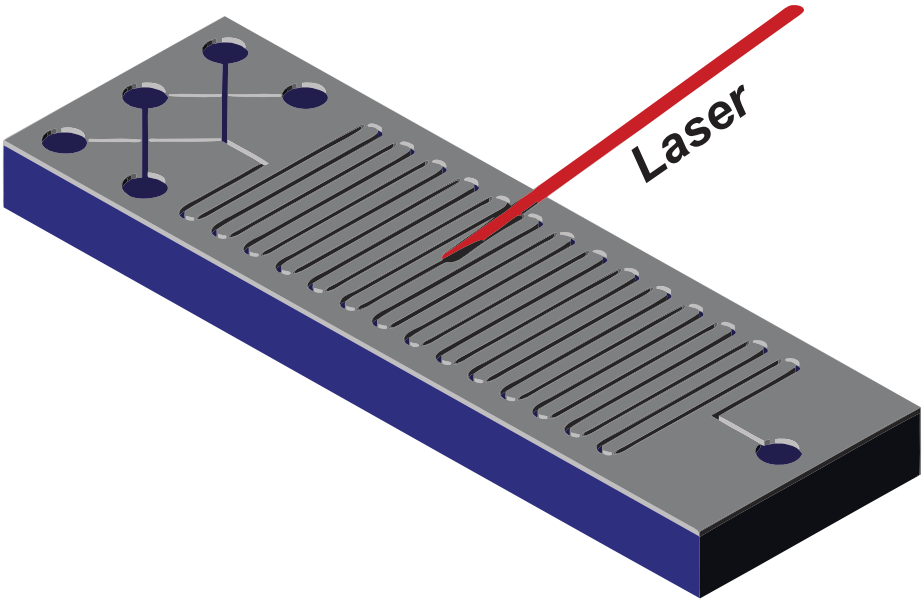

b.)

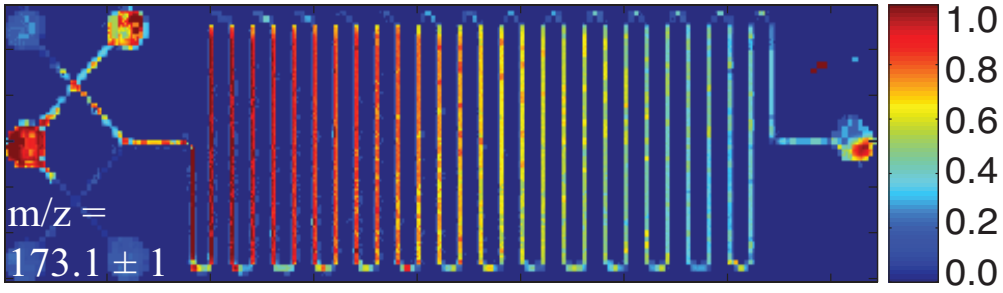

Figure 2 – Chapter 5. a.) Enzyme and substrate droplets combine in the microchannel and deposit a small amount of residue on the channel walls. This residue can later be detected and quantified relatively using mass spectrometry b.) Mass spectrometry imaging of a porous silicon channel at 173.1±1 m/z (arginine). Intensity correlates with relative concentration. This concentration data can be used to produce a kinetic curve.

Notable Previous Microfluidic Systems for Enzyme Kinetics

Song and Ismagilov: Droplet-Based Multi-Phase System

Song and Ismagilov described a microfluidic system for sub-millisecond resolution enzyme kinetic measurement using multiphase (oil/water) droplet microfluidics.[20] The aqueous phase met the oil phase at a t-shaped intersection, and pinched off in consistent droplet sizes depending on flow rates. The droplets were passed through an oscillating channel mixing section. Single-turnover kinetics of Ribonulease A (RNase A) were measured through fluorescent imaging of 140 nL droplets containing µM-scale enzyme and substrate. A fluorogenic substrate was cleaved by RNase A, and fluorescence intensity tracked as a function of time.

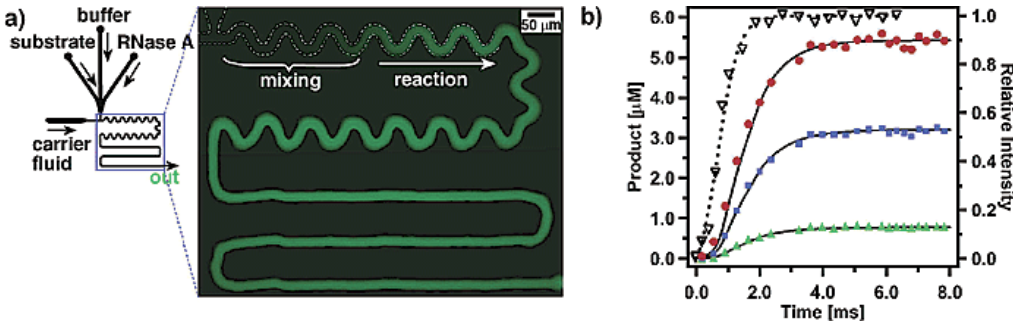

Figure 3 – Single-turnover kinetics of RNase A, from Song and Ismagilov.[20] (a) 2 second exposure micrograph, averaging individual droplets, and a schematic of the microsystem (b) graph of reaction progress at a pH of 7.5. for substrate concentrations: 5.8 µM, 3.3 µM, 0.8 µM. Used with permission of the American Chemical Society.

By integrating images over 2-4 seconds, images such as Figure 3 were obtainable. Though it may be possible to incorporate quenching and offline MS measurement using an analogous system, this has not yet been demonstrated.

Peterson et al.*: Continuous Flow Single Phase System*

Peterson *et al.* presented an enzymatic microreactor that utilized trypsin immobilized on porous polymer monoliths.[21] Michaelis-Menten kinetics (steady state kinetics) were probed using the low molecular weight substrate N-α-benzoyl-L-arginine ethyl ester. The primary limitation of this system is its use of a single, continuously flowing phase. Dispersion and diffusion in such a system limit its utility for pre-steady-state kinetics.

It is our view that the general strategy of utilizing droplets to probe enzyme kinetics, originally demonstrated by Song and Ismagilov, and adapted in various forms for mass spectrometry in this thesis, represents a superior method of probing enzyme kinetics, due to the lack of dispersion, faster mixing, and discrete nature of the sampling.

Overview of Enzyme Kinetics

Enzymes are biomolecules that catalyze chemical reactions. Enzyme kinetics is the study of the biochemical reactions catalyzed by enzymes. Methods for enzyme kinetics can be broken up into two general approaches: steady state, and pre-steady-state. Steady state methods rely on varying a parameter of an experiment such as substrate or enzyme concentration and fitting the resulting data to a model that explains the enzyme behavior. Pre-steady-state kinetics directly traces a reaction in time by monitoring substrate/product concentrations or enzyme intermediate concentrations, usually for the purpose of analyzing enzymes that do not fit standard models, or when it is necessary to understand the details of enzyme-substrate intermediates for mechanistic purposes.

Michaelis-Menten Kinetics

The most common model for describing steady state enzyme kinetics is the Michaelis-Menten model, first proposed in 1913 by Leonor Michaelis and Maud Menten.[22] The Michaelis-Menten model takes advantage of the saturable property of reactions to produce useful kinetic constants for describing reactions. Figure 4 shows an example of a typical saturation curve. The Michaelis-Menten model is valid only when the concentration of enzyme is much lower than the concentration of substrate, and when the enzyme is not subject to allosteric regulation. In certain multi-substrate reactions, Michaelis-Menten kinetics will also apply, although their interpretation is not as straightforward.[23]

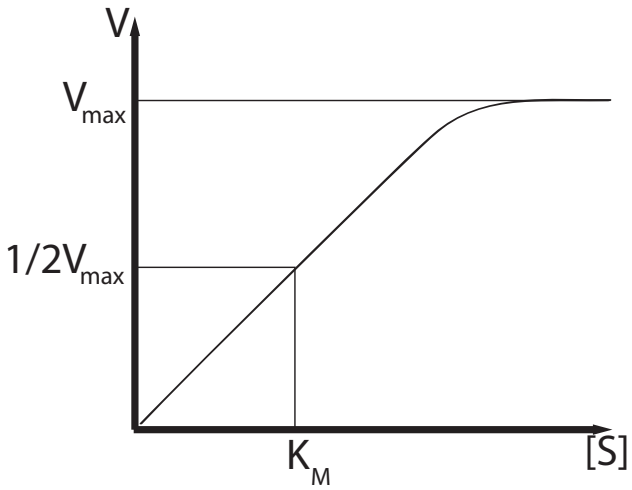

Figure 4 – Michaelis-Menten kinetics. A saturation curve showing the relationship between substrate concentration and the rate of reaction. Measurements are taken at steady state. V_{max} is the maximum rate of reaction. K_M is defined as ½ V_{max}.

Pre-Steady-State Kinetics

The initial moments after an enzyme combines with its substrate is studied by pre-steady-state kinetics. As shown in Figure 5, there is an initial burst phase after the initiation of a reaction that will be completely masked if one probes the kinetics using only steady state kinetic methods. Pre-steady-state enzyme kinetics are typically interrogated using quench-flow systems,[14] a category which includes the devices presented here.

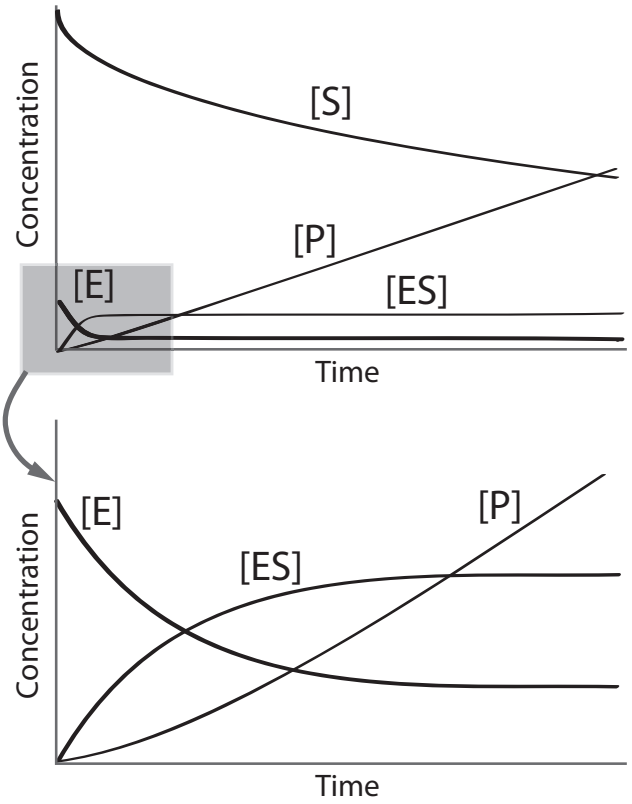

Figure 5 – Pre-steady-state kinetics. The burst phase following the initiation of a reaction can have important implications in understanding the mechanisms of a reaction.

References

(1) Connors, K. A. *Chemical Kinetics: The Study of Reaction Rates in Solution*; VCH Publishers: New York, 1990.

(2) Chakraborti, S.; Mandal, M.; Das, S.; Mandal, A.; Chakraborti, T., Regulation of matrix metalloproteinases: An overview, *Mol. Cell. Biochem.* **2003**, *253*, 269-285.

(3) Golde, T. E., Alzheimer disease therapy: Can the amyloid cascade be halted?, *J. Clin. Invest.* **2003**, *111*, 11-18.

(4) Murad, F., Cyclic Guanosine-Monophosphate as a Mediator of Vasodilation, *J. Clin. Invest.* **1986**, *78*, 1-5.

(5) Ma, Q.; Lu, A. Y. H., The challenges of dealing with promiscuous drug-metabolizing enzymes, receptors and transporters, *Curr. Drug Metab.* **2008**, *9*, 374-383.

(6) Fleet, M.; Osman, F.; Komaragiri, R.; Fritz, A.; Raj, D. S. C., Protein catabolism in advanced renal disease: role of cytokines, *Clinical Nephrology* **2008**, *70*, 91-100.

(7) Chou, T. C.; Talalay, P., Quantitative-Analysis of Dose-Effect Relationships - the Combined Effects of Multiple-Drugs or Enzyme-Inhibitors, *Advances in Enzyme Regulation* **1984**, *22*, 27-55.

(8) Favata, M. F.; Horiuchi, K. Y.; Manos, E. J.; Daulerio, A. J.; Stradley, D. A.; Feeser, W. S.; Van Dyk, D. E.; Pitts, W. J.; Earl, R. A.; Hobbs, F.; Copeland, R. A.; Magolda, R. L.; Scherle, P. A.; Trzaskos, J. M., Identification of a novel inhibitor of mitogen-activated protein kinase kinase, *J. Biol. Chem.* **1998**, *273*, 18623-18632.

(9) Fabian, M. A.; Biggs, W. H.; Treiber, D. K.; Atteridge, C. E.; Azimioara, M. D.; Benedetti, M. G.; Carter, T. A.; Ciceri, P.; Edeen, P. T.; Floyd, M.; Ford, J. M.; Galvin, M.; Gerlach, J. L.; Grotzfeld, R. M.; Herrgard, S.; Insko, D. E.; Insko, M. A.; Lai, A. G.; Lelias, J. M.; Mehta, S. A.; Milanov, Z. V.;

Velasco, A. M.; Wodicka, L. M.; Patel, H. K.; Zarrinkar, P. P.; Lockhart, D. J., A small molecule-kinase interaction map for clinical kinase inhibitors, *Nat. Biotechnol.* **2005**, *23*, 329-336.

(10) Mccay, P. B., Vitamin-E - Interactions with Free-Radicals and Ascorbate, *Annu. Rev. Nutr.* **1985**, *5*, 323-340.

(11) Vane, J. R.; Botting, R. M., New Insights into the Mode of Action of Antiinflammatory Drugs, *Inflammation Res.* **1995**, *44*, 1-10.

(12) Mannervik, B.; Danielson, U. H., Glutathione Transferases - Structure and Catalytic Activity, *Crc Critical Reviews in Biochemistry* **1988**, *23*, 283-337.

(13) Miller, R. H.; Harper, A. E., Branched-Chain Amino-Acid (Bcaa) Metabolism in the Isolated Perfused Rat-Kidney, *Federation Proceedings* **1983**, *42*, 543-543.

(14) Houston, C. T.; Taylor, W. P.; Widlanski, T. S.; Reilly, J. P., Investigation of enzyme kinetics using quench-flow techniques with MALDI TOF mass spectrometry, *Anal. Chem.* **2000**, *72*, 3311-3319.

(15) Brody, J. P.; Yager, P.; Goldstein, R. E.; Austin, R. H., Biotechnology at low Reynolds numbers, *Biophys. J.* **1996**, *71*, 3430-3441.

(16) Brivio, M.; Tas, N. R.; Goedbloed, M. H.; Gardeniers, H. J. G. E.; Verboom, W.; van den Berg, A.; Reinhoudt, D. N., A MALDI-chip integrated system with a monitoring window, *Lab Chip* **2005**, *5*, 378-381.

(17) Brivio, M.; Fokkens, R. H.; Verboom, W.; Reinhoudt, D. N.; Tas, N. R.; Goedbloed, M.; van den Berg, A., Integrated microfluidic system enabling (bio)chemical reactions with on-line MALDI-TOF mass spectrometry, *Anal. Chem.* **2002**, *74*, 3972-3976.

(18) Figeys, D.; Pinto, D., Lab-on-a-chip: A revolution in biological and medical sciences., *Anal. Chem.* **2000**, *72*, 330A-335A.

(19) Squires, T. M.; Quake, S. R., Microfluidics: Fluid physics at the nanoliter scale, *Reviews of Modern Physics* **2005**, *77*, 977-1026.

(20) Song, H.; Ismagilov, R. F., Millisecond kinetics on a microfluidic chip using nanoliters of reagents, *J. Am. Chem. Soc.* **2003**, *125*, 14613-14619.

(21) Peterson, D. S.; Rohr, T.; Svec, F.; Frechet, J. M. J., Enzymatic microreactor-on-a-chip: Protein mapping using trypsin immobilized on porous polymer monoliths molded in channels of microfluidic devices, *Anal. Chem.* **2002**, *74*, 4081-4088.

(22) Michaelis, L.; Menten, M. L., The kenetics of the inversion effect., *Biochemische Zeitschrift* **1913**, *49*, 333-369.

(23) Nelson, D. L.; Cox, M. M. *Lehninger Principles of Biochemistry*, 4th Edition ed.; W. H. Freeman, 2004.

Chapter 2

A Digital Microfluidic System for the Investigation of Pre-Steady-State Enzyme Kinetics Using Rapid Quenching with MALDI-TOF Mass Spectrometry

This chapter describes a digital microfluidic system, based on electrowetting, developed to facilitate the investigation of pre-steady-state reaction kinetics using rapid quenching and matrix-assisted laser desorption/ionization time-of-flight mass spectrometry (MALDI-TOF MS). The device consists of individually addressable electrodes arranged to allow the combination of liquid droplets at well-defined time intervals, and an integrated, electrohydrodynamically driven mixer. The device combines two droplets to initiate a reaction, then, with precise timing, combines a third droplet to quench the reaction, and finally combines a fourth droplet to form a matrix. Improvements to throughput when compared to traditional lab scale methods, and previous MALDI-TOF MS digital microfluidic systems, were made. The device was tested against a model protein tyrosine phosphatase system, and results agreed well with published data. The system therefore allows for the analysis of reaction kinetics that were previously too rapid to analyze using MALDI-TOF MS.

Portions of this chapter were published in:

1) Nichols, K. P.; Gardeniers, H. J. G. E. *Analytical Chemistry*, 2007, 79, 8699-8704.

2) Nichols, K. P.; Gardeniers, H. J. G. E. In *Miniaturization and Mass Spectrometry*; le Gac, S., van den Berg, A., Eds.; Royal Society of Chemistry: Cambridge, UK, 2009, pp. 277-288.

3) Nichols, K. P.; Gardeniers, H. J. G. E. In *Proceedings of MicroTAS 2006*, 2006, pp. 582-584.

Introduction

The work presented in this chapter is an optimized combination of the work of Houston *et al.*, who demonstrated the utility of matrix-assisted laser desorption/ionization time-of-flight mass spectrometry (MALDI-TOF MS) in studying pre-steady-state kinetics using quench-flow techniques,[1] and the work of Wheeler *et al.*, who developed an elegant system for manipulating microliter scale droplets on planar surfaces for subsequent analysis using MALDI-TOF MS.[2, 3] The purpose of this work is to improve the pre-steady-state kinetic analysis technique of Houston *et al.* by using digital microfluidic techniques to analyze the smallest liquid volume possible with the most rapid quenching possible; it attempts to overcome the "fundamental limitations"[1] previously encountered in pre-steady-state kinetic studies. Typically, for pre-steady-state kinetic analysis, one combines enzyme with substrate and quenches the reaction after specified time intervals. Pre-steady-state kinetic analysis is particularly challenging due to the extremely short time scales typically involved, on the order of milliseconds.[4] The digital microfluidic system previously described by Wheeler *et al.* for use with MALDI-TOF MS was not suitable for this particular application due to unexpected throughput issues, and due to unavoidable contamination from protein fouling, thus necessitating a significant rethinking of its design. We discuss how, for certain applications of digital microfluidics to MALDI-TOF MS, the removal of the on-chip reservoirs and droplet handling systems of the Wheeler *et al.* device allows for higher throughput than can be achieved by their inclusion. Additionally, we describe a novel electrohydrodynamic mixing scheme incorporated in our device.

The purpose of combining these previously described techniques and including the novel mixing scheme described in this chapter was to enhance the throughput of the Houston *et al.* method for pre-steady-state kinetic analysis, allowing for the analysis of inherently noisy samples. We sought to create a lab-on-a-chip implementation of the Houston *et al.* method that was capable of overcoming the

inherent inaccuracy in certain pre-steady-state kinetic measurements. We achieved this by designing a system with adequate throughput to produce sufficient data to overcome the noise inherent in pre-steady-state kinetic analysis. The advantage of this system over that of Houston *et al.* is not necessarily greater accuracy of individual measurements, but higher throughput, allowing for innate inaccuracy to be overcome.

Lab-on-a-chip systems have been demonstrated to have great utility for Analytical Chemistry.[5-7] In general, lab-on-a-chip systems seek to miniaturize traditional bench scale operations, which are normally carried out in glassware on the order of milliliters to liters, to chip scale operations in channels and droplets, on the order of nanoliters to microliters. The majority of lab-on-a-chip devices proposed thus far utilize predefined sealed channels on the order of micrometers. These sealed channels are constructed using a variety of geometries, and combined in such a way as to recreate traditional wet chemistry protocols on a smaller scale. When used in such a manner, these sealed channels are referred to as "continuous flow" microfluidic channels.[8-10]

Recently, a method for constructing lab-on-a-chip devices without continuous flow microfluidics has emerged. It is referred to as digital microfluidics. Digital microfluidics utilizes discrete liquid droplets manipulated on electrode arrays instead of the sealed channels of continuous flow microfluidics. The primary advantages of digital microfluidic systems include: low dispersion / cross-talk between droplets, rapid homogenization within the droplet, more straightforward translations from bench-scale to chip-scale processes, greater reconfigurability leading to more "general-purpose" devices, and reduction of dead-volumes associated with macro to micro interconnections due to the high degree of integration possible between sample reservoirs, dispensing systems, and structures for droplet manipulation. The primary disadvantage of digital microfluidic systems is that they require high voltages and polarizable liquids.[2, 3, 11-14] Digital microfluidic systems are distinct from droplet-based continuous flow microfluidic systems. Digital microfluidic systems manipulate droplets on a plane with x-y movement restricted only by the presences of electrode

pads, while droplet-based continuous flow systems produce nL scale droplets in traditional continuous flow microfluidics using multiple phases. [15-18]

The most common digital microfluidic fluid actuation techniques utilize a combination of strategically placed electrodes and changes in contact angle induced by one of two principles: electrowetting on dielectric (EWOD) or dielectrophoresis (DEP). EWOD and DEP can be considered the low and high frequency cases, respectively, of the application of a sufficient electric field to polarizable liquids along the correct axes.[19-21]

EWOD based digital microfluidic devices typically require a planar electrode covered by a hydrophobic dielectric film, above which droplet actuation occurs. For reversible droplet actuation, a ground plane integrated on a cover above the droplet is typically required. Upon application of a sufficient voltage, the charge imbalance at the liquid-dielectric interface results in an electrochemical (Coulombic) force that causes a change in contact angle, and subsequent droplet movement. A simple digital microfluidic EWOD device can be constructed by arranging two adjacent coplanar electrodes, coated with a hydrophobic dielectric, above which is a polarizable liquid droplet covered by a ground plane. By selectively applying a DC potential to one of the two bottom coplanar electrodes, the apparent hydrophobicities of the surfaces above these two electrodes will vary, causing a droplet placed above one of the two electrodes to move preferentially towards the regions of higher field strength.[11, 22-25]

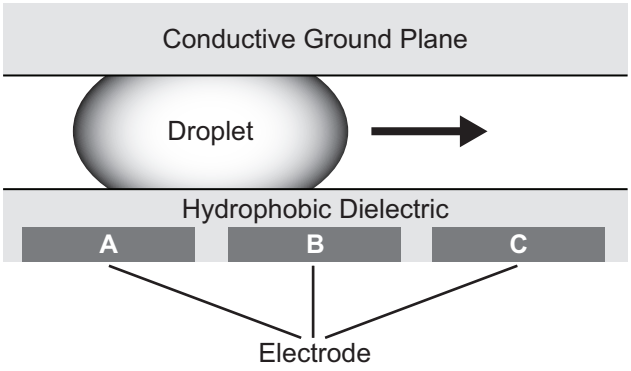

Figure 1 – A cross-section of a typical EWOD (electrowetting on dielectric) system. If a sufficient voltage is applied between two bottom electrodes, the droplet will center itself between the bottom electrodes (shown). If a sufficient voltage is applied between any individual bottom electrodes and the ground plane, the droplet will center itself directly over that bottom electrode (not shown). Our system does not use a ground plane (lid), so droplet manipulation is accomplished solely using the bottom electrodes. For example, to move the droplet from left to right, first a voltage would be applied between electrodes A and B, and then between B and C.

EWOD based digital microfluidics have already been combined with MALDI-TOF MS by Wheeler *et al.*[2] However, the Wheeler *et al.* device would have several drawbacks when used in pre-steady-state kinetic studies, including lower throughput, for reasons explained in the discussion section, and the absence of a mixing element. Further, while Paik *et al.*[11] have demonstrated droplet mixers for EWOD based digital microfluidic systems, their mixing system is not rapid enough to be of use in pre-steady-state kinetics.

MALDI-TOF MS has been demonstrated as a useful tool in pre-steady-state kinetic research by Houston *et al.*, who combined it off-line with quench-flow methods to follow the appearance of a protein tyrosine phosphatase (PTPase) reaction intermediate.[1] Houston *et al.*, were capable of measuring rate constants up to 30 s^{-1},

with k_2/k_3 ratios up to approximately 15. The device described within extends this technique to measure rate constants approximately 5 times greater, with k_2/k_3 ratios approximately twice previously measurable values using mass spectrometry alone. MALDI-TOF MS is typically conducted on a centimeter scale conducting plate; the digital microfluidic system employed is a square plate approximately 2 cm on each side, with 16 experimental units per chip, that can be placed directly inside a standard MALDI-TOF MS plate that has been machined appropriately. By grounding the exposed wires on the otherwise insulated chip, charging is negligible.

There are a variety of other spectroscopy techniques available for investigating reaction kinetics. However, MALDI-TOF MS allows for the determination of rate constants regardless of the incorporation of a chromophore, and at a wide variety of buffer concentrations. Both of these advantages are useful if one wishes to study enzymatic reactions under naturally occurring conditions. Without the use of mass spectrometry, if an optical readout is required, the experiment will either be restricted to substrates and products from which a colorimetric or fluorescent measurement may be taken, or the substrate or product must be modified such that it can be probed by an optical method. The advantages of MALDI-TOF MS can be compared to spectrophotometric methods, which require a chromophore, and electrospray ionization mass spectrometry, which is sensitive to buffer concentrations. As MALDI-TOF MS is an off-line technique requiring quenching for the analysis we performed, a rapid mixer must be incorporated into the system, or the system must be designed so that mixing is inherently fast. The optimization of a rapid, active mixing system for digital microfluidic systems, including optimized frequencies of use, is discussed in detail in chapter 3, and has been published by us elsewhere.[26]

Yop51 Protein Tyrosine Phosphatase (PTPase)[27] was analyzed as a model system. Deprotonated PTPases act as nucleophilic thiolates during attacks on phosphates. Mass-spectrometric analyses of PTPases are possible due to the predictable formation of a covalent phosphoenzyme intermediate.[1] Once

phosphorylized, the enzyme has a mass difference that is readily detectable using mass spectrometry. In this study, unphosphorylated enzyme is used as an internal standard to permit quantitation of the phosphorylated to unphosphorylated enzyme ratio, used to determine pre-steady-state kinetic values. The ratio of these two enzyme forms is tracked throughout the initial burst-phase of the reaction.

Experimental

Device Fabrication

A complete process flow describing the device fabrication in detail is provided at the end of the chapter.

The digital microfluidic system used to obtain kinetic values consists of individually addressable Cr/Au electrodes (Figure 2), covered by 100 nm of silicon dioxide, 500 nm of silicon nitride (which together act as a sufficient dielectric layer), and 1 μm of Teflon AF 601S1-x-6 (DuPont) film. The total length and width of each electrode shown is 0.75 mm.

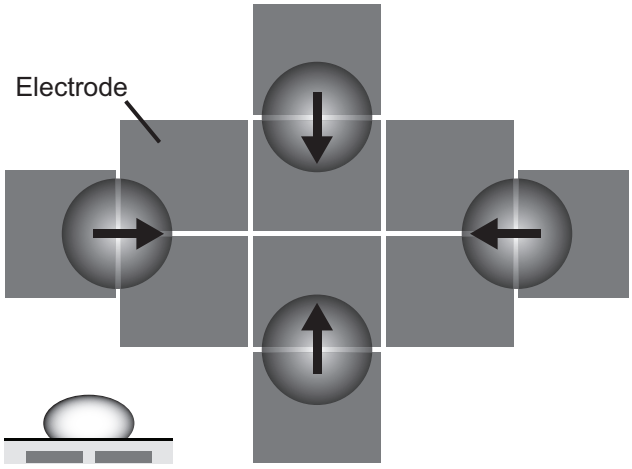

Figure 2a – A simplified top-down and cross-sectional (inset) view of one experimental unit on the chip. Droplets are loaded robotically or manually at each of the four outermost positions shown. During loading, all the central electrodes are set to negative DC voltage, and all the outer electrodes are set to positive DC voltage, to facilitate easier, more accurate droplet placement. This also allows smaller volumes to be accurately dispensed, as capillary forces in the pipette tip can be overcome. The droplets are then sequentially

combined using AC voltage (enzyme with substrate, then quench, then matrix). The cross-section shows a droplet over an electrode gap and a hydrophobic dielectric. Wires are not shown. During analysis, charging is negligible if the system is grounded, since small areas of the wires are in direct (uninsulated) contact with the matrix.

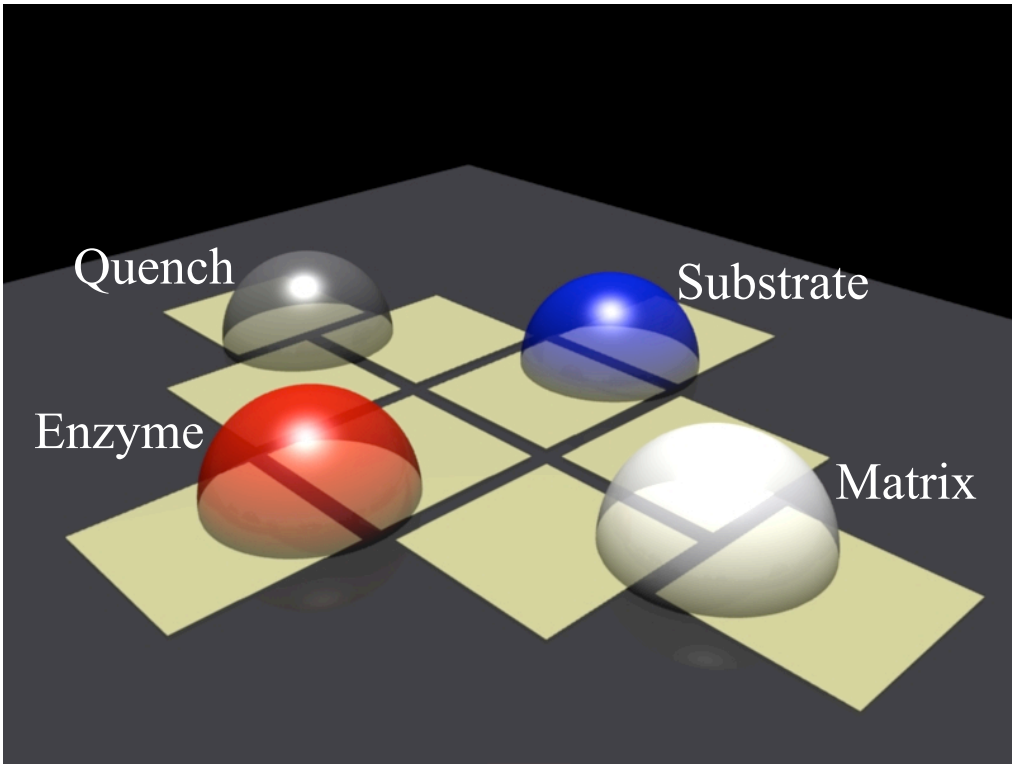

Figure 2b – A 3D rendering of the device shown in Figure 2a.

All patterns were designed using CleWin (WieWeb Software, the Netherlands). Cr masks were produced using a Heidelberg Instruments DWL 2.0 (Germany) laser pattern generator. Double-side-polished glass wafers were metalized using a 20 nm Cr adhesion layer and a 200 nm Au thin film was sputtered using a custom built sputtering tool available at the MESA+ Institute for Nanotechnology

(University of Twente, the Netherlands). Standard photolithography techniques were employed to produce a photoresist etch mask for the metallization layer. The photoresist etch mask was oxidized using a standard ozone reactor, prior to wet etching using standard Cr and Au etching recipes. The Silicon Dioxide and Silicon Nitride layers were deposited using PECVD, and patterned using reactive ion etching (RIE). In devices where it was necessary, vias for wiring were patterned by leaving holes in the dielectric layer that a 200 nm Cr layer was sputtered onto at $2 \cdot 10^{-2}$ bar using the above-mentioned sputtering device. A hydrophobic Teflon AF 600 film (DuPont, USA) was manually dispensed and spun to a thickness of approximately 1 μm. Adhesive tape was applied over the contact pads before pouring and spinning the Teflon layer, allowing for very simple patterning. After removing the adhesive tape, the Teflon AF was baked at 150˚C for 20 minutes. Individual 2 cm chips were diced using a Disco DAD-321 (Disco Corporation, Japan) dicing saw.

MALDI-TOF MS Kinetic Analysis on Chip

When voltage is applied across adjacent electrodes at 1000 Hz, 250 V_{RMS}, liquid droplets quickly center themselves over the inter-electrode gap. Using the voltage patterns illustrated in Figure 3, an enzyme and a substrate droplet can be combined, allowed to react for an arbitrary time, and then quenched using a strong acid and the matrix necessary for mass spectrometry. As discussed in chapter 3, electrohydrodynamic forces act as an efficient mixer in such a system.

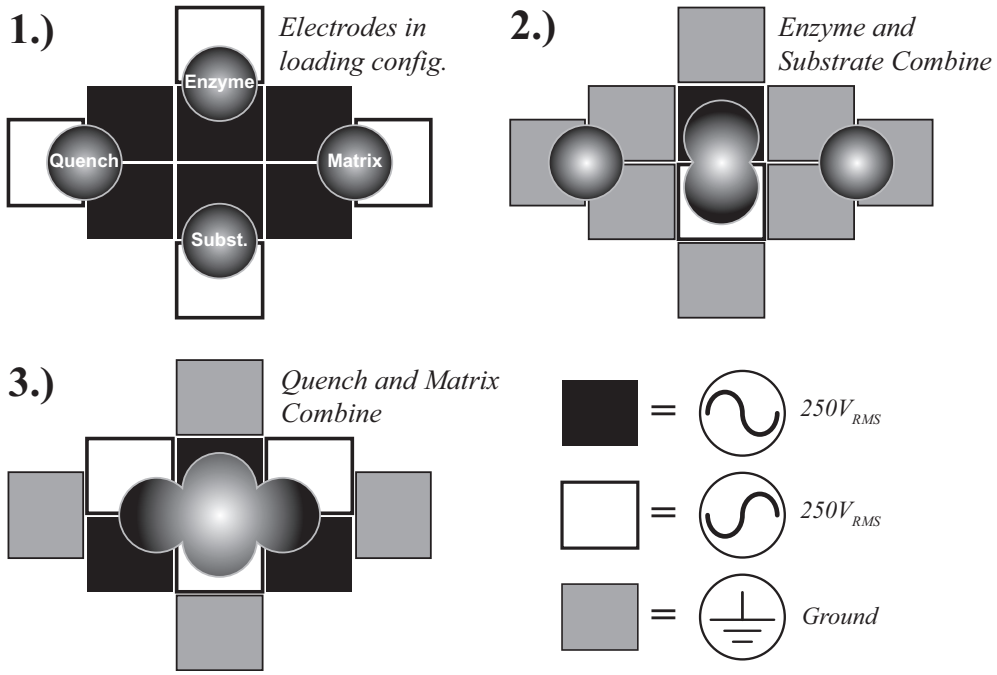

Figure 3 – Voltage patterns to load, combine and mix droplets. 1.) Droplets are loaded robotically or manually at each of the four outermost positions, with the voltage centering the droplets over the inter-electrode gap. 2.) The enzyme and substrate droplets combined using only the two central electrodes. 3.) The quench and matrix combine with the reacting enzyme, stop the reaction, and allow subsequent MALDI-TOF MS.

Experiments were conducted by sequentially combining 0.5 μl buffered 50 μM Yop51 PTPase (Sigma, USA) at pH 7.2 with its substrate, 20mM *p*-nitrophenyl phosphate (Acros), then quenching the reaction with 1 M dichloroacetic acid (Acros), and finally forming a matrix using 25 mg/ml ferulic acid in 2:1 H_2O/acetonitrile (Acros). The temperature of the system was controlled at 30°C using a simple resistive heater and thermistor element. Samples were directly analyzed on the digital microfluidic chip using an Applied Biosystems Voyager MALDI-TOF MS. The electrodes were grounded during analysis. This effectively minimized charging by making use of the uninsulated vias described in the fabrication section.

Combination and mixing of droplets at well-defined time intervals was accomplished using a custom-built relay board interfaced with a laptop PC controlled using MATLAB. Each 0.5 μl droplet was manually loaded across one of the outermost electrode gaps, and then brought into the center for rapid mixing. Protein Tyrosine Phosphatase (PTPase) was analyzed as a model system. Deprotonated PTPases act as nucleophilic thiolates during attacks on phosphates.

Details of the model PTPase reaction are available.[1, 27] An equation derived by Bender, Kezdy and Wedler[28] describing the pre-steady-state kinetics of α-Chymotrypsin, an enzyme whose physiological role is the hydrolysis of protein amide bonds, was used to deduce the rate constants k_1 and k_2., where:

$$E + S \overset{K_S}{\rightleftharpoons} E \cdot S \xrightarrow{k_2} ES' \xrightarrow[P_1]{k_2} E + P_2 \qquad (1)$$

E is the enzyme, S is the substrate, P indicates a product, and ES'/EP is the covalently bound enzyme/product intermediary. It has been shown that our model PTPase follows this same scheme, and that the Bender derivation is valid since, as is the case with α-Chymotrypsin $k_3 >> k_2$.[1]

Based on the analysis by Houston *et al.*,[1] our model PTPase followed the scheme:

$$E + S \underset{k_{-1}}{\overset{k_1}{\rightleftharpoons}} E \cdot S \xrightarrow[phenol]{k_2} EP \xrightarrow{k_3} E + P_i \qquad (2)$$

The Bender *et al.* derivation can then be used to determine the following parameters:

$$C = \frac{k_2}{\left(k_2 + k_3\right)\left(1 + \frac{K_m}{[S]_0}\right)} \tag{3}$$

$$b = k_3 + \frac{k_2}{1 + \frac{\left(k_2 + k_3\right) \cdot K_m}{k_3 \cdot [S]_0}} \tag{4}$$

$$\frac{[EP]}{[E]_0} = C \cdot \left(1 - e^{-bt}\right) \tag{5}$$

K_m is the Michaelis–Menten constant. $[S]_0$ is the initial product concentration.

Nonlinear regression using MATLAB was used to fit eq. 5 to K_m values obtained from literature[27], experimentally relevant concentrations, and scaled $[EP]/[E]_0$ data calculated as the area under EP divided by the sum of the EP and E areas.

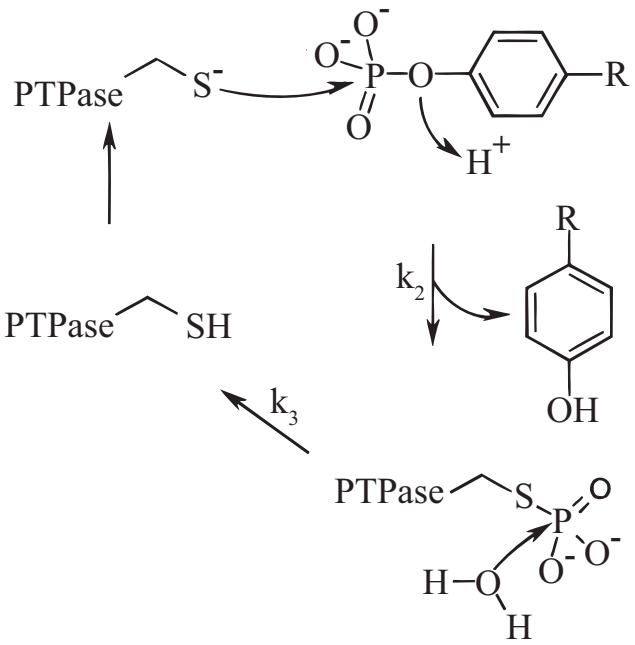

Figure 4 – Protein tyrosine phosphatase mechanism (PTPase). The EP intermediate can be detected by MALDI-TOF MS when $k_2 >> k_3$. Figure adapted from Houston *et al.*[1]

Calibration of Electrohydrodynamic Mixer

Two reactions were analyzed to determine mixing behavior: the mixing of 0.5 µl droplets of 10^{-5} M fluorescein (Sigma, USA) with 0.5 µl DI water droplets (Figure 2), and the mixing of 0.5 µl droplets of 10^{-5} M fluorescein with 0.5 µl droplets of 1 M acetic acid (Sigma, USA).

A standard function generator and a Krohn-Hite 7602M (Krohn-Hite Corporation, USA) amplifier operating at 250 V_{RMS} generated AC voltages with frequencies ranging from 1 Hz to 300000 Hz.

Mixing efficiency was analyzed using a HI-CAM high-speed video camera (Lambert Instruments, the Netherlands) and MATLAB 7.1 (MathWorks, USA).

There is no standard metric available to define "percent mixed" as a single scalar quantity. Instead, the most common technique in the literature is to define a point at which mixing is "complete," and use this value only.[11] The definition of "complete" is often ambiguous. For our system, we found it difficult to define complete mixing, since our end stages of mixing were particularly difficult to differentiate. Therefore, we utilized a common circuit analysis technique, where a time constant τ is defined as the point at which 63% of a signal has decayed. In this case, our signal is the "completeness" of mixing, though utilizing this method means only the asymptote (of intensity, for example) that "complete" mixing eventually reaches is needed, and not a precise determination of "completeness."

To construct the curve from which this time constant was extracted, we calculated the variance of the mean gradient magnitude as a function of time. To determine this value, each video frame was converted into a 2D matrix, with each pixel assigned a value from 0 to 1. Videos were manually inspected to verify the image sensor was not saturated. For each pixel, in each video frame, the magnitude of the gradient was calculated. Subsequently, the variance in the x and y directions were calculated. This produced two vectors, from which the mean value was extracted. This mean value was then plotted as a function of time, for each frame of the video.

Calculating either the gradient magnitude or variance alone led to obviously unmixed regions being identified as mixed. Mixing has many subtleties, and many of these will inevitably be lost when converting from a 2D matrix to a single number. However, this method seemed most suitable for our application. It is believed that this value can provide an accurate metric for mixing analysis, as long as images are manually inspected to confirm that the last image in the series is homogenized.

Hi-speed video analysis was also used to measure average droplet speeds during transfer to the center of the device. This time was then used to define the zero point in eq. 5.

Results and Discussion

Primary Results

Houston *et al.* reported the capability to measure pre-steady-state kinetics using "rapid chemical quench flow methods" coupled with MALDI-TOF MS. However, they reported difficulties in obtaining accurate pre-steady-state kinetic measurements from systems with high k_2/k_3 ratios. They reported that above a certain critical value, random error prevents the differentiation of slightly varying progress curves. The highest k_2/k_3 ratio reported by Houston *et al.* was approximately 15 ([29.2 +/- 3.8] / [1.89+/-0.46] for p-fluorophenyl phosphate and the enzyme Stp1).[1]

To demonstrate the improved performance possible using our system, we performed an equivalent set of measurements, though using an enzyme/substrate system with a higher k_2/k_3 ratio. Yop51 PTPase at pH 7.2 with its substrate, 20mM *p*-nitrophenyl phosphate has a reported k_2/k_3 ratio of 30.1 (193/6.5).[27] Unphosphorylated enzyme is used as an internal standard to permit quantitation of the phosphorylated to unphosphorylated enzyme ratio (Figure 5), which is used to determine pre-steady-state kinetic values. As is shown in Figure 6, performing a sufficiently large number of measurements (10 per time point) will produce enough normally distributed data to overcome even relatively high k_2/k_3 ratios. Our analysis produced a k_2 value of 170±10, and a k_3 value of 8±3. Since previous studies of Yop51 PTPase have not provided standard deviations for their results (presumably due to the difficulty in obtaining them) it is not possible to tell precisely how close our values are to previously measured values. However, our results do not appear to greatly deviate from published results. Note that the rate constants cited above (not our own measurements) were not determined using MALDI-TOF MS. Our study thus demonstrates the highest rate constants yet measured with this particular analysis technique. The advantages of using MALDI-TOF MS are described in the introduction.

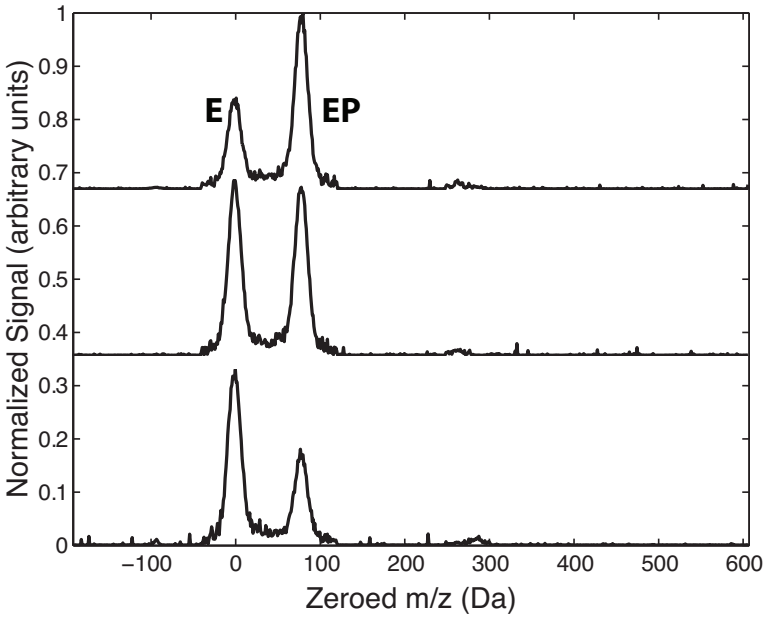

Figure 5 - Typical MALDI-TOF MS spectra acquired at three sequential time intervals, after signal processing. Curves are smoothed using the Savitzky-Golay method and leveled to facilitate proper definition of limits of integration. Occasionally, if samples are offset on the device, charging will occur since the sample is, in that case, not grounded. The delta m/z remains constant however, and data can still be obtained if zeroed as shown. The absence of other large peaks makes this possible. The two peaks represent unphosphorylated (E) and phosphorylated (EP) PTPase, respectively. This image is comparable to Figure 5 in Houston *et al.*[1]

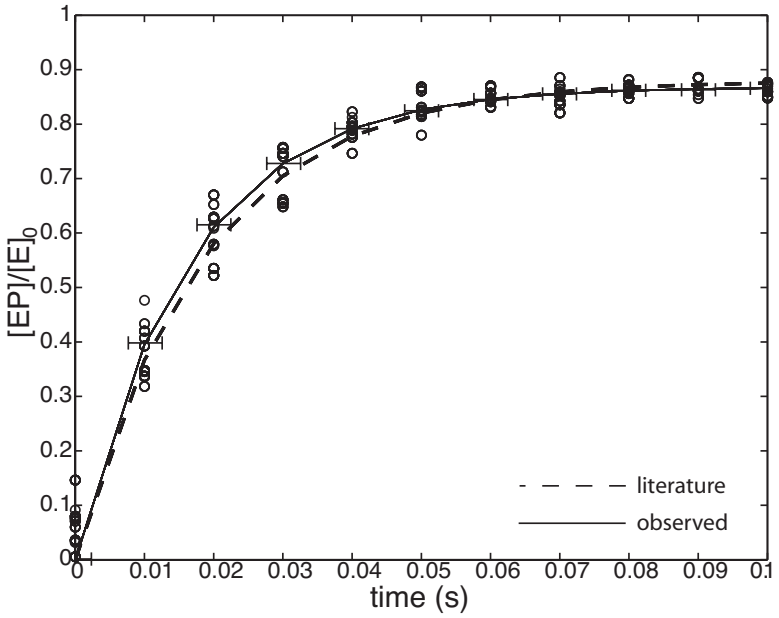

Figure 6 – Literature data (parameters from Zhang *et al.*[15], model described in Experimental section) and observed data from our experiments. Greater scatter is observed at earlier time points. The horizontal error bars represent two standard deviations from the mean mixing time for these droplet volumes and actuation frequencies, as determined in separate experiments. Our parameters were: k_2 = 170 +/- 10 and k_3 = 8 +/- 3. Zhang's parameters were: k_2 = 193; k_3 = 6.5; and K_m = 2.5 mM.

The absence of sophisticated droplet dispensing and handling systems in our device

As can be seen in Figure 2, our device does not have the elegant sample preparation and dispensing systems demonstrated in the Wheeler *et al.* device for MALDI-TOF MS measurements in a digital microfluidic system. While our initial designs did include analogous systems, we quickly found that, using the best practices currently published, they require too much space on the chip to be of practical use for our system, for the following reasons: The Wheeler *et al.* system performs a relatively

simpler set of chemical operations; they move an impure sample to a specific location, dry and rinse the sample, and then move a matrix forming solution over the sample. Their system therefore requires two reservoirs. Since our system combines a larger number of droplets (an enzyme, a substrate, a quench, and a matrix forming solution) it has additional complications associated with having an additional two reservoirs. Further, since even slight contamination between any of these droplets will catastrophically affect the pre-steady-state kinetic experiment, and, since some protein (enzyme) absorption on a hydrophobic surface is inevitable, separate lanes leading from each of the four reservoirs are required. The difficulties with routing such a network without crossing lanes are obvious: to do so requires that as much, if not more, space on the chip be devoted to droplet handling as is devoted to positions on the chip where the actual experiments are carried out.

The inclusion of a droplet handling system is therefore only justified if the time it saves is greater than the time that is lost due to being able to perform fewer experiments per chip. Performing a large number of time-stepped MALDI-TOF MS measurements, as we wished to do, requires two primary expenditures of time. The most obvious expenditure is that required by droplet dispensing. Incorporating on-chip reservoirs and droplet handling systems as in the Wheeler *et al.* device reduces this time expenditure. However, the second, and in our case, greater expenditure of time comes from loading the MALDI-TOF MS plate into the MALDI-TOF MS system. In a typical MALDI-TOF MS system, it takes approximately 1 minute to properly position the tray in the device, and as many as 5 to 10 minutes for the system to load the tray, move it into position, and pump the system down to a vacuum level sufficient for analysis. Unloading the system takes an additional 1 to 2 minutes. There is, therefore, a tradeoff between the time that can be saved by using on-chip dispensing systems, and the time that can be saved by using this space for additional measurements per loading cycle. In our case, eliminating droplet dispensers was the better choice.

Therefore, due to the unintended consequences associated with the inclusion of an on-chip droplet dispensing system, an external robotic droplet dispenser is superior to on-chip droplet handling systems for our particular application, despite being in disagreement with the general design ethos of lab-on-a-chip systems. Even dispensing by hand takes at most one to two seconds per droplet, and is surprisingly easy if the electrodes are properly energized to "automatically" center the droplet. Robotic dispensing is already a common tool for MALDI-TOF MS analysis, and is not difficult to integrate with our system.

Calibration of Electrohydrodynamic Mixer

Convective electrohydrodynamic (EHD) flow, utilized in our system for mixing within a droplet, is a consequence of the tangential stress at the interface between a droplet and its surrounding medium, where tangential viscous stress arises to directly balance tangential electric stress.[29] While we believe the use of EHD based mixing to be novel as applied to a digital microfluidic system, a physical model is beyond the scope of this analytical chemistry focused chapter. However, EHD is a well-established field, and papers spanning several decades confirm the effects we describe.[30-33] Therefore, we only discuss the basic characteristics and limitations of the device to the extent necessary that it could be duplicated in a similar digital microfluidic system.

Most digital microfluidic systems described already contain the necessary components for an EHD based mixer. EHD flow can be initiated by placing a conductive droplet over an insulated electrode gap, and applying a sufficient voltage at the correct frequency across the electrodes. However, care should be taken, as the presence of a lid will decrease the efficiency of EHD mixing. EHD mixing will be most efficient in a suspended droplet not pinned to any surface, and should decrease proportionally to the level of pinning present. Thus, EHD flow in a confined microchannel will not occur under typical conditions, though EHD mixing in a

microchannel between liquids with "different electrical properties" has recently been reported.[34] Likewise, EHD mixing will be most efficient in a digital microfluidic device without a lid, and will decrease as the ratio of pinned to unpinned droplet surface increases. This is another factor making the inclusion of the droplet handling systems described by Wheeler *et al.* problematic, as analogous droplet actuation without a grounded lid is significantly more difficult.

Efficient EHD driven mixing was achieved at 250 V_{RMS} from 150 Hz to 2250 Hz. Above 2250 Hz, mixing efficiency decreases as the decreasing impedance of the dielectric reaches a critical threshold allowing for the pinning of a greater percentage of the droplet to the floor of the device. Above 46000 Hz, impedance is low enough to permit sufficient current to cause unacceptable Joule heating. At the chosen frequency of 1000 Hz, mixing time for 0.5 μL droplets was approximately 15 ms (Figure 7, white square). This time was used to calibrate the kinetic model as described in the Experimental section.

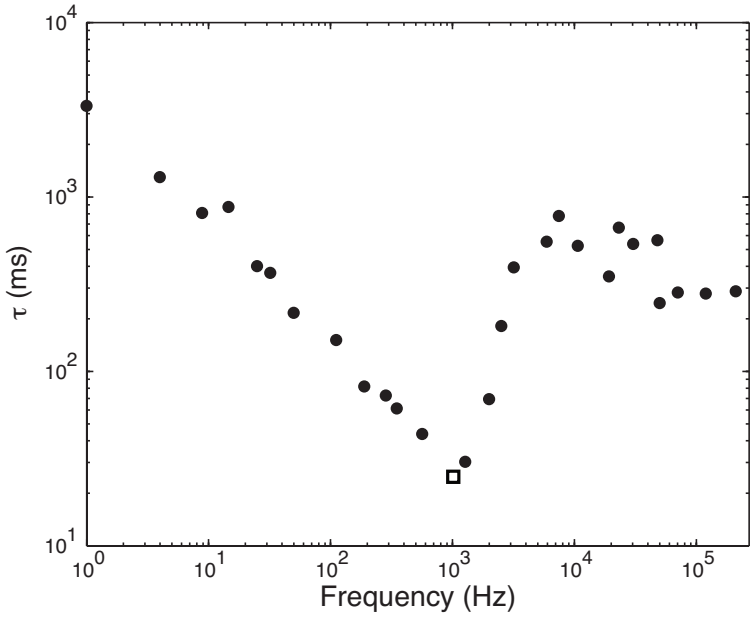

Figure 7 – The mixing constant τ for the EHD mixer as a function of frequency. Black circles represent the means of between 2 and 4 measurements. The white square at 1000 Hz was used to calibrate the device as described in the experimental section. At higher frequencies, operation becomes more complicated as additional phenomena begin to affect the droplet.

Analysis of the high-speed videos shows that mixing in this frequency regime appears to be the result of spiraling fluid flow originating at the center of the droplet, moving outwards, curving around the droplet wall, and returning to the center of the droplet, as would be expected in an EHD driven flow field.

Suitability for applications in varying salt concentrations, and the absence of Joule heating at 1000 Hz

As shown in Table 1, varying the KCl concentration from $0.5 \cdot 10^{-5}$ M to 1 M does not significantly affect mixing time when mixing 1 μL droplets of KCl with 1 μL droplets of DI water. For broad compatibility with a wide variety of chemical and biochemical reactions, this is a critical tolerance. One significant advantage of MALDI-TOF MS over electrospray ionization MS for kinetic studies is its relative insensitivity to salt concentration.

Additionally, it was demonstrated that at 1000 Hz, 250 V_{RMS}, no measurable Joule heating occurs. Droplets were left on the device (without a lid) and continuously mixed until no visible liquid remained. No significant difference in evaporation rate was observed between mixing at 1000 Hz, 250 $V_{RMS,}$ and droplets left on the device without the application of any external potential.

Table 1 - Effect of KCl concentration on the mixing τ of 1 µl of KCl with 1 µl of DI water at 750 Hz. For the EHD mixing scheme described to be broadly useful, it must also be usable over a broad range of salt concentrations (conductivities). As can be seen, KCl concentration does not affect τ over the measured range. Standard deviations of τ are slightly larger than in other experiments due to a larger droplet being used (0.5 µl as opposed to 1 µl), which travels somewhat more irregularly. Smaller droplets will have more repeatable results.

KCl (M)	Mean τ (ms)	Std Dev (ms)
0.5E-5	42	1
1.0E-5	51	13
0.5E-4	39	1
1.0E-4	56	1
0.5E-3	44	7
1.0E-3	44	10
0.5E-2	49	7
1.0E-2	43	7
0.5E-1	40	9
1.0E-1	46	10
0.5E0	42	1
1.0E0	40	4

Conclusions

We have demonstrated a lab-on-a-chip system for the study of pre-steady-state chemical kinetics utilizing digital microfluidics and MALDI-TOF MS. The device incorporates an EHD mixing scheme, and is designed with the particularities of pre-steady-state kinetics in mind. Future work should focus on an on-chip droplet dispensing system that would meet the requirements discussed within. If a device could be constructed capable of moving droplets over multiple planes (a 3D digital microfluidic system), and with a removable lid, it would be possible to obtain the densities required for a true high-throughput MALDI-TOF MS digital microfluidic system.

Acknowledgements

The technology program of the Ministry of Economic Affairs of the Netherlands (project no. 6626) and the Technology Foundation STW, the applied science division of the NWO, financially supported this research.

Detailed Process Flow

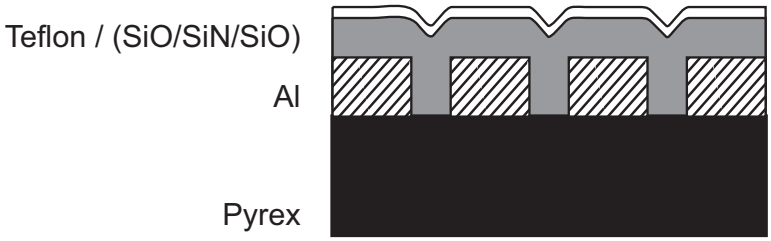

Figure 8 – Cross-section of completed digital microfluidic chip, showing electrode pads, covered by dielectric. The ridge in the dielectric between the electrodes is insignificant in scale compared to the droplets. It must be thick enough, however, to completely cover the electrodes and prevent short circuits even at the corner.

This design requires two masks. The first mask defines the electrode pattern, and the second mask defines areas left exposed for later wire-bonding or direct electrical connections by test-probe tips. Dimensions are discussed in further detail in chapter 3.

Process Steps

All steps refer to machinery available at the MESA+ Institute for Nanotechnology cleanroom as of 2008. In general however, these steps should be broadly applicable to other equipment with only slight modifications. It should be noted that an attempt was made by a colleague at K.U. Leuven to fabricate these devices using a lift-off protocol (instead of that shown below), and short-circuits between the electrode pads were found to limit yield below acceptable levels. The protocol below was then duplicated with success.

Substrate Selection

Step Name	Details	Comments
Substrate selection – Pyrex Glass	CR112B Diameter: 100 mm Thickness: ca. 0.5 mm	A batch consists of 5 (4 + 1 reserve) wafers. Note that MESA+ transitioned to borofloat wafers as of late-2008. However, Pyrex should be able to be replaced with borofloat without subsequent changes being required.

Electrode Layer

Step Name	Details	Comments
Cleaning Glass	CR112B / Wet-Bench 3-4 HNO_3 (100%) Selectipur: MERCK 100453 • Beaker 1: HNO_3 (100%) 5 min. • Beaker 2: HNO_3 (100%) 5 min. • Quick Dump Rinse <0.1 µS • Spin drying	
Sputtering of Al (Sputterke)	CR106A / Sputterke Al Target • Electrode temp.: water cooled electrode • Ar flow: 81 sccm • Base pressure: 1.0 e-6 mbar • Sputter pressure: 6.6 e-3mbar • Power: 200W • Time: 10 min	200 nm
Lithography - Coating Olin907-17 (Headway)	CR112B / Headway Spinner Olin 907-17 • Spinning speed: 4000 rpm • Spinning time: 20 sec. • Prebake (95°C): 90 sec.	
Lithography - Alignment & Exposure Olin 907-17 (EV)	CR117B / EVG 20 Electronic Vision Group 20 Mask Aligner • Exposure time: 4 sec.	
Lithography - Development Olin Resist	CR112B / Wet-Bench 11 Developer: OPD4262 Hotplate 120°C (CR112B or CR117B))	Mask 1

	• After Exposure Bake (120°C): 60 sec. Development: • Time: 30 sec. in Beaker 1 • Time: 15-30 sec. in Beaker 2 • Quick Dump Rinse <0.1µS • Spin drying	
Lithography - Post bake standard	CR112B / Hotplate 120°C • Time: 30 min.	
Ozone anneal of Olin 907 (to improve wetting)	CR116B-1 / UV PRS-100 • Time: 300 sec.	To improve wetting during etching of Chromium layers
Etching of Al Wet -	Al Wet etch 55º C	
Cleaning fuming HNO_3 user made	CR116B / Wet-Bench 2 HNO_3 (100%) Selectipur: MERCK 100453 • Beaker 1: HNO_3 (100%) 5 min • Quick Dump Rinse <0.1µS • Spin drying	

Dielectric Layer

Step Name	**Details**	**Comments**
PECVD of SiO-SiN-SiO layer (Oxford)	CR102A / OXFORD Plasmalab 80 + • Electrode temp. = 300°C o SiO o SiN o SiO	
Lithography - Coating Olin907-35 (Headway)	CR112B / Headway Spinner Olin 907-35 • Spinning speed: 4000 rpm • Spinning time: 20	

	sec. • Prebake (95°C): 90 sec.	
Lithography - Alignment & Exposure Olin 907-35 (EV)	CR117B / EVG 20 Electronic Vision Group 20 Mask Aligner • Exposure Time: 8 sec.	Mask 2
Lithography - Development Olin Resist	CR112B / Wet-Bench 11 Developer: OPD4262 Hotplate 120°C (CR112B or CR117B)) • After Exposure Bake (120°C): 60 sec. Development: • Time: 30 sec. in Beaker 1 • Time: 15-30 sec. in Beaker 2 • Quick Dump Rinse <0.1µS • Spin drying	
Lithography - Postbake standard	CR112B / Hotplate 120°C • Time: 30 min.	
Plasma etching SiN (Etske)	CR102A / Elektrotech PF310/340 Time >10min Dirty chamber Styros electrode • Electrode temp.: 10°C • CHF3 flow: 25sccm • O2 flow: 5sccm • pressure: 10mTorr • power: 75W Etchrate SiN: 50nm/min (for VD: -460V) Etchrate SiN: 75 nm/min (for VDC: -580V) Etchrate Olin resist: 95nm/min	Check electrical contact with Multimeter

	If DC-Bias < 375V apply chamber clean	
Dice	CR128C / Disco DAD dicing saw Default Pyrex dicing parameters	Dicing lines are thick, unbroken lines on outside of chips

Teflon Layer

Step Name	**Details**	**Comments**
Teflon	Teflon AF 601S1-x-6 • Spin at 2000 RPM • Bake at 200º C o 2 min	Pattern using adhesive tape to mask electrode areas.

References

(1) Houston, C. T.; Taylor, W. P.; Widlanski, T. S.; Reilly, J. P., Investigation of enzyme kinetics using quench-flow techniques with MALDI TOF mass spectrometry, *Anal. Chem.* **2000**, *72*, 3311-3319.

(2) Wheeler, A. R.; Moon, H.; Bird, C. A.; Loo, R. R. O.; Kim, C. J.; Loo, J. A.; Garrell, R. L., Digital Microfluidics with in-Line Sample Purification for Proteomics Analyses with MALDI-MS, *Anal. Chem.* **2005**, *77*, 534-540.

(3) Moon, H.; Wheeler, A. R.; Garrell, R. L.; Loo, J. A.; Kim, C. J., An integrated digital microfluidic chip for multiplexed proteomic sample preparation and analysis by MALDI-MS, *Lab Chip* **2006**, *6*, 1213-1219.

(4) Zhou, X. Z.; Medhekar, R.; Toney, M. D., A continuous-flow system for high-precision kinetics using small volumes, *Anal. Chem.* **2003**, *75*, 3681-3687.

(5) Stone, H. A.; Stroock, A. D.; Ajdari, A., Engineering flows in small devices: Microfluidics toward a lab-on-a-chip, *Annual Review of Fluid Mechanics* **2004**, *36*, 381-411.

(6) Rios, A.; Escarpa, A.; Gonzalez, M. C.; Crevillen, A. G., Challenges of Analytical Microsysterns, *Trac-Trends in Analytical Chemistry* **2006**, *25*, 467-479.

(7) Squires, T. M.; Quake, S. R., Microfluidics: Fluid physics at the nanoliter scale, *Reviews of Modern Physics* **2005**, *77*, 977-1026.

(8) Manz, A.; Graber, N.; Widmer, H. M., Miniaturized Total Chemical-Analysis Systems - a Novel Concept for Chemical Sensing, *Sensors and Actuators B-Chemical* **1990**, *1*, 244-248.

(9) Gardeniers, J. G. E.; Van Den Berg, A., Lab-on-a-Chip Systems for Biomedical and Environmental Monitoring, *Anal. Bioanal. Chem.* **2004**, *378*, 1700-1703.

(10) Nichols, K. P.; Ferullo, J. R.; Baeumner, A. J., Recirculating, passive micromixer with a novel sawtooth structure, *Lab Chip* **2006**, *6*, 242-246.

(11) Paik, P.; Pamula, V. K.; Fair, R. B., Rapid droplet mixers for digital microfluidic systems, *Lab Chip* **2003**, *3*, 253-259.

(12) Urbanski, J. P.; Thies, W.; Rhodes, C.; Amarasinghe, S.; Thorsen, T., Digital microfluidics using soft lithography, *Lab Chip* **2006**, *6*, 96-104.

(13) Nichols, K. P.; Gardeniers, H. J. G. E., A digital microfluidic system for the investigation of pre-steady-state enzyme kinetics using rapid quenching with MALDI-TOF mass spectrometry, *Anal. Chem.* **2007**, *79*, 8699-8704.

(14) Fair, R. B., Digital microfluidics: Is a true lab-on-a-chip possible?, *Microfluidics and Nanofluidics* **2007**, *3*, 245-281.

(15) Tice, J. D.; Song, H.; Lyon, A. D.; Ismagilov, R. F., Formation of droplets and mixing in multiphase microfluidics at low values of the Reynolds and the capillary numbers, *Langmuir* **2003**, *19*, 9127-9133.

(16) Song, H.; Chen, D. L.; Ismagilov, R. F., Reactions in droplets in microflulidic channels, *Angew. Chem., Int. Ed.* **2006**, *45*, 7336-7356.

(17) Huebner, A.; Sharma, S.; Srisa-Art, M.; Hollfelder, F.; Edel, J. B.; Demello, A. J., Microdroplets: A sea of applications?, *Lab Chip* **2008**, *8*, 1244-1254.

(18) Grigoriev, R. O.; Schatz, M. F.; Sharma, V., Chaotic mixing in microdroplets, *Lab Chip* **2006**, *6*, 1369-1372.

(19) Jones, T. B.; Wang, K. L.; Yao, D. J., Frequency-dependent electromechanics of aqueous liquids: Electrowetting and dielectrophoresis, *Langmuir* **2004**, *20*, 2813-2818.

(20) Ahmed, R.; Jones, T. B., Optimized liquid DEP droplet dispensing, *Journal of Micromechanics and Microengineering* **2007**, *17*, 1052-1058.

(21) Ahmed, R.; Jones, T. B., Dispensing picoliter droplets on substrates using dielectrophoresis, *Journal of Electrostatics* **2006**, *64*, 543-549.

(22) Mugele, F.; Baret, J. C., Electrowetting: From Basics to Applications, *Journal of Physics-Condensed Matter* **2005**, *17*, R705-R774.

(23) Saeki, F.; Baum, J.; Moon, H.; Yoon, J. Y.; Kim, C. J.; Garrell, R. L., Electrowetting on Dielectrics: Reducing Voltage Requirements for Microfluidics., *Abstracts of Papers of the American Chemical Society* **2001**, *222*, U341-U341.

(24) Chatterjee, D.; Hetayothin, B.; Wheeler, A. R.; King, D. J.; Garrell, R. L., Droplet-based microfluidics with nonaqueous solvents and solutions, *Lab Chip* **2006**, *6*, 199-206.

(25) Paik, P.; Pamula, V. K.; Pollack, M. G.; Fair, R. B., Electrowetting-based droplet mixers for microfluidic systems, *Lab Chip* **2003**, *3*, 28-33.

(26) Nichols, K. P.; Gardeniers, J. G. E. In *Proceedings of MicroTAS 2006*, 2006, pp 582-584.

(27) Zhang, Z. Y.; Palfey, B. A.; Wu, L.; Zhao, Y., Catalytic function of the conserved hydroxyl group in the protein tyrosine phosphatase signature motif, *Biochemistry* **1995**, *34*, 16389-16396.

(28) Bender, M.; Kezdy, F.; Wedler, F., Alpha-chymotrypsin: enzyme concentration and kinetics, *J. Chem. Educ.* **1967**, *44*, 84-88.

(29) Feng, J. Q., Electrohydrodynamic behaviour of a drop subjected to a steady uniform electric field at finite electric Reynolds number, *Proceedings of the Royal Society of London Series a-Mathematical Physical and Engineering Sciences* **1999**, *455*, 2245-2269.

(30) Taylor, G., Studies in Electrohydrodynamics I. Circulation Produced in a Drop by an Electric Field, *Proceedings of the Royal Society of London Series a-Mathematical and Physical Sciences* **1966**, *291*, 159.

(31) Melcher, J. R., Traveling-Wave Induced Electroconvection, *Phys. Fluids* **1966**, *9*, 1548.

(32) Melcher, J. R.; Taylor, G. I., Electrohydrodynamics - a Review of Role of Interfacial Shear Stresses, *Annual Review of Fluid Mechanics* **1969**, *1*, 111.

(33) Saville, D. A., Electrohydrodynamics: The Taylor-Melcher Leaky Dielectric Model, *Annual Review of Fluid Mechanics* **1997**, *29*, 27-64.

(34) El Moctar, A. O.; Aubry, N.; Batton, J., Electro-Hydrodynamic Micro-Fluidic Mixer, *Houille Blanche-Revue Internationale De L Eau* **2006**, 31-37.

Chapter 3

Optimization of Electrohydrodynamic Mixing in a Digital Microfluidic System

Optimal frequencies for electrohydrodynamic (EHD) mixing in electrowetting on dielectric (EWOD) and open air based digital microfluidic systems were determined. 1 µl liquid droplets can be mixed in approximately 100 ms when actuated at 500 Hz, 250 V_{RMS}. This represents a decrease of one order of magnitude for this liquid volume compared to previously reported digital microfluidic mixers. As tested, the device exhibits an approximately linear increase in efficiency up to 2250 Hz. From 2250 Hz to 50000 Hz, mixing is inhibited. Above 50000 Hz this inhibition diminishes. This chapter gives a qualitative description of the mixing; experimentally determined optimal actuation frequencies; a simple computational fluid dynamics (CFD) model that qualitatively duplicates the observed flow patterns, and can be used for scaling analysis; and, it provides a brief overview of the current published models of such mixing.

Portions of this chapter were published in:
Nichols, K. P.; Gardeniers, H. J. G. E. In *Proceedings of MicroTAS 2006*, 2006, pp. 582-584.

Introduction

Mixing in the closed channels of traditional, continuous flow, microfluidic systems presents numerous challenges due to the low Reynolds numbers typically involved.[1] Similar problems exist in digital microfluidic chips where liquid droplets are individually manipulated on a specially designed surface, instead of in closed channels. Most digital microfluidic systems utilize electrowetting on dielectric (EWOD) effects for droplet actuation.[2-9] EWOD devices require a planar electrode covered by a hydrophobic dielectric film, above which droplet actuation occurs. Reversible droplet actuation typically requires a ground plane integrated on a cover above the droplet. Upon application of a sufficient voltage, the charge imbalance at the liquid-dielectric interface results in an electrochemical (Coulombic) force that causes a change in contact angle, and subsequent droplet movement.

At low frequencies (under 2250 Hz), aqueous droplets placed over a micron-scale interelectrode gap will exhibit mixing in each of the four quadrants of the droplet.[10] This chapter gives a qualitative description of the mixing; experimentally determined optimal actuation frequencies; a simple computational fluid dynamics (CFD) model that qualitatively duplicates the observed flow patterns and can be used for scaling analysis; and, it provides a brief overview of the current published models of such mixing.

While mixing in continuous flow microfluidics is a mature field, with a wide variety of mixer types proposed, tested, and in use,[1] digital microfluidic mixing is not as fully developed. Paik *et al.* have described a pattern of droplet actuation across an electrode array designed to optimize mixing behavior in EWOD digital microfluidic systems. The pattern moves droplets either back and forth, or across several electrodes. The droplet then folds over itself, bringing into contact fluidic elements that were previously separated. The Paik *et al.* system, currently the best published system for µl scale droplet mixing in EWOD devices,

can mix 1 µl droplets in approximately 2 seconds.[3, 4] In this chapter we demonstrate that optimized electrohydrodynamic (EHD) mixing can decrease this time by an order of magnitude.

Experimental

Empirical Optimization

Using a high-speed camera system, we have demonstrated that a standard EWOD system, when operated under the conditions presented in this chapter, is capable of mixing 1 µl droplets in 0.1 second, a reduction of more than one order of magnitude compared to mixing times previously reported using non-optimized conditions. Further, the device is tolerant of salt concentrations from $0.5 \cdot 10^{-5}$ M to 1 M, and does not exhibit measurable Joule heating when operated at its recommended parameters of 500 Hz, 250 V_{RMS}.

Two electrode patterns were tested: square electrodes, and an Archimedean spiral electrode pattern. The square electrodes were each 1.0 mm, with 50 µm gaps between them. The Archimedean spiral electrodes had line widths of 40 µm, inter-electrode gaps of 50 µm, and a total footprint of 1.0 mm. The electrodes were fabricated on Pyrex wafers, and metalized using a sputtered 20 nm Cr adhesion layer and a 200 nm Au thin film. Standard photolithography techniques were employed to produce a photoresist etch mask. A 4 µm SU-8 (MicroChem, USA) dielectric layer and a 1 µm Teflon AF (DuPont, USA) hydrophobic layer covered the electrodes. For experiments designed to test the device's compatibility with existing EWOD systems, an ITO coated glass lid was supported using silicon wafers of varying thicknesses.

Two reactions were analyzed to determine mixing behavior. First, the mixing of 1 µl droplets of 10^{-5} M fluorescein (Sigma, USA) with 1 µl DI water droplets was analyzed, to allow streamlines to be followed throughout the entire

mixing process. Second, the mixing of 1 µl droplets of 10^{-5} M fluorescein with 1 µl droplets of 1 M acetic acid (Sigma, USA) was analyzed to determine accurate mixing times. Side views were unnecessary, since the pH dependency of fluorescein fluorescence eliminated the possibility of unmixed regions being hidden by mixed regions above them; if one level (in the z direction) of the device is not mixed, this will be visible.

A standard signal generator and a Krohn-Hite 7602M (Krohn-Hite Corporation, USA) amplifier operating at 250 V_{RMS} generated AC voltages with frequencies ranging from 1 Hz to 300 kHz actuated the droplets.

Mixing efficiency was analyzed using a HI-CAM high-speed video camera (Lambert Instruments, The Netherlands). We used a gated, intensified, high-speed camera with a maximum frame rate of 1825 fps. An image intensifier was required since fluorescent droplets were analyzed to determine mixing times. Videos were analyzed using MATLAB 7.1 (MathWorks, USA) to determine the mean gradient of the variance as a function of time. For a given frequency, a time constant τ was defined as the point at which 63% of the final gradient (see Ch. 2, pg. 29) was reached. Droplets were combined under air, and also under octane (Sigma, USA) to decrease the standard deviation of τ due to occasional droplets sticking to the substrate when actuated in air. The mean τ for experiments conducted in air fell within one standard deviation of the mean for experiments conducted in octane. Highly efficient mixing (approximately 100 ms τ for 1 µL) was demonstrated in segments of the DC to 2250 Hz regime. The 500 Hz column of Figure 1 clearly indicates that rapid homogenization is possible at these frequencies. We confirmed that mixing was homogenous, and that we were not merely seeing a composite of all levels, by also testing the mixing time of fluorescein with acetic acid, which will inhibit fluorescence on mixing. If mixing is incomplete in any level of the droplet, fluorescence from that level will show through the otherwise transparent droplet. Observed τ were not significantly higher between the two sets of measurements. Analysis of the videos shows that

mixing in this frequency regime appears to be the result of spiraling fluid flow originating at the center of the droplet, moving outwards, curving around the droplet wall, and returning to the center of the droplet.

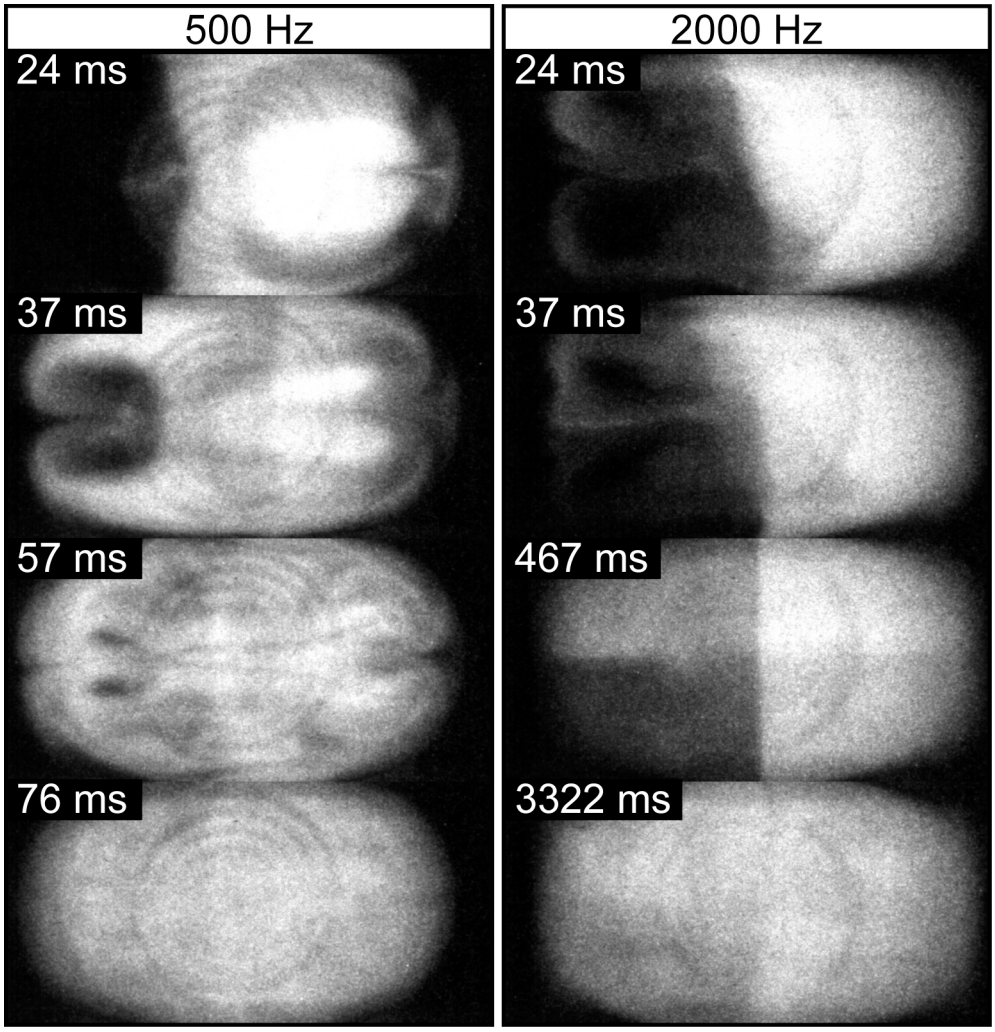

Figure 1 – Representative images from videos of mixing behavior at 500 Hz (left), and 2000s Hz (right). Mixing at 500 Hz appears to be the result of spiraling fluid flow originating at the center of the droplet, moving outwards, curving around the droplet wall, and returning to the center of the droplet.

Relatively inefficient mixing was found in the 2250 Hz to 50000 Hz frequency regime. A representative example from this regime is shown in the 2000 Hz column of Figure 1. In the 467 ms image, distinguishable concentration variations are clearly visible.

Figure 2 shows the effect of frequency on τ for three sets of experiments using the two electrode designs described above. There are three regimes of interest in Figure 2. In the first regime, extending from DC to 2250 Hz, τ decreases linearly with increasing frequency under all experimental conditions. In the second regime, from 2250 Hz to 50000 Hz, there is significant increase in τ. In the third regime, above 50000 Hz, the τ in the spiral electrode device achieves an efficiency approximately two times greater than that achieved in the low frequency regime, while the τ in the square electrode device does not significantly recover.

Above 50000 Hz, significant current was measured passing through the system. This is the only regime where electrode shape effects mixing. Figure 2 shows the great differences in mixing efficiency between the spiral and square electrode mixer that are induced at such frequencies.

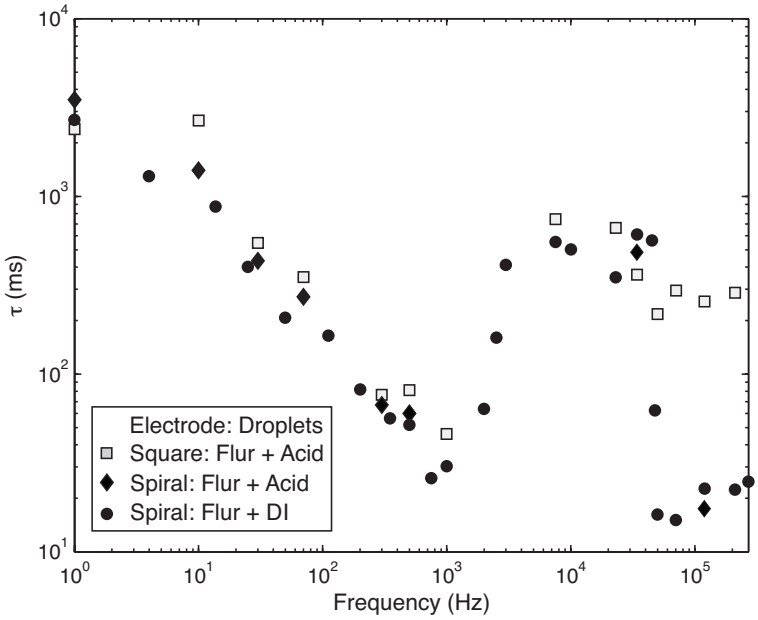

Figure 2 – Mixing obtained by high-speed image analysis of the mixing of 1 µl of 10^{-4} M fluorescein with 1 µl of DI water, and the mixing of 1 µl of 10^{-4} M fluorescein with 1 µl of 1 M acetic acid. τ is defined as the point at which 63% of mixing is complete.

EWOD digital microfluidic devices typically employ a lid. Since mixing under the conditions described above occurs as a result of shear stresses balanced at the droplet interface, mixing will be least inhibited when operated without a lid. However, using a lid, we were able to achieve mixing at the same rate, provided the gap height was large enough to prevent excessive pinning, which under our conditions was found to be 750 µm. Apart from the absence of a lid, the device as tested is constructed in the same manner as previously reported EWOD digital microfluidic devices. While EWOD devices typically use DC signals to manipulate droplets, an AC signal could be applied to a dedicated mixing component without difficulty.

Varying the KCl concentration from $0.5 \cdot 10^{-5}$ M to 1 M does not significantly affect mixing time when mixing 1 µL droplets of KCl with 1 µL droplets of DI water. For broad compatibility with a wide variety of chemical and biochemical reactions, this is a critical tolerance.

Additionally, at the recommended mixing parameters, 500 Hz, 250 V_{RMS}, no measurable Joule heating occurs. Droplets were left on the device (without a lid) and continuously mixed until no visible liquid remained. No significant difference was observed for mixing at 500 Hz, 250 V_{RMS} and droplets left on the device without the application of any external potential.

Mixing Theory and Modeling

A number of physical mechanisms have been proposed to account for mixing effects described in this chapter. To briefly summarize the current theoretical framework: in a recent *Langmuir* letter, Ko, Lee, and Kang summarized the current state of the theoretical modeling of such flows as such, "Flows in electrowetting have very important consequences. They can be beneficially utilized to enhance mixing of fluids… However, the details and origin of such hydrodynamic flows are still not understood very well. It is even unclear whether the flows are truly generated purely by the oscillation of the interface, or in combination with electrohydrodynamic effects."[11]

Davoust *et al.* have proposed that Taylor-Melcher type electrohydrodynamic effects are entirely responsible for the flow patterns discussed in this chapter. They propose that EHD stresses and shear stresses are balanced at the droplet interface, resulting in convective flows when the droplet shape deviates from a hemisphere, as it does in both of the electrode configurations tested.[12, 13]

Earlier work by Green *et al*. attributed most of the flow to a combination of dielectrophoresis and thermal effects: "The high electrical fields, which are required to produce sufficient force to move a particle, result in heat dissipation in the medium. This in turn produces thermal gradients, which may give rise to fluid motion through buoyancy, and electrothermal forces." However, at the frequencies suggested in our device, we observed no temperature increase. Further, since water remains highly polarizable up to microwave frequencies, and will exhibit positive dielectrophoresis throughout the frequency range, it is unlikely that this was the primary cause of fluid flow in our system, due to the trough at 10^3 Hz (Figure 2). Additionally, since dielectric responses are relaxation phenomena, the onset of diminished mixing near 2 kHz and the return to good mixing at ~50 kHz occur too rapidly with changes in frequency to be explainable by dielectric responses alone.

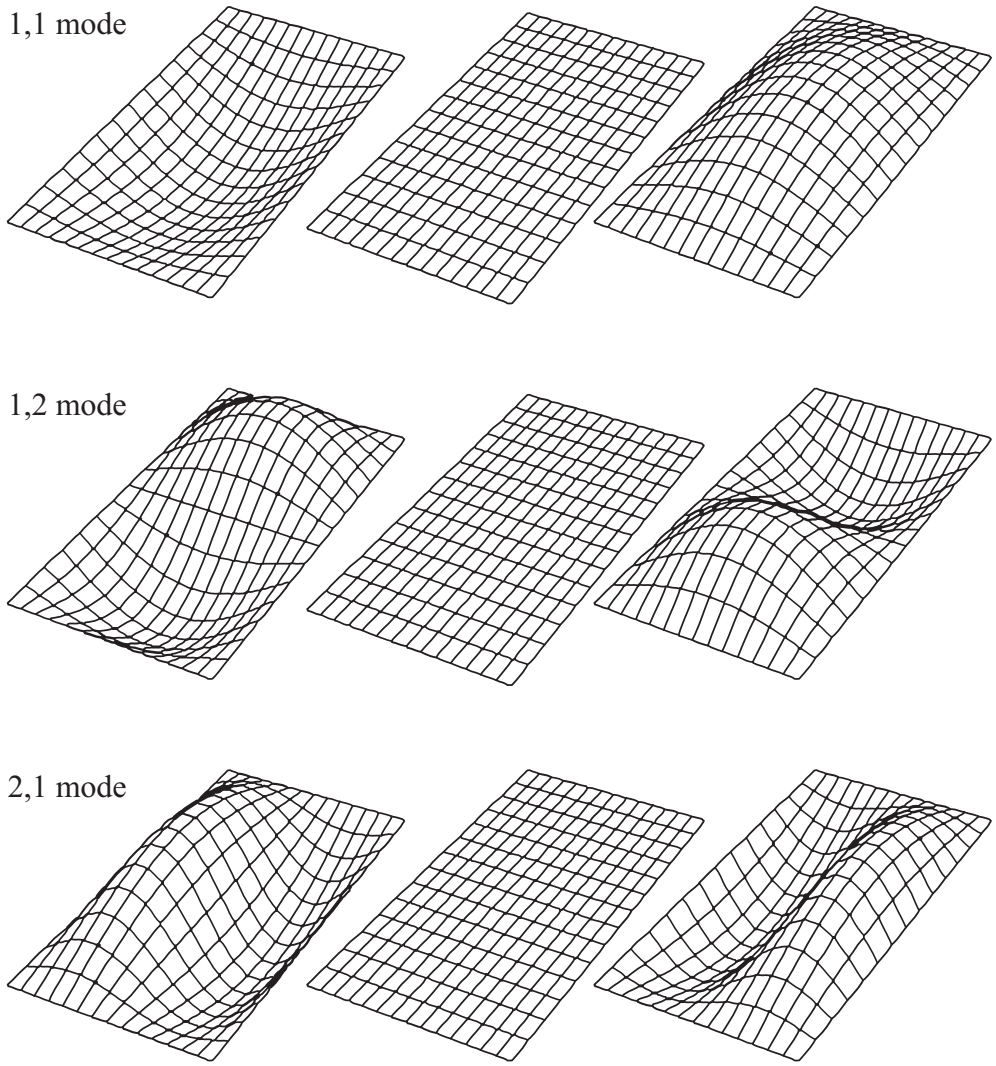

Figure 3 – Vibrational modes of a rectangular mesh. This image shows the 1,1; 1,2; and 2,1 vibrational modes. Qualitatively, there are similarities to the quadrants shown in Figure 2. Adapted from animations provided by Dr. Dan Russel, Kettering University.

It is also possible that the behavior shown in Figure 1 is due to overlaying acoustical resonance effects, such as a superposition of the 1,1; 2,1; and 2,2 resonant modes shown in Figure 3. These modes would be expected above the low frequency cut-off of acoustic resonance, with the excitation of additional modes occurring with increasing frequency until an eventual cutoff frequency. However, if this is in fact the cause, why the cutoff is so dramatic is not understood.

Computational Fluid Dynamics (CFD) Model

In the absence of a single model to describe the system, we constructed a simple computational fluid dynamics simulation with a hemispherical aqueous droplet, where each quadrant of the droplet rotates about the line from the origin to the central point of the quadrant – the four lines from $(r, \theta, \varphi) = (0,0,0)$ to $(r, \frac{1}{4}\pi, \frac{\pi}{4})$; $(r, \frac{3}{4}\pi, \frac{\pi}{4})$; $(r, \frac{5}{4}\pi, \frac{\pi}{4})$ and $(r, \frac{7}{4}\pi, \frac{\pi}{4})$ – in the appropriate directions and rotational speed as experimentally determined. The vector field of only the rotating wall is as shown in Figure 4.

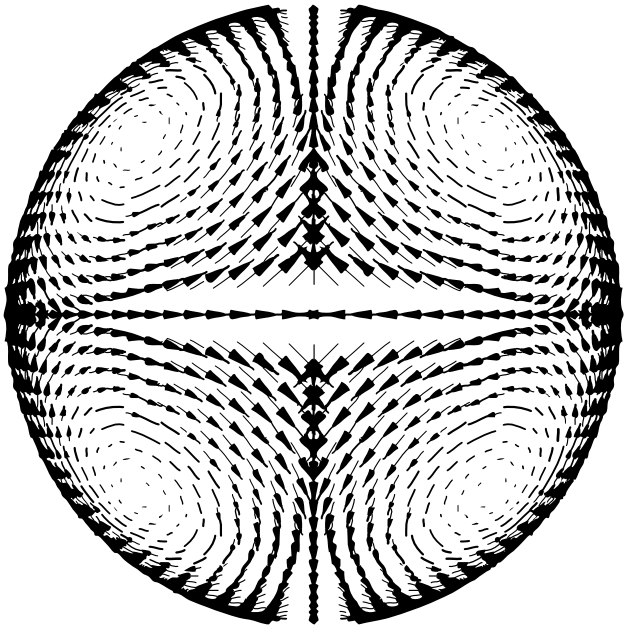

Figure 4 – Vector Fields resulting from the rotation of the four droplet quadrants.

This approximation was based on the single characteristic that most of the models discussed above possess: at the air/liquid interface, shear stresses are balanced through rotational flows. Oscillation and flows originating inside the droplet were not modeled. A full model, incorporating the known electric fields, would of course be more useful, as it would allow the design of optimized electrodes.

Ko *et al.* investigated the hydrodynamic flow patterns inside a droplet under various AC electrowetting conditions. While they were not able to construct a single, unified model to describe the various flow regimes, they did make a number of qualitative conclusions. In general, their observations are similar to those we made, though they identified slightly different frequency cutoffs for what were refer to as the "no mixing" regime.

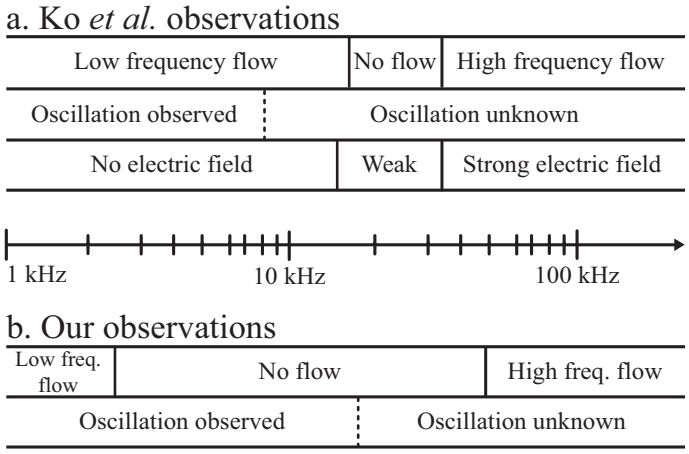

Figure 5 – Comparison of flow regimes as observed by a.) Ko *et al.*[11], and b.) in our work. Both sets of observations show three distinct flow regimes. The three regimes in our work are noticeable as the areas of fast mixing, slow mixing, and fast mixing again at the various frequencies investigated in Figure 2.

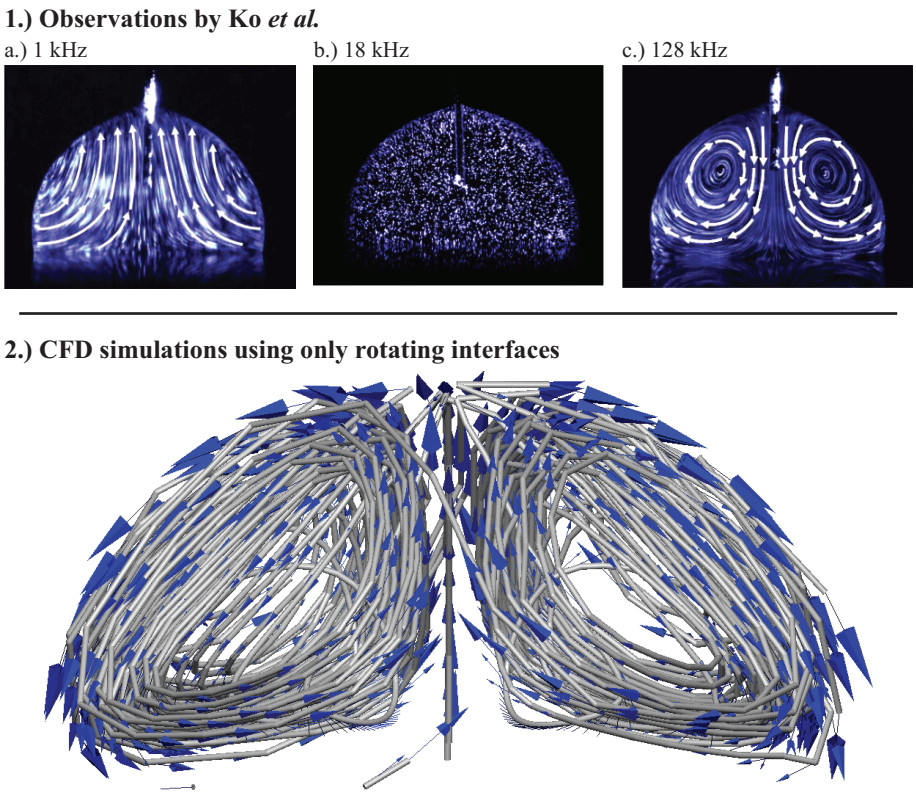

Figure 6 – Comparison of observed hydrodynamic flows in electrowetting behavior 1.) by Ko *et al.*[11] (photographs used with permission of the American Chemical Society) and 2.) our CFD simulations using rotating walls. The CFD simulation is qualitatively similar, and was found to be useful to describe scaling properties of the system.

Qualitatively, the CFD simulation (streamlines shown in Figure 6.2) appears to match well with observed results, and should at least be useful for analyzing the scaling properties of the system. Compare, for example, the flow patterns shown in Figure 6.1.a. at 1 kHz with the CFD results.

Diffusion of model proteins was also simulated to determine mixing times for the numerically calculated flow patterns. Example mixing times, as determined using this method, are shown in Figure 7.

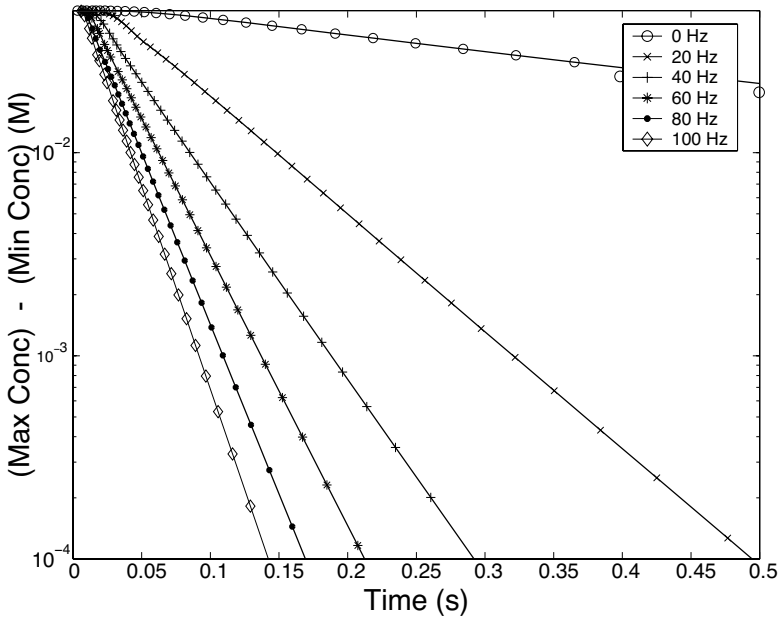

Figure 7 – Protein concentration range (max – min) as a function of time. Two droplets are combined, one with an enzyme with a diffusivity of 1E−7 m^2 s^{-1}, and one of DI water. As mixing nears completion, the difference between the volumetric element with the highest enzyme concentration and the lowest enzyme concentrations approaches zero.

Conclusions

For digital microfluidic systems intended to actuate volumes in the microliter range, the technique presented in this chapter represents the most efficient mixing method yet developed. While volumes lower than the microliter range can be mixed in shorter timeframes, there are a variety of applications where nanoliter volumes are simply too low to be manageable using the interconnections currently available, or for which nanoliter volumes do not produce sufficient product volumes. The device presented in this chapter is broadly applicable in a variety of microliter scale digital microfluidic devices, owing to its absence of measurable Joule heating, and its tolerance of a wide range of salt concentrations.

Acknowledgements

The technology program of the Ministry of Economic Affairs of The Netherlands (project no. 6626) and the Technology Foundation STW, the applied science division of the NWO, financially supported this research.

References

(1) Nguyen, N. T.; Wu, Z. G., Micromixers - a review, *Journal of Micromechanics and Microengineering* **2005**, *15*, R1-R16.

(2) Fair, R. B., Digital microfluidics: Is a true lab-on-a-chip possible?, *Microfluidics and Nanofluidics* **2007**, *3*, 245-281.

(3) Paik, P.; Pamula, V. K.; Pollack, M. G.; Fair, R. B., Electrowetting-based droplet mixers for microfluidic systems, *Lab Chip* **2003**, *3*, 28-33.

(4) Paik, P.; Pamula, V. K.; Fair, R. B., Rapid droplet mixers for digital microfluidic systems, *Lab Chip* **2003**, *3*, 253-259.

(5) Wheeler, A. R.; Moon, H.; Bird, C. A.; Loo, R. R. O.; Kim, C. J.; Loo, J. A.; Garrell, R. L., Digital Microfluidics with in-Line Sample Purification for Proteomics Analyses with MALDI-MS, *Anal. Chem.* **2005**, *77*, 534-540.

(6) Chatterjee, D.; Hetayothin, B.; Wheeler, A. R.; King, D. J.; Garrell, R. L., Droplet-based microfluidics with nonaqueous solvents and solutions, *Lab Chip* **2006**, *6*, 199-206.

(7) Mugele, F.; Baret, J. C., Electrowetting: From Basics to Applications, *Journal of Physics-Condensed Matter* **2005**, *17*, R705-R774.

(8) Mugele, F.; Baret, J. C.; Steinhauser, D., Microfluidic mixing through electrowetting-induced droplet oscillations, *Appl. Phys. Lett.* **2006**, *88*, 204106.

(9) Moon, H.; Wheeler, A. R.; Garrell, R. L.; Loo, J. A.; Kim, C. J., An integrated digital microfluidic chip for multiplexed proteomic sample preparation and analysis by MALDI-MS, *Lab Chip* **2006**, *6*, 1213-1219.

(10) Nichols, K. P.; Gardeniers, H. J. G. E., A digital microfluidic system for the investigation of pre-steady-state enzyme kinetics using rapid quenching with MALDI-TOF mass spectrometry, *Anal. Chem.* **2007**, *79*, 8699-8704.

(11) Ko, S. H.; Lee, H.; Kang, K. H., Hydrodynamic flows in electrowetting, *Langmuir* **2008**, *24*, 1094-1101.

(12) Fouillet, Y.; Jary, D.; Brachet, A. G.; Berthier, J.; Blervaque, R.; Davous, L.; Roux, J. M.; Achard, J. L.; Peponnet, C., Limerick, Ireland 2006.

(13) L. Davoust, Y. F., Y. Ishida In *MicroTAS 2007*: Paris, France, 2007.

Chapter 4

A Digital Nanofluidic System Using Nanochannels in SU-8 with floor and ceiling metal electrodes and integrated microchannels

Sacrificially etched 2-D nanofluidic channels and nanospaces with integrated floor and ceiling electrodes and arbitrary channel geometries have been demonstrated with channel heights from 20 nm to 400 nm, widths from 800 nm to 40 μm, and lengths up to 3 mm, using SU-8 as the channel structural material. The system was investigated for use as a digital nanofluidic system analogous to the previously described digital microfluidic system, though heat dissipation in the system was not great enough to permit its use with enzymes.

Portions of this chapter were published in:
1) Nichols, K. P.; Eijkel, J. C. T.; Gardeniers, H. J. G. E. *Lab Chip* 2008, *8*, 173-175.
2) Nichols, K. P.; Eijkel, J. C. T.; Gardeniers, J. G. E. In *Proceedings of MicroTAS 2007*, 2007, pp. 982-984

Introduction

In Chapter 2, we described a digital microfluidic system that sequentially combined liquid droplets at well-defined time intervals for the purpose of obtaining enzyme kinetic data. In this chapter, we describe an attempt to further miniaturize this system into a nanofluidic system. While heat generation during operation was too high to use the device as intended, it nonetheless represents an interesting fabrication technique that may be useful elsewhere.

Nanochannels are channels with at least one dimension in the nanometer range.[1] A variety of top-down and bottom-up approaches for nanochannel fabrication have been reported.[1-6] Here, we present a technique for the fabrication of nanochannels and nanospaces in SU-8, a commonly used, photo-definable epoxy for MEMS devices, with integrated floor and ceiling electrodes.

Much attention has been focused on the benefits of using very small working electrodes in electrochemical systems, where electron transfer to the electrode surface is less likely to be limited by mass transport.[7-9] Further applications for integrated electrodes in nanochannels may include surface functionalization with DNA and proteins,[10, 11] fluidic control in nanochannels,[12] surface enhanced Raman scattering (SERS),[13-15] and single molecule studies[16] of large molecules such as DNA.

Adhesion of the metal layers in a nanochannel system with floor and ceiling electrodes is a significant problem that we have demonstrated can be overcome using SU-8 or SU-8 3000. Additionally, utilizing SU-8 allows for direct integration with SU-8 based MEMS and microfluidics; simple patterning of interconnections due to the photo-definable nature of SU-8;[17] sufficiently thick channel roofs to prevent bending due to capillarity induced negative pressure, as has previously been problematic;[18] and arbitrary nanochannel geometries due to the conformal nature of SU-8 dispensing.

Nanochannels have previously demonstrated utility in fundamental studies of liquid behavior,[19] single molecule analysis,[19-22] single cell analysis,[20] and in other studies where surface phenomena dominate over bulk phenomena.[2]

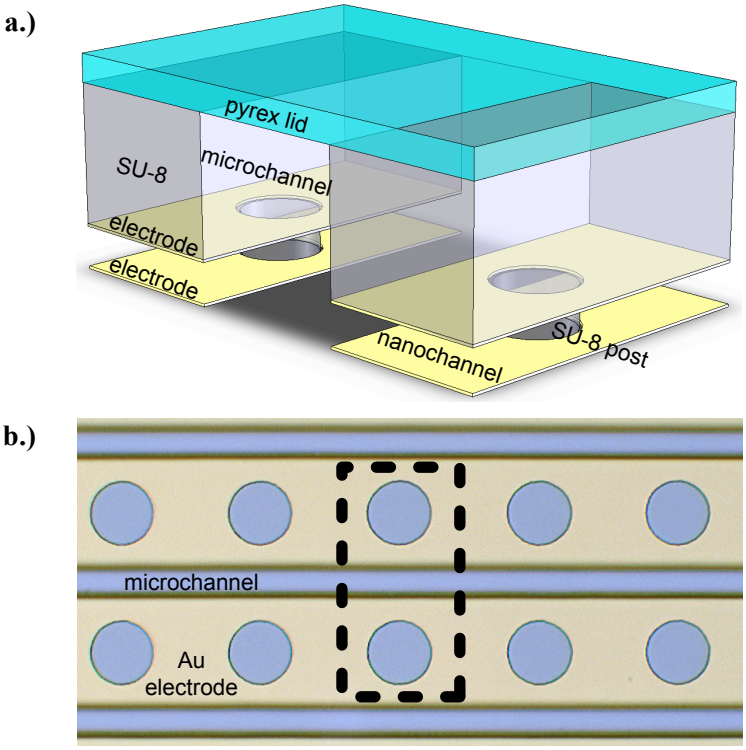

Figure 1 – a.) a drawing of a glass covered (plate on top) SU-8 microchannel (center of drawing, SU-8 shown by rectangles and pillars), and nanochannels (gaps under SU-8 walls) with Au electrodes (not to scale). The circles in the electrode layers allow posts of SU-8 to support the structure. b.) a micrograph of such a system viewed from above, with the area shown in the top image indicated by the dashed line. The electrode layer is in focus.

Experimental

Nanochannel Fabrication

Fabrication of the device followed standard photolithography procedures. A sequence of metal layers was deposited on a substrate such that the bottom and top layers were usable as electrodes, and the middle layer could be sacrificially removed without affecting the electrode layers. The substrate was then coated with SU-8 (Microchem, USA) to provide the lid of the nanochannel along with fluidic inlets and outlets. Finally, the sacrificial layer was removed. Since the nanochannel structural material is SU-8, if this is patterned, microchannels or reservoirs can be directly included. If a lid for these microchannels is required, glass or PDMS can be easily bonded. Simple nanochannels without electrodes were also constructed using only a patterned sacrificial layer.

An overview of a wet-etching protocol is presented in Figure 2, and a detailed protocol for ion beam etching is given at the end of the chapter. In step 1, the top and bottom electrode were defined on a Si substrate, along with the sacrificial layer between the electrodes. Metallization was accomplished using a custom built sputtering tool, though most common metallization tools should produce equivalent results. Metal stacks were deposited without breaking vacuum. A wide variety of electrode/sacrificial layers are possible (Table 1). As an example, the channels in Figure 1 were fabricated using a stack of Ta/Au/Cr/Au with heights of 20 nm / 100 nm / 100 nm / 100 nm deposited by sputtering. For galvanically coupled metals, care should be taken to design the photoresist masks to minimize total etched area, since underetching will be significantly accelerated if large metal areas are exposed. Additionally, the top and bottom metal layers must be underetched relative to the sacrificial layer, to prevent short circuits. Previous work has demonstrated good adhesion of SU-8 to a variety of metal layers.[21]

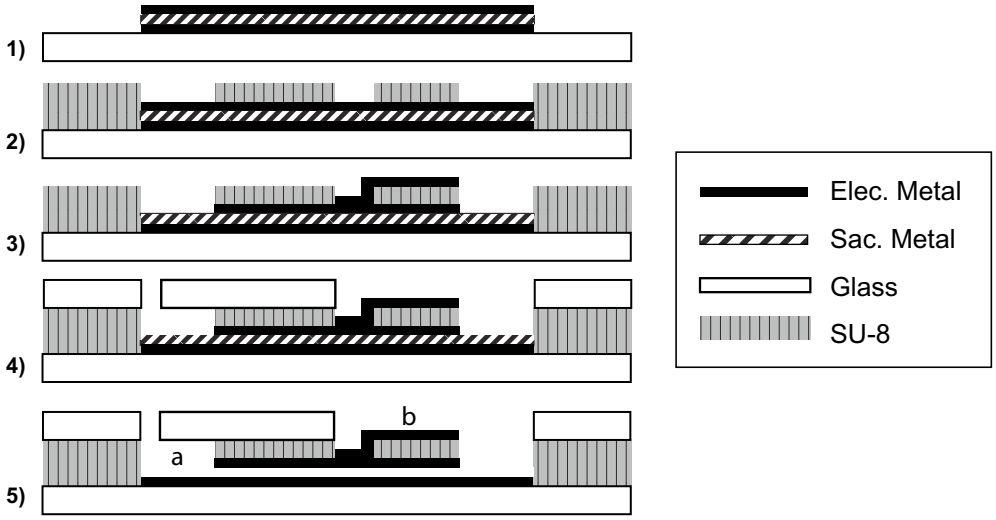

Figure 2 – Process for SU-8 Nanofluidic Channel with Top/Bottom Electrodes and Integrated Microchannels – 1) Top electrode, bottom electrode (black, solid) and sacrificial layer (thick black slanted line) patterned. 2) SU-8 (gray, vertical black lines) patterned with microchannels and electrode access holes/vias. 3) Metal layer sputtered for contact pads and contact with top electrode. 4) Patterned glass or PDMS bonded to structural SU-8 5) Sacrificial layer removed. (a) represents a microchannel (running into the plane) or a contact pad for the bottom electrode, (b) represents the top electrode contact pad. The bottom electrode contact pad and the microchannels are shown colocated, though this is not necessary. The via to the left of (b) must be small enough at the bottom such that the metal membrane will not significantly deflect, or an additional layer of SU-8 must be used as a structural support.

In step 2, a single layer of SU-8 was dispensed to a thickness of 15 μm and patterned to create microfluidic channels and access to the top and bottom electrodes. Standard manufacturer recommended processing (Microchem, USA) was used.

In step 3, an additional metal layer was sputtered and patterned to create contact pads and electrical contacts with the top electrode. This layer should be

sputtered at a pressure sufficient to ensure good step coverage. We obtained sufficient step coverage at $1 \cdot 10^{-2}$ bar. Ideally, this via should be small enough at the bottom such that insignificant deflection of the metal membrane occurs, and no additional support is needed. However, this requires careful tuning specific to the device, equipment, and surface reflectivity. If not initially practical, an additional SU-8 layer can be used to support the thin metal membrane.

In step 4, the microchannels that connect to the nanochannels are sealed using a patterned glass or PDMS lid. Standard PDMS processing can be used for PDMS lids. For glass lids, holes were etched using powder blasting, and bonding was achieved using a simple office laminator set to 150 °C. Interconnections with glass and PDMS lids have been well documented elsewhere.

Before sacrificial etching, it is important to once again expose and bake the SU-8 device for at least three times the recommended exposure time. For short channels that require minutes to hours of etching, this is less critical.

In step 5, the sacrificial layer was removed. Cr was etched in BASF Selectipur Chromium Etch, an ammonium cerium (IV) nitrate based etchant. Au was etched in $KI:I_2:DI = 4:1:40$. Etching within channels is limited by diffusion, and thus will be highly dependent on device geometry. Certain metal combinations will result in galvanic coupling that will significantly affect etch rates.[22, 23] Calibration for a specific system is possible by monitoring the impedance across the electrodes, as the etch proceeds.

We achieved equivalent results with SU-8, and the newer SU-8 3000 series, a version of SU-8 formulated in a solvent specifically designed to improve adhesion. The major difference was in yield; SU-8 3000 was far less sensitive to fouling of the metal surfaces. SU-8 2000 was not investigated.

Integration with Microfluidic Channels

Since the nanochannel structural material is SU-8, microchannels can be patterned in a single lithographic step. A variety of alternative designs could easily be constructed, such as interdigitated microchannels with nanochannels connecting the two sides. A lid can be attached to the SU-8 microchannels by bonding a patterned piece of glass[24] or PDMS.[25]

The ability to easily integrate microchannels in a single lithographic step is an important feature of the design. Connections from the macro world to the micro world already present many complications. Attempting to connect directly from the macro world to a nanofluidic system is only possible under a limited set of circumstances.

Bonding of a glass lid to a single layer SU-8 microchannel is trivial, with a number of examples reported.[24, 26, 27] In general, all that is needed is a slight amount of heat and pressure. PDMS can also be used as a lid, simply by applying pressure from above. For example, an uncured layer of PDMS will form a tight seal with an SU-8 microchannel[28] that can be strengthened if clamped underneath a glass coverslip. Bonding multiple SU-8 layers together to form an encapsulated microchannel entirely of SU-8 can be problematic, due to non-uniform film thicknesses. Methods have been proposed to overcome this, [24, 27, 29, 30] though we experienced significant difficulty replicating them.

Channel Geometries

Simple electrode geometries with planar channels can be constructed in a single lithography step. More complicated geometries require an additional step to define the electrodes/channel independently. For example, a channel with 3D grooves could be constructed using two steps instead of the single step shown in Figure 2, step 1. Any arbitrary structure that can be lithographically patterned can be used to define the nanochannels.

Nanochannels with widths from 800 nm to 40 microns were fabricated. Channels with widths below 1 micron can be fabricated using e-beam lithography, or more advanced photolithography techniques. Channels with widths above 40 microns should be avoided due to channel collapse. For wide structures, pillars may be placed every 40 microns or less to extend the device's width (Figure 1). Channels with heights from 20 nm to 400 nm were fabricated.

Stability of SU-8 in Various Etchants

SU-8 is a highly functionalized epoxy; removal typically requires harsh etchants or plasma treatments.[31] Nonetheless, some slow dissolution will occur. To measure these slow etch rates, a thick grid pattern was fabricated on an SU-8 surface. For Au etchant testing and Cr etchant testing, a 1 μm thick Pyrex mask was sputtered using a Nordiko NM2000 (Nordiko, UK) onto an unpatterned, fully crosslinked SU-8 substrate, and was subsequently patterned in BHF using a Cr mask. For BHF testing, a 500 nm Cr mask was sputtered using a custom sputtering tool. Subsequently, etching experiments were conducted, the mask was removed, and an AFM scan (Digital Instruments Nanoscope III, Veeco, USA) was used to determine the relative SU-8 height before and after etching. Testing as described above revealed SU-8 etch rates in BASF Selectipur Chromium Etch to be less than 2 nm / day, and in BHF to be less than 1 nm / day. SU-8 etch rates in $KI:I_2:DI = 4:1:40$ (Au etchant) were too low to be measurable. It is important to note that this testing is only valid for SU-8 that has been cross linked far in excess of the recommended exposure times. High resolution is still achievable in these substrates however, as the resist can be exposed normally, developed, and then reexposed to improve cross-linking.

Table 1 - Compatibility of structural materials, sacrificial layers, and electrode layers. A "+" symbol indicates inertness in the indicated etch solution. A "-" symbol indicates either dissolution or pitting, except for Cu in Au etch, which forms solid CuI. For example, a channel could be constructed in SU-8 using Ta electrodes, and an Au sacrificial layer.

	SU-8	*Pyrex*	*Cr*	*Au*	*Ti*	*Ti/W*	*ITO*	*Pt*	*Cu*	*Ta*
"Cr Etch" [a]	+	+	-	+	-	-	-	+	-	+
"Au Etch" [b]	+	+	+	-	+	+	+	+	-	+
BHF	+	-	+	+	-	-	-	+	+	-

[a] *"Cr etch" is BASF Selectipur, an ammonium cerium(IV) nitrate based etchant.* [b] *"Au Etch" is KI:I_2:DI = 4:1:40*

Metal Layer Surface Roughness

All metal/etchant combinations marked as "+" in Table 1 were measured using a Digital Instruments Nanoscope III (Veeco Inc., USA) to determine the surface roughness of the thin films before and after etching (Table 2). Measurements were made on metalized, but unpatterned Si wafers (bare wafers without SU-8 structuring, or sacrificial layer removal) before and after 24 hours of exposure to the indicated etchants. The wafers were annealed at 95 °C for 15 minutes to simulate processing.

Table 2 - Surface roughness (in nm) of stable metal/etchant combinations (stability defined by "+" symbol in Table 1) before and after 24 hours in the indicated etchants. 50 nm thin films were tested on Si wafers with an initial surface roughness of 0.05 nm. For Au and Pt thin films, a 10 nm Ta adhesion layer was used. After deposition, films were annealed for 15 minutes at 95 °C to simulate processing conditions. "Cr Etch" and "Au Etch" are defined above.

	Cr	Au	Ti	Ti/W	ITO	Pt	Cu	Ta
Cr Etch[a]	-	2.8 2.6	-	-	-	1.2 3.7	-	0.4 3.9
Au Etch[b]	1.5 1.4	-	0.9 0.6	0.4 0.8	0.7 3.0	1.2 1.2	-	0.4 0.3
BHF	1.5 3.9	2.8 1.0	-	-	-	1.2 9.8	5.2 4.9	-

Channel Hydrophobicity

The hydrophobic/hydrophilic combination of the SU-8 nanochannel on a Si or Pyrex substrate (without electrodes) spontaneously fills with both DI water and Octane. Metalized nanochannels will fill depending on the surface properties of the metal.

Heat Generation During Droplet Actuation

The original purpose of the nanochannel system device described within was to miniaturize the digital microfluidic system described in Chapter 2. It was planned to split "droplets" in a nanochannel system using direct current (using two electrodes directly in contact with the liquid), and then to move and combine these droplets using only electric fields produced by a separate set of electrodes (only one of which was directly in contact with the liquid). Simulations indicated that heat dissipation in the SU-8 layer would be rapid enough to allow droplet splitting without negatively

affecting enzyme activity. A multilayered nanochannel system was constructed to investigate this approach.

a.) Multilayered nanochannel droplet manipulator, from below

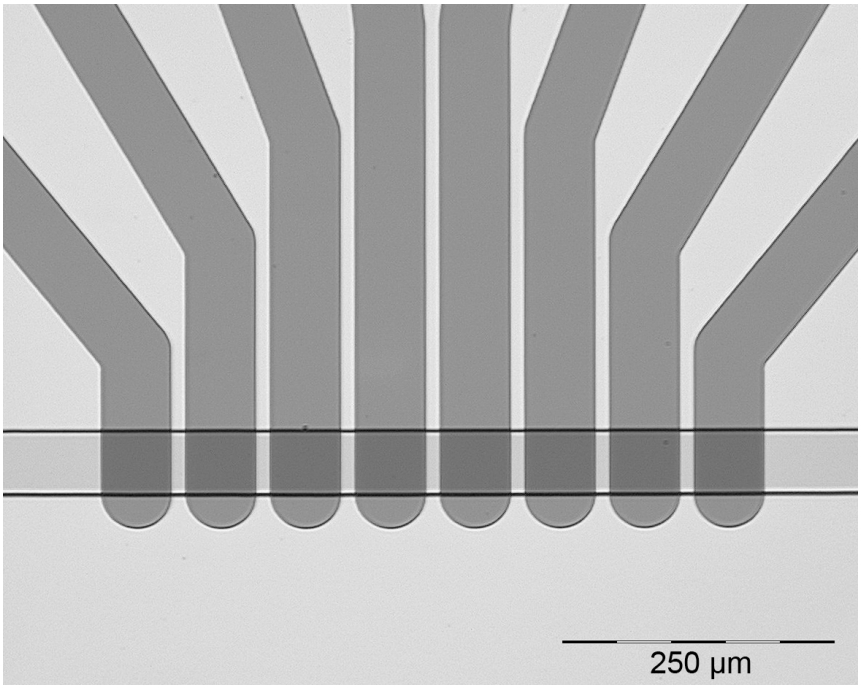

b.) Cross-section

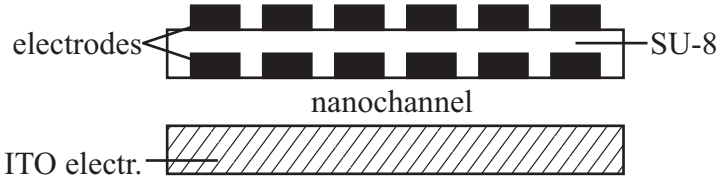

Figure 3 – A multilevel nanochannel/electrode system for splitting and recombining droplets. The middle electrode can either be used to pass current through a droplet ("splitting") or as a floating electrode (charged from above) to manipulate (attract) droplets from elsewhere in the channel.

Using a series of variations on the electrode system described above, it was determined that the maximum droplet width that could be split and actuated in a 100 nm high system was 50 microns. Above this width, droplets could not be moved using electric fields alone for all voltages tested, up to a voltage sufficient to cause breakdown in the SU-8 dielectric layer.

Unfortunately, heat dissipation in the droplets was not as anticipated based on simulations, and enzyme activity was severely degraded when droplets were actuated at voltages necessary to cause "splitting" in a reasonable time frame. Two enzyme systems were investigated: a phosphatase, and a glucosidase. Droplets were loaded in the system, actuated, and the enzyme was subsequently extracted for analysis by diffusion over 48 hours. The QuantiChrom β-Glucosidase Assay Kit and pNPP Phosphatase Assay Kit by BioAssay systems (BioAssay, Inc., USA) were used to assess enzyme activity.

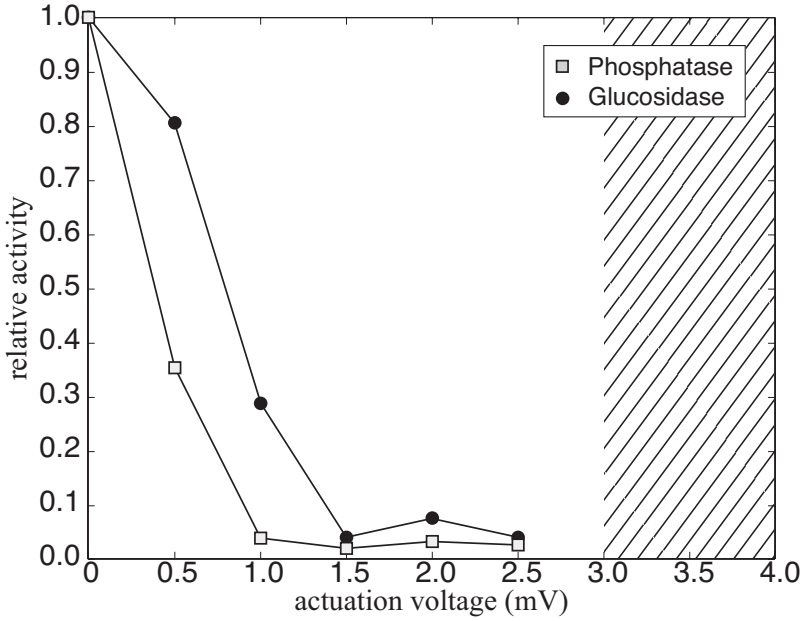

Figure 4 – Phosphatase and glucosidase activity after droplet "splitting" at indicated voltages, as measured as a percentage of activity after identical handling, though without voltage application. The cross-hatched area indicates voltages that caused obvious, excessive droplet heating.

Once it was determined that the voltages required to split the droplets would cause excessive enzyme loss, the system was not investigated further, though we expect the general system structure (a nanochannel with electrodes on the channel floor and ceiling) may have other uses.

Detailed Process Flow

The process as described in the Lab on a Chip paper this work was originally published in (and briefly mentioned in this chapter) has been modified here for Ion Beam Etching instead of wet etching. Ion beam etching allows for significantly higher yield, since shorts of the top and bottom electrode due to over-etching are less likely.

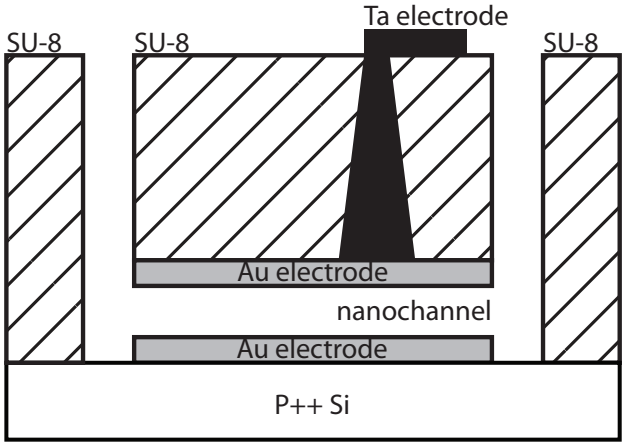

Figure 5 – Cross-section of completed device.

This design requires four masks. The first mask defines the electrode geometry. The second mask defines the microfluidic access channels. The third mask is used to connect the contact pads to the top electrode through the via. The fourth mask is a support layer for the via.

Process Steps

All steps refer to machinery available at the MESA+ Institute for Nanotechnology cleanroom as of 2008. In general however, these steps should be broadly applicable to other equipment with only slight modifications.

Substrate Preparation

Step Name	Details	Comments
P++ doped Silicon	0.025 Ohm cm	Wafers were used without RCA cleaning, directly from the supplier as SEMI-clean.

Definition of Nanochannel Area

Step Name	Details	Comments
Evaporation of metal layers	Machine • Balzers BAK 600 Materials (in order of evaporation) • Ta - 50 nm • Au - 50 nm • Cr - 100 nm • Au - 50 nm	The Au height can be modified to produce channels of different heights. Thickness should be monitored (i.e., crystal monitoring, etc.) and subsequently verified.
Patterning of etch mask	Spin Photoresist • OiR 907-17 • Spin at 4000 RPM • Soft bake 1 min @ 95º C Expose • Mask Layer 11 • 4 s, 12 W/cm^2 Develop • 1 min OPD 4262	HMDS on Au forms a layer that can be difficult to remove. Since adhesion is not critical in IBE, an adhesion layer is not recommended.
Ion beam etching	Time: 120 min Accelerator • Voltage: 500 V • Current: 2 mA Beam • Voltage: 500 V • Current: 20 mA Pressure • Base: 7E-7 mTorr • Process: 3E-4 mTorr Angle = 20º Rotation = ~0.1 Hz	

Resist removal	Microstrip® 5010 • 80º C • 5 hours Ion Beam Etch • Same parameters as above, 2 min	Hard baking in vacuum (as is done in Ion Beam Etching) produces a very difficult to remove mask. Oxygen plasma removal may also be used (though not if a Cr layer is used as the sacrificial layer, as is done here). Optical inspection should always be performed to ensure complete removal. An additional (short) IBE step is necessary after Microstrip use to ensure good SU-8 adhesion.

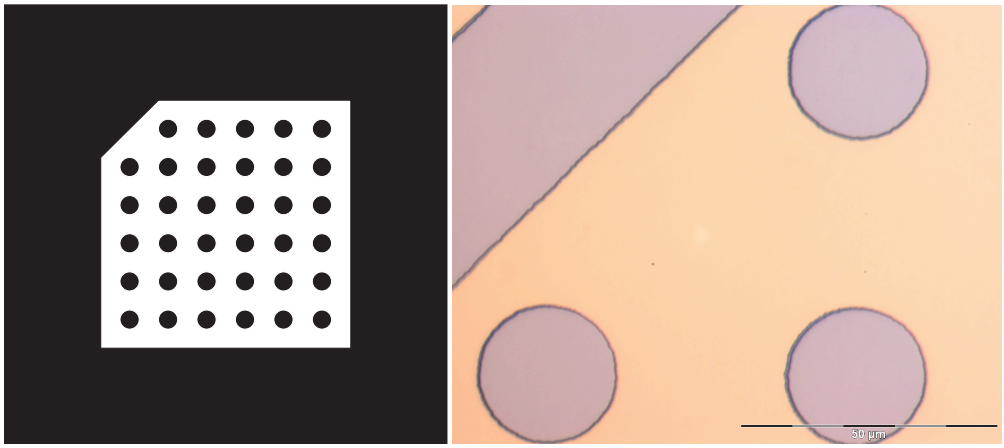

Figure 6 - Top down view: Holes/border patterned by Ion beam etching. In the left image, the white area is protected from etching, and will be the top electrode pattern. The micrograph shows the gold top electrode, and the silicon substrate.

SU-8 Support/Channels Layer

Step Name	Details	Comments
SU-8 processing	SU-8 25 Pour, to cover 2/3 of wafer Spin @ 3000 RPM Soft bake • 5 min @ 65°C • 2 min @ 95°C	SU-8 should be poured (if manually dispensed) from a small bottle, as close to the substrate surface as possible. Inspect the wafer under a microscope to

	(per Microchem datasheet) Expose • Hard contact, with vacuum • Delay before exposure, 4 minutes • 60 seconds (on 12 mW/cm2 EVG 620) Post exposure bake • 5 min @ 65°C, 2 min @ 95°C (per Microchem datasheet) Develop • RER 600, 5 min, with agitation	ensure complete development. If the vias/channels will not completely develop before the SU-8 begins to crack, the easiest way to reduce this problem is to obtain better contact between the mask and the resist (use hard contact, vacuum, etc). Note that the channels in this particular design are not meant to have macro-interconnects; they are simply the access points for a droplet that is dispensed over the entire device.

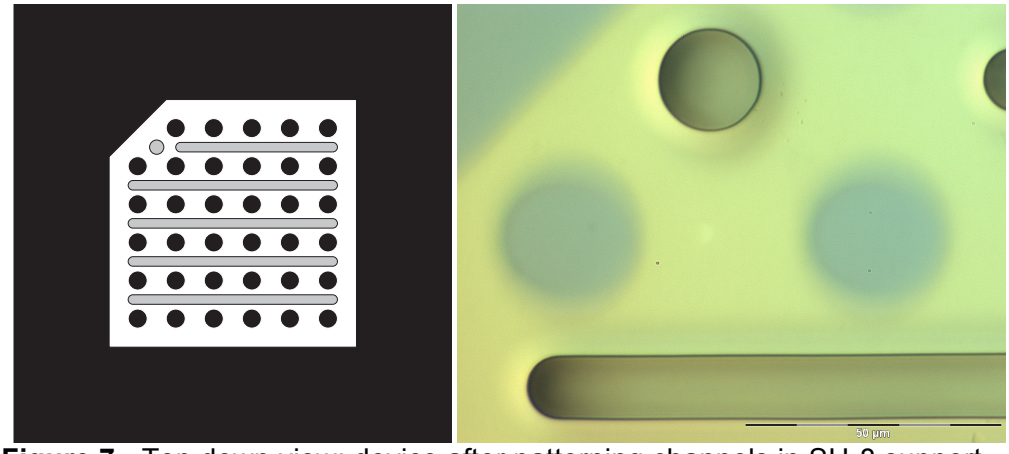

Figure 7 - Top down view: device after patterning channels in SU-8 support layer. Microchannels are lines between circles. The gray circle in the upper left is a via hole. The micro channels allow access to the nanochannels. In the micrograph, the focal plane is at the top of the SU-8 microchannels.

Vias

Step Name	Details	Comments
Sputtering of Ta	Ta • Time = 4 min • Pressure = 1.0E-2 mBar • Power = 200 W	Estimated thickness: Ta = 20 nm Au = 150 nm After this step, a layer of Ta will coat the entire wafer. This is not patterned until the contact pads are defined
SU-8 processing	SU-8 25 Pour, to cover 2/3 of wafer Spin @ 3000 RPM Soft bake • 5 min @ 65°C, • 2 min @ 95°C (per Microchem datasheet) Expose • Hard contact, with vacuum • Delay before exposure, 4 minutes • 35 seconds (on 12 mW/cm2 EVG 620) Post exposure bake • 5 min @ 65°C • 2 min @ 95°C (per Microchem datasheet) Develop • RER 600, 5 min, with agitation	The purpose of this SU-8 layer is to provide support for the via so it does not collapse after etching the sacrificial layer.

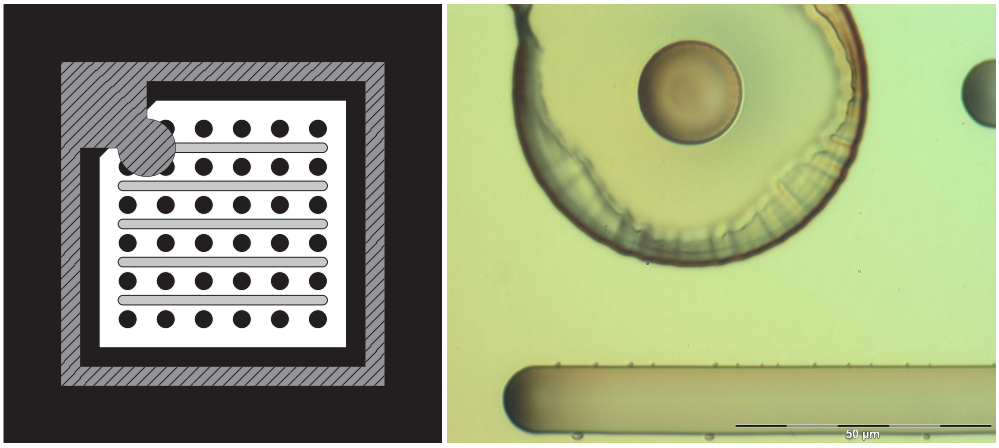

Figure 8 - Top down view: device after patterning SU-8 support layer for via. This top SU-8 support layer serves only to hold up the wire connecting to the top electrode. The SU-8 is optimally exposed for the center of the via, which results in overexposure and slight deformation along the edge.

Wiring to Contact Pads

Step Name	Details	Comments
Patterning of etch mask	Spin Photoresist • OiR 907-17 • Spin at 4000 RPM • Soft bake 1 min @ 95C Expose • 4 sec @ 12 W/cm^2 Develop • 1 min OPD 4262	Highly variable based on device geometry and metal combinations

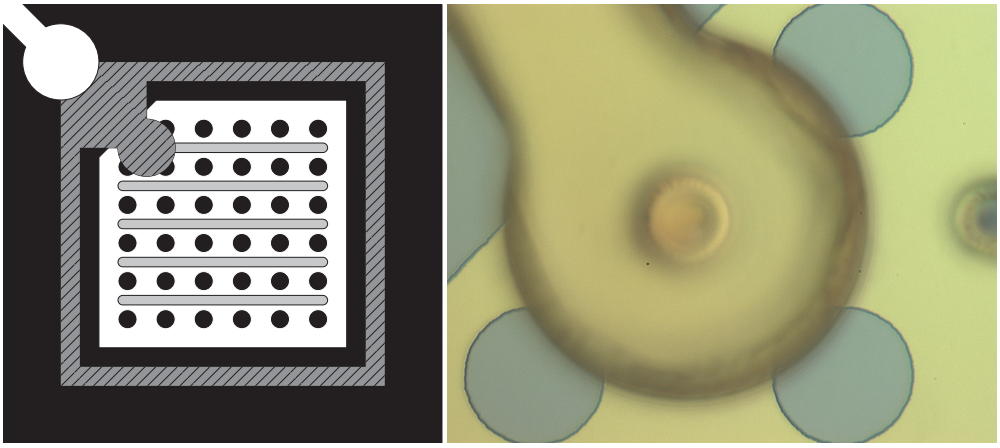

Figure 9 - Top down view: device after patterning wiring to contact pads. The wire on the upper left leads to the contact pads. Gold covers the entire surface, and it is removed except in the area covered by either SU-8 (shown in photo), or positive resist. The focal plane in this image is on the gold top electrode layer. Electrical connection with the via is made on the sides of the SU-8 support layer, under the protected circle in the upper left.

Sacrificial Layer Etching

Step Name	Details	Comments
Sacrificial etching of Cr	BASF Selectipur • 24 Hours • An ammonium cerium(IV) nitrate based Cr etchant • Rinse DI Water: 48 hours	Highly variable based on device geometry and metal combinations
Removal of photoresist used to pattern Ta contact pads	Tepla 300 E plasma asher • 500 W • 1 mbar • 50 SCCM O2	Leaving PR on until this stage gives extra protection against SU-8 peeling up along chip edges during Cr etch.

Dicing, Packaging

Step Name	Details	Comments
	Dicing, Disco Dicing Saw DAD-321 • 30,000 RPM • 10mm/sec Packing • PC board edge connector • 0.1" pitch • Breadboard connectable • Farnell part no: 965893	

Acknowledgements

This research was financially supported by the Technology Foundation STW, applied science division of NWO and the technology program of the Ministry of Economic Affairs of The Netherlands (project no. 6626).

References

(1) Eijkel, J. C. T.; Bomer, J.; Tas, N. R.; van den Berg, A., 1-D Nanochannels fabricated in polyimide, *Lab Chip* **2004**, *4*, 161-163.

(2) Mijatovic, D.; Eijkel, J. C. T.; Van Den Berg, A., Technologies for Nanofluidic Systems: Top-Down Vs. Bottom-up - a Review, *Lab Chip* **2005**, *5*, 492-500.

(3) Stern, M. B.; Geis, M. W.; Curtin, J. E., Nanochannel fabrication for chemical sensors, *Journal of Vacuum Science & Technology B: Microelectronics and Nanometer Structures* **1997**, *15*, 2887.

(4) Ilic, B.; Czaplewski, D.; Zalalutdinov, M.; Schmidt, B.; Craighead, H. G., Fabrication of flexible polymer tubes for micro and nanofluidic applications, *Journal of Vacuum Science & Technology B: Microelectronics and Nanometer Structures* **2002**, *20*, 2459.

(5) Nam, W. J.; Bae, S.; Kalkan, A. K.; Fonash, S. J., Nano-and microchannel fabrication using column/void network deposited silicon, *Journal of Vacuum Science & Technology A: Vacuum, Surfaces, and Films* **2001**, *19*, 1229.

(6) Yang, B.; Pang, S. W., Multiple level nanochannels fabricated using reversal UV nanoimprint, *Journal of Vacuum Science & Technology B* **2006**, *24*, 2984-2987.

(7) Arrigan, D. W. M., Nanoelectrodes, nanoelectrode arrays and their applications, *Analyst* **2004**, *129*, 1157-1165.

(8) Pumera, M.; Sanchez, S.; Ichinose, I.; Tang, J., Electrochemical nanobiosensors, *Sensors and Actuators B-Chemical* **2007**, *123*, 1195-1205.

(9) Bard, A. J.; Fan, F. R. F.; Kwak, J.; Lev, O., Scanning Electrochemical Microscopy - Introduction and Principles, *Anal. Chem.* **1989**, *61*, 132-138.

(10) Ge, B. X.; Huang, Y. C.; Sen, D.; Yu, H. Z., Electrochemical investigation of DNA-modified surfaces: From quantitation methods to experimental conditions, *J. Electroanal. Chem.* **2007**, *602*, 156-162.

(11) Calzolari, A.; Di Felice, R., Surface functionalization through adsorption of organic molecules, *Journal of Physics-Condensed Matter* **2007**, *19*, 305018-305028.

(12) Schasfoort, R. B. M.; Schlautmann, S.; Hendrikse, L.; van den Berg, A., Field-effect flow control for microfabricated fluidic networks, *Science* **1999**, *286*, 942-945.

(13) Olk, P.; Renger, J.; Hartling, T.; Wenzel, M. T.; Eng, L. M., Two particle enhanced nano Raman microscopy and spectroscopy, *Nano Lett.* **2007**, *7*, 1736-1740.

(14) Wang, X.; Cui, Y.; Ren, B., Fabrication of Au tips for tip-enhanced Raman spectroscopy, *Chemical Journal of Chinese Universities-Chinese* **2007**, *28*, 522-525.

(15) Bishnoi, S. W.; Rozell, C. J.; Levin, C. S.; Gheith, M. K.; Johnson, B. R.; Johnson, D. H.; Halas, N. J., All-optical nanoscale pH meter, *Nano Lett.* **2006**, *6*, 1687-1692.

(16) Xu, B. Q.; Tao, N. J. J., Measurement of single-molecule resistance by repeated formation of molecular junctions, *Science* **2003**, *301*, 1221-1223.

(17) Cheng, G. J.; Pirzada, D.; Dutta, P., Design and fabrication of a hybrid nanofluidic channel, *Journal of Microlithography Microfabrication and Microsystems* **2005**, *4*, 013009.

(18) Tas, N. R.; Mela, P.; Kramer, T.; Berenschot, J. W.; van den Berg, A., Capillarity induced negative pressure of water plugs in nanochannels, *Nano Lett.* **2003**, *3*, 1537-1540.

(19) Hibara, A.; Saito, T.; Kim, H. B.; Tokeshi, M.; Ooi, T.; Nakao, M.; Kitamori, T., Nanochannels on a Fused-Silica Microchip and Liquid Properties Investigation by Time-Resolved Fluorescence Measurements, *Anal. Chem* **2002**, *74*, 6170–6176.

(20) Andersson, H.; van den Berg, A., Microtechnologies and nanotechnologies for single-cell analysis, *Curr. Opin. Biotechnol.* **2004**, *15*, 44-49.

(21) Nordstrom, M.; Johansson, A.; Nogueron, E. S.; Clausen, B.; Calleja, M.; Boisen, A., Investigation of the bond strength between the photo-sensitive polymer SU-8 and gold, *Microelectron. Eng.* **2005**, *78-79*, 152-157.

(22) Roberge, P. R. *Handbook of Corrosion Engineering*; McGraw-Hill Professional, 1999.

(23) Sparreboom, W.; Eijkel, J. C. T.; Bomer, J.; van den Berg, A., Rapid sacrificial layer etching for the fabrication of nanochannels with integrated metal electrodes, *Lab Chip* **2008**, *8*, 402-407.

(24) Blanco, F. J.; Agirregabiria, M.; Garcia, J.; Berganzo, J.; Tijero, M.; Arroyo, M. T.; Ruano, J. M.; Aramburu, I.; Mayora, K., Novel three-dimensional embedded SU-8 microchannels fabricated using a low temperature full wafer adhesive bonding, *Journal of Micromechanics and Microengineering* **2004**, *14*, 1047-1056.

(25) Wang, L. S.; Flanagan, L.; Lee, A. P., Side-wall vertical electrodes for lateral field microfluidic applications, *Journal of Microelectromechanical Systems* **2007**, *16*, 454-461.

(26) Pan, C. T.; Yang, H.; Shen, S. C.; Chou, M. C.; Chou, H. P., A low-temperature wafer bonding technique using patternable materials, *Journal of Micromechanics and Microengineering* **2002**, *12*, 611-615.

(27) Tuomikoski, S.; Franssila, S., Free-standing SU-8 microfluidic chips by adhesive bonding and release etching, *Sensors and Actuators a-Physical* **2005**, *120*, 408-415.

(28) Kastantin, M. J.; Li, S.; Gadre, A. P.; Wu, L. Q.; Bentley, W. E.; Payne, G. F.; Rubloff, G. W.; Ghodssi, R., Integrated fabrication of polymeric devices for biological applications, *Sensors and Materials* **2003**, *15*, 295-311.

(29) Gracias, A.; Feng, X. J.; Xu, B.; Castracane, J., Novel microfabrication approach of embedded SU8 (TM) fluidic networks for cell transport on chips, *Journal of Microlithography Microfabrication and Microsystems* **2006**, *5*, -.

(30) Jasbir, N. P.; Bozena, K.; Bonnie, L. G.; Byron, D. G., PDMS as a sacrificial substrate for SU-8-based biomedical and microfluidic applications, *Journal of Micromechanics and Microengineering* **2008**, 095028.

(31) Dentinger, P. M.; Clift, W. M.; Goods, S. H., Removal of SU-8 photoresist for thick film applications, *Microelectron. Eng.* **2002**, *61-2*, 993-1000.

Chapter 5

Enzyme Kinetics By Directly Imaging A Porous Silicon Microfluidic Reactor Using DIOS Mass Spectrometry

Enzyme kinetics were obtained in a porous silicon microfluidic channel by combining an enzyme and substrate droplet, allowing them to react and deposit a small amount of residue on the channel walls, and then analyzing this residue by directly ionizing the channel walls using a matrix assisted laser desorption/ionization mass spectrometry (MALDI-MS) laser source. The porous silicon of the channel walls functions in a manner analogous to the matrix in MALDI-MS, and is referred to as a desorption/ionization on silicon mass spectrometry (DIOS-MS) target when used in this configuration. Mass spectrometry signal intensity of substrate residue correlates with relative concentration, and position in the microchannel correlates with time, thus allowing determination of kinetic parameters. The system is especially suitable for initial reaction velocity determination. This microreactor is broadly applicable to time-resolved kinetic assays as long as at least one substrate or product of the reaction is ionizable by DIOS-MS.

Portions of this chapter were published in:

1) Nichols, K.P.; Gardeniers, H.J.G.E.; Azoz, S. *Analytical Chemistry*, 2008, 80, 8314-8319

2) Nichols, K.P.; Gardeniers, H.J.G.E. In *Proc. of the Am. Soc. for Mass Spectrometry 2008, (digital publication, no page numbers*).

3) Nichols, K. P.; Gardeniers, H.J.G.E. In *Proc. of MicroTAS 2008*, 2008, pp. 1943-1945

Introduction

In chapter two, we reported a method to obtain pre-steady-state enzyme kinetics using a digital microfluidic (liquid droplet) system coupled with matrix assisted laser desorption/ionization time-of-flight mass spectrometry (MALDI-TOF MS).[1] Our system utilized individually addressable electrodes covered by a hydrophobic dielectric to combine droplets with precise timing. Enzyme droplets were sequentially combined with their substrates, then quenched with a strong acid, and finally combined with a matrix. By varying the time until the quench, a time-sequence was obtained and analyzed using MALDI-TOF MS to extract pre-steady-state kinetic constants of a model protein tyrosine phosphatase. MALDI-TOF MS allows for the determination of rate constants regardless of the incorporation of a chromophore, and at a wide variety of buffer concentrations. Both of these are useful advantages if one wishes to study enzymatic reactions under naturally occurring conditions. While this previously described system did represent a high throughput method for obtaining the kinetics of certain reactions, its primary weakness was its requirement of an internal standard, a set of molecules that would ionize in equivalent molar ratios. Without this internal standard to aid in calibration, local variations in concentration across and between dried droplets prevented even relative quantitation. Numerous authors have described local variations in solute concentration after the drying of a droplet, sometimes referred to as a "coffee stain" effect.[2, 3] Modeling has typically been accomplished by assuming pinned contact lines, low Reynolds numbers, and a hemispherical droplet shape.[4-6]

The system described in this chapter has the same basic goal as the devices we described in previous chapters: high throughput kinetics. However, to eliminate the need for an internal standard, this new system takes a very different approach to the microfluidic system design. Instead of analyzing an array of droplets on a planar electrode surface, each of which is separately quenched at discrete time intervals to produce a kinetic curve, only a single reacting droplet is analyzed, using a system that

can continuously and smoothly extract a small amount of product or substrate residue from this droplet. The droplet travels down a porous silicon microfluidic channel, depositing a trace amount of residue in the silicon pores, which are later analyzed by desorption/ionization on silicon mass spectrometry (DIOS-MS). The pores are tuned to be smaller than the enzyme, but larger than the reaction product, thus quenching the reaction. This effectively eliminates the intra-droplet and inter-droplet variability of our previous system, allowing for quantitation without internal standards. An additional benefit is the absence of dead time between the initiation of mixing and the point at which measurements can be taken, since measurements are possible along the entire channel.

Desorption/ionization on silicon mass spectrometry (DIOS-MS) is a vaporization technique for generating gas-phase ions in which nanostructured silicon is used as a replacement for the crystalline matrix of matrix assisted laser desorption/ionization mass spectrometry (MALDI-MS).[7] By eliminating matrix interference, DIOS-MS extends the observable mass range to small biomolecules, such as metabalomes.[8] Further, combining dynamic electrowetting with DIOS-MS allows for greatly enhanced mass spectrometry sensitivity.[9]

MALDI imaging mass spectrometry (MALDI-IMS) is a type of MALDI-MS that has been utilized to investigate the distribution of ionizable molecules within thin sections of biological tissues.[10] In MALDI-IMS, after slicing a tissue sample into a thin section, a matrix material is deposited, typically by spotting or spraying, and a raster scan of the tissue sample is made by the laser source in a MALDI mass spectrometer. In this way, the relative concentration of a specific molecule (identified by its m/z) at a specific location can be identified without labeling. The system described within is in many ways similar to MALDI-IMS, though instead of scanning a tissue sample spotted with matrix, a microfluidic channel constructed of porous silicon (DIOS-MS) is scanned. And, instead of obtaining information about the spatial distribution of a molecule in a tissue sample, our system reveals the temporal concentration profile of an enzymatic reaction, since, in this microfluidic system,

spatial position corresponds with a specific point in time, and the residue deposited by a droplet traveling through the channel is proportional to substrate or product concentration at that point in time.

The majority of microfluidic devices previously described use a continuously flowing single liquid phase. Where applicable, using a two-phase system with monodisperse droplets has the advantage of rapid mixing within the droplet and low dispersion.[11-13] Thorsen *et al.* first reported droplet generation in a microfluidic system in 2001 using a T-junction with one oil channel and one water channel. At proper differential inlet pressures, monodisperse droplets are formed by shearing and pinching off segments from one of the two phases.[14] Variations on this technique have been widely used for kinetics,[15] crystallization,[16] and encapsulation of single cells.[17]

In this chapter, we utilize DIOS-MS, droplet-based microfluidics, and well-established silicon micromachining techniques to produce a microfluidic system capable of determining various kinetic parameters by analyzing the residue of a reacting enzyme and substrate droplet as it travels down the length of a porous silicon microfluidic channel. The most obvious use for such a device is to rapidly obtain enzyme initial velocity measurements. These measurements can be determined directly from the relative substrate or product concentrations determined by mass spectrometry as a function of time/position, as shown in Figure 6. However, if sufficient additional information is known about the enzymes in question (such as adherence to Michaelis-Menten kinetics) there are a variety of non-linear regression techniques suitable for deducing kinetic parameters directly from an enzyme progress curve.[18-20]

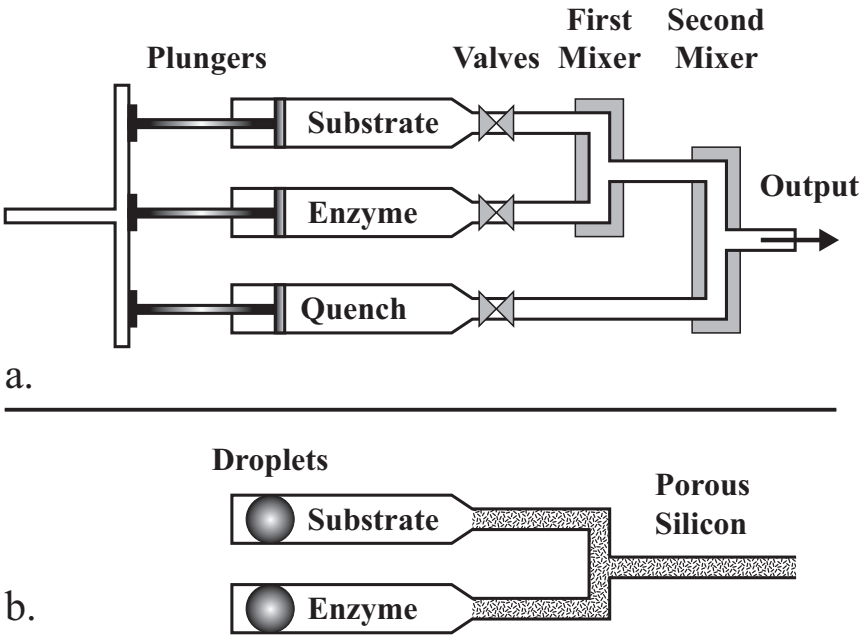

Figure 1 – Comparison of bench-scale stopped flow system for kinetic analysis (top) with microfluidic analog (bottom). The microfluidic system is simpler, allows faster mixing, and permits analysis of the reaction at the point where mixing initiates. The microfluidic system is analogous to a bench-scale capillary tubing based system, but with a small percentage of the reaction products depositing on the capillary walls, and capable of being analyzed in place after the experiment using mass spectrometry.

As shown in Figure 1, our system is conceptually similar to a traditional bench-scale stopped flow system for kinetic analysis. However, our system is simpler, due to the elimination of multiple valves and the need for a quench; it allows for faster mixing, due to the use of rapidly mixing droplets; and, it permits analysis along the entire length of the capillary in which the reaction occurs instead of only at a single outlet.

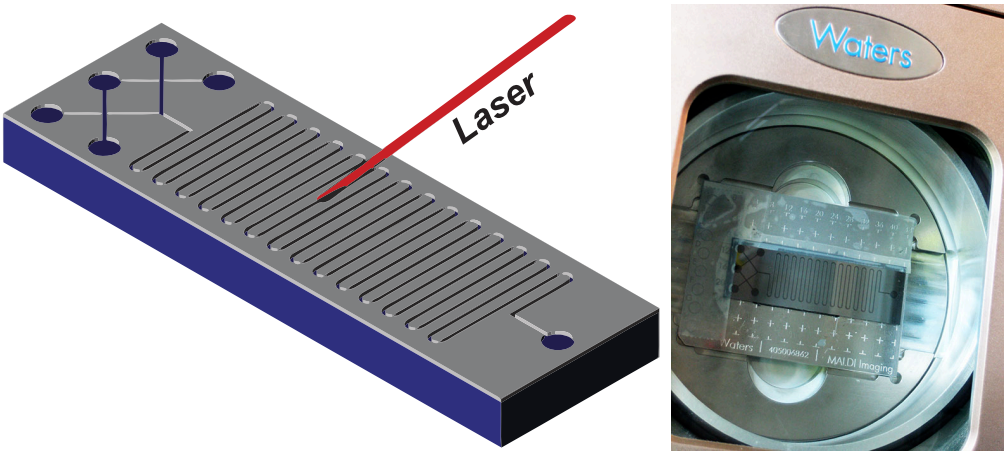

Figure 2 – Enzyme and substrate droplets combine in the microchannel and deposit a small amount of residue on the channel walls. This residue can later be detected and quantified relatively using mass spectrometry

Figure 2 shows an overview of the device being analyzed. After the reaction is complete, the porous silicon chip is removed from its holder, and placed directly in a mass spectrometer. Mass spectrometry readings were correlated with a position on the chip using a combination of software provided by the instrument manufacturer and a MATLAB script. Images such as that shown in Figure 6 were then constructed.

Materials And Methods

A cross section of the porous Si kinetic analysis chip during use is shown in Figure 3. Prior to the point in time shown in the figure, the device first combines an enzyme droplet and a substrate droplet. This combined enzyme/substrate droplet then travels down the channel, depositing a trace amount of reaction substrate and product on the channel walls. After the droplet has passed through the channel, the lid is removed, and the chip is analyzed using DIOS-MS. The chip consists of a patterned porous silicon "floor," with SU-8 walls, and a removable polydimethylsiloxane (PDMS) lid. The electrode embedded in the PDMS lid enhances wetting and improves DIOS-MS detection sensitivity.[9] After the droplet has traveled the length of the channel, the lid is removed, and the bottom half of the chip is placed directly into a mass spectrometer.

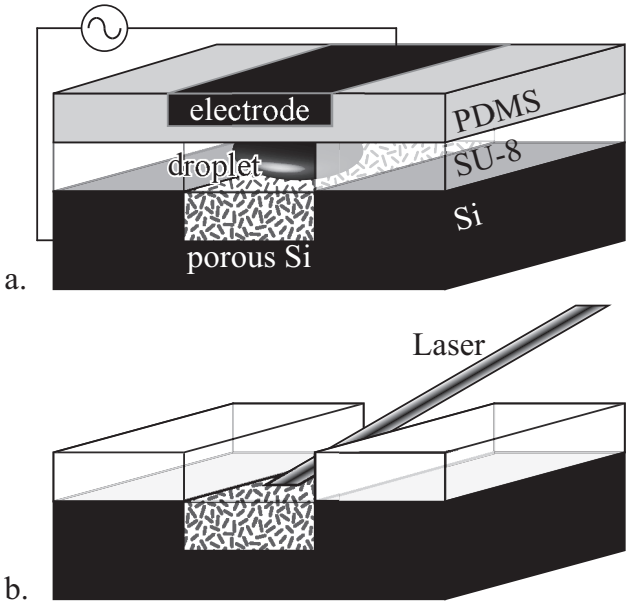

Figure 3 – Cross section of porous Si kinetic analysis chip during enzymatic reaction, as droplet travels down the channel depositing reaction product on the channel walls (top), and during DIOS-MS analysis (bottom). The chip consists of a patterned porous silicon "floor," with SU-8 walls, a removable polydimethylsiloxane (PDMS) lid, and an electrode embedded in the PDMS. After the droplet has traveled the length of the channel, the lid is removed, and the bottom half of the chip is placed directly into a mass spectrometer.

Fabrication

Photolithography masks were designed using CleWin (WieWeb Software, the Netherlands). Chromium masks were produced using a Heidelberg Instruments DWL 2.0 (Germany) laser pattern generator. Microchannel side walls were patterned using SU-8 50 (Microchem, USA), a photo-definable epoxy, spun to a height of 50 microns and patterned using standard photolithography techniques. The channel width was 250 microns, an even multiple of the MALDI-MS laser width. The porous silicon microchannel floors were fabricated using a custom-built anodization cell. Porous

silicon pore size was tuned to be larger than the substrate and product, though smaller than the mean diameter of arginase, using the parameters detailed in Table 1. This allows continuous substrate diffusion into the pores, negating the need for a quench since the pores sterically hinder the enzymatic reaction, and allows for subsequent DIOS-MS directly on the chip. It will therefore be necessary to tune the porous silicon surface differently if significantly larger or smaller enzymes are used. Details for tuning pore diameter as a function of anodization conditions are available.[21] The specific parameters used in this study were 3 mA / cm^2 passed through 5% HF and the bulk of a P++ doped Si wafer for 5 minutes. Pore sizes were determined using the Barrett–Joyner–Halenda (BJH) method.[22] The lid was cured Polydimethylsiloxane (PDMS), attached to the microchannel using the pressure from an external holder. The PDMS was not oxidized prior to attachment, since it was not permanent; after droplets were passed through the channel, the lid was removed. A holder was constructed using ABS plastic, with NanoPort connectors (Upchurch Scientific, USA) to fit standard fused silica capillary tubing (inner diameter 50 microns). Harvard Apparatus PHD 2000 (Harvard Apparatus, USA) syringe pumps were connected to the capillary tubing to provide a pressure gradient.

Table 1 – Formation conditions and characteristics of porous silicon on flat substrates. This data was used to tune the porous silicon such that the pores were smaller than the enzyme, but larger than the substrate and product. Data used with permission from Tiggelaar, Verdoold, Eghbali, Desmet and Gardeniers.

Galvanostatic formation conditions			**Characteristics porous silicon layer**			
Electrolyte [wt %]	Current [mA]	Process time [min]	Thickness [nm]	Pore size [nm]	Porosity ε [%]	A_{BET} [m^2/cm^3]
5% HF	50	5	612 ± 4	4.2 ± 0.2	23	300
	100		745 ± 7	4.9 ± 0.1	36	410
	200		1640 ± 10	5.4 ± cc0.1	55	350
15% HF	50	5	890 ± 20	-	-	-
		10	1485 ± 6	3.2 ± 0.2	21	170
	100	5	1630 ± 20	-	-	-
		10	2130 ± 20	3.6 ± 0.3	27	370
	200	5	2270 ± 20	4.4 ± 0.5	47	290
20% HF	50	5	950 ± 9	2.1 ± 0.5	20	140
	100		2164 ± 5	2.5 ± 0.4	35	130
	200		3201 ± 4	3.5 ± 0.3	39	200

Droplet Dispensing

Using a two phase system with monodisperse droplets has the advantage of rapid mixing within the droplet and low dispersion.[11] Mixing times were numerically simulated using CFD-ACE 2008 (CFD Research Corp., USA) using the "Flow," "Chemistry/Mixing," "Free Surface (VOF)" and "Grid Deformation" modules. In cases where the time steps required were excessively low (below 1E-9 sec), damping was used to decrease simulation time. Adaptive meshing was used as described by Cristini and Tan.[23]

Droplets were dispensed using the scheme shown in Figure 4. The scheme is conceptually similar to the loading loop common in HPLC setups. During droplet dispensing, custom-made rubber seals were inserted in the threaded holes otherwise occupied by the NanoPort connectors, as indicated in the scheme. Shear forces at the perpendicular junction between the air and liquid flows form the droplets. The reason for the use of this non-standard droplet dispensing system is detailed in the Results and Discussion section.

In a two phase oil and water system, Thorsen *et al.* reported that droplet volume is primarily dependent only on the differential inlet pressures.[14] Numerical simulations using CFD-ACE 2008 (CFD Research Corp., USA) were used to verify that the same is true for a two phase water and air system.

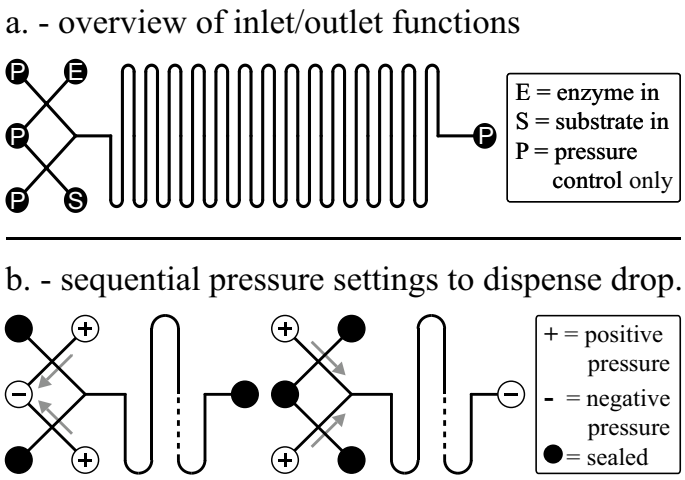

Figure 4 – Pressure settings used to dispense droplets. In the left image of figure b., the top "+" reservoir contains the enzyme, and the bottom "+" reservoir contains the substrate. Enzyme and substrate droplet are then pulled towards the "-" outlet. When the pressures are set as shown in the right image of figure b., an enzyme droplet and a substrate droplet pinch off at the "x" shaped intersections, combine, and traverse the channel. The only liquid reservoirs are the "enzyme" and "substrate" inlets. Pressure controls are only connected to a syringe containing air. Black reservoirs are sealed using a rubber stopper.

Electrowetting

An insulated electrode in the form of a P++ doped porous silicon wafer coated with a 50 nm PECVD silicon dioxide dielectric was embedded in the PDMS ~50 µm from the bottom PDMS surface (50 µm from the channel). The electrode was elevated during PDMS curing using SU-8 posts. A 150 V_{RMS} signal at 100 kHz was utilized. Special care should always be taken with high voltages. The voltage and frequency required is specific to the dielectric properties of the insulator and PDMS, and should thus be tuned for each device such that the minimum energy needed to

affect the contact angle is used. Electrowetting has previously been demonstrated to produce dramatic increases in sensitivity for DIOS-MS.[9]

Model Enzyme

The model enzyme system investigated was the arginine to ornithine reaction by arginase. Enzyme concentrations from a wide variety of enzyme and substrate concentrations were investigated. Mass spectrometry was performed using a Waters Synapt HDMS system (Waters, USA), examining 173.1 m/z in the case of arginine.

Enzyme concentrations from 0.03 to 10.1 mM of L-arginase from bovine liver (Sigma-Aldrich, USA and ABCR, Germany) and arginine initial concentrations from 10 μM to 100 mM were investigated. All reactions were conducted at 37°C in a Binder BD 53 incubator (Binder, Germany). Syringe pumps were kept outside the incubator, though capillary tubes leading into the incubator were kept as short as this configuration would allow. The chips and chip holders were continuously stored and utilized in the incubator. After loading the reservoirs with 10 μL of liquid (enzyme, or substrate), the system was allowed to equilibrate for 5 minutes. Prior to loading, liquid temperatures were either at room temperature or 4°C.

Control experiments verified that nonspecific enzyme adsorption to the porous silicon is insignificant, and that, while diffusion of trace amounts of substrate into the porous silicon is high enough to be detected by DIOS-MS, it is low enough (~1%) that it can be ignored during kinetic modeling. Detail is given in the Results and Discussion section.

Mass Spectrometry

Before quantitation, all data was post processed in MassLynx (Waters, USA) using the following protocol: Savitzky-Golay smoothing (2 times, 3 channels); background subtraction (polynomial order: 15, below curve%: 10, tolerance: 0.01); spectrum centering (min peak width at half height: 4, centroid top%: 80). When attempting to quantitate mass spectrometry results, it is important to always precisely follow the exact same post-processing steps, whatever specific steps are chosen.

All measurements were performed using the Enhanced Duty Cycle (EDC) mode on the Waters SYNAPT HDMS (Waters, USA). EDC increases the duty cycle for a narrow m/z range to levels approaching 100%. The masses of interest are pre-defined, and discrete ion packets are formed in the collision cell at synchronized time intervals with the pusher.[24] Though this method limits the available mass range that can be investigated, in our case, it increased arginine sensitivity 20-fold. Using this method, or an equivalent method available through another manufacturer, is highly recommended to measure the trace samples on the porous silicon surface.

Results and Discussion

Though no internal standard for DIOS-MS is present, the continuous, smooth decrease in substrate signal can be used to extract rapid kinetic constants, after controlling for substrate loss (diffusion) into the pores unrelated to the enzyme. Since the final point of mixing overlaps with what is typically referred to as the "observation cell" in such a system, and since the entire surface of the microchannel can be analyzed using DIOS-MS, there is zero dead time. We successfully utilized our system with arginase, detecting the conversion of arginine into ornithine (Figure 6).

Droplet Dispensing

It was rapidly determined that standard continuous flow microfluidics, without droplet formation, would not be satisfactory for the desired measurements. Dispersion produced low temporal resolution, and mixing times for acceptable channel geometries were excessive, as determined by CFD. Channel geometries were limited by the minimum width of the MALDI-MS source laser.

Typically, droplets in a two-phase microfluidic system are produced by combining streams from the two phases at a T-intersection. At proper differential flow rates, droplets of one phase will pinch off into the second phase. Simulations indicated that this approach would not work well for our device since our device has a relatively complex wall structure compared to most other droplet microfluidic systems. It has one PDMS wall, two SU-8 walls, and one porous silicon wall. The varied contact angles of the four walls made pinching off of one of the droplet phases problematic using previously published methods.

Computational fluid dynamics was used to verify mixing time for our system is on the millisecond timescale, as expected based on previous work.[11, 25, 26] Direct visualization of mixing was not possible in our system due to the presence of multiple

opaque layers. Mixing times could most likely be improved by having the two droplets come into contact with each other "back to front," as opposed to "side to side," using a recently demonstrated method.[27]

Changing the air and water inlet flow rates (labeled as "pressure control" and "enzyme/substrate" in Figure 4) is the primary method of controlling droplet volume. In this case, the higher the air inlet pressure (flow rate), the smaller the droplets will be, since they are sheared off from the liquid phase more quickly. If the air flow rate is too low, shearing will not occur. This is shown in Figure 5. Since our device already has an electrode present above and below the droplet, it may be possible to produce more varied droplets under a wider range of conditions using the method of Mallogi *et al.*[28]

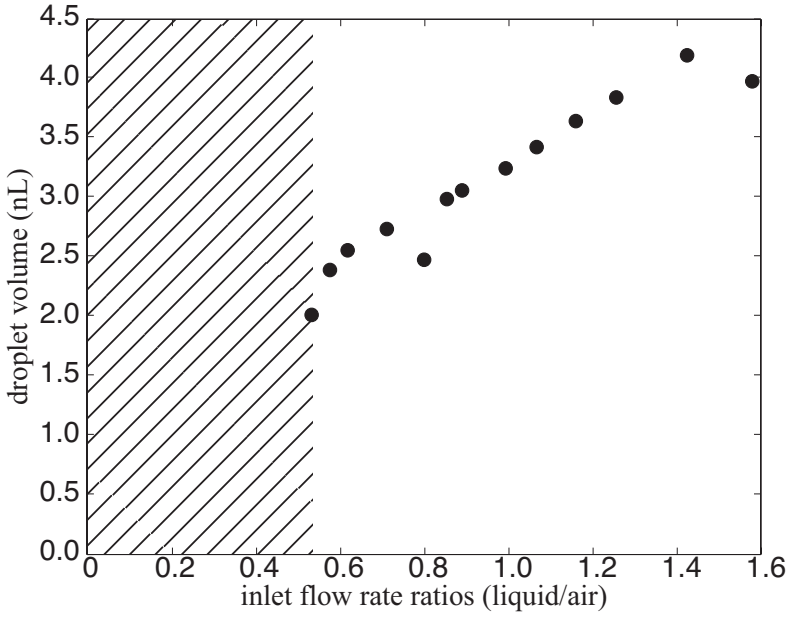

Figure 5 – Droplet volume as a function of inlet flow rate ratios at the perpendicular intersection of the channels shown in Figure 4. The crosshatched area indicates the regime where air pressure is insufficient to shear off a droplet.

MS Imaging of Whole Chip

Figure 6 shows a complete raster scan of a porous silicon chip, after an enzymatic reaction has taken place within it. Significant substrate signal is visible in three of the four wells. The presence of substrate in the leftmost wells is due to the use of these wells in loading the droplet. The presence of a significant substrate signal in the rightmost well, which is only used as an outlet, is due to the remaining droplet volume that does not exit the system. Since the signal in the main channel is due only to trace residue from this droplet, there is still a significant signal at the outlet since the total number of molecules that eventually localize here from the droplet bulk is orders of magnitude higher than in the main channel. In practice, it is not necessary to scan the entire chip. We have obtained initial velocity measurements with an R^2 of 0.96 with as few as 29 measurement points. Scanning more points will improve this value considerably though, as the contribution of local noise, from, for example, air bubbles created during the anodization process, will be minimized.

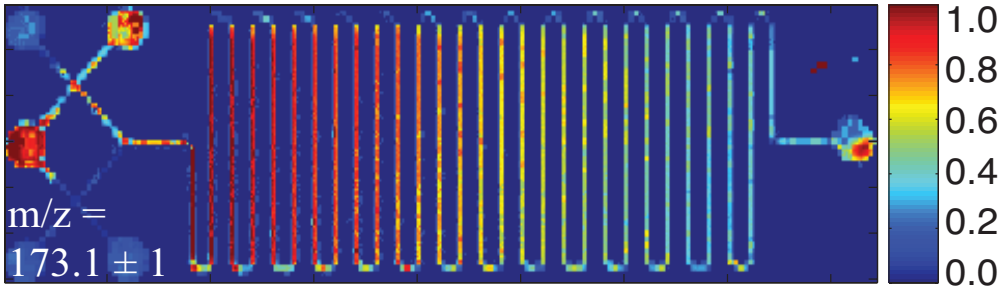

Figure 6 – Imaging of porous silicon channel using mass spectrometry at 173.1±1 m/z (arginine). Intensity correlates with relative concentration. In practice, it is not necessary to scan the entire chip. If signal intensity is too low, multiple lines can be summed together, though with some reduction in temporal resolution. The decrease in intensity along the top "curves" of the channels is due to shadowing of the laser by the microchannel walls.

Initial Velocity Measurements

The primary value of such scans as shown in Figure 6 is to rapidly obtain initial velocity measurements. After controlling for potential non-linearity in droplet speed due to the pressure driven nature of the flow, these can be determined directly from the relative substrate or product concentrations, determined by mass spectrometry as a function of time/position. Figure 7 shows just such an initial velocity measurement, over a variety of enzyme concentrations. The total number of measurements, and time, required to obtain such a graph is dramatically reduced from that required using traditional bench-scale techniques through the use of a porous silicon microreactor in the manner demonstrated. Further, if sufficient additional information is known about the enzymes in question (such as adherence to Michaelis-Menten kinetics) there are many non-linear regression techniques capable of deducing kinetic parameters directly from an enzyme progress curve, which at proper flow rates and enzyme concentrations, can be extracted directly from the data in Figure 6.[18-20]

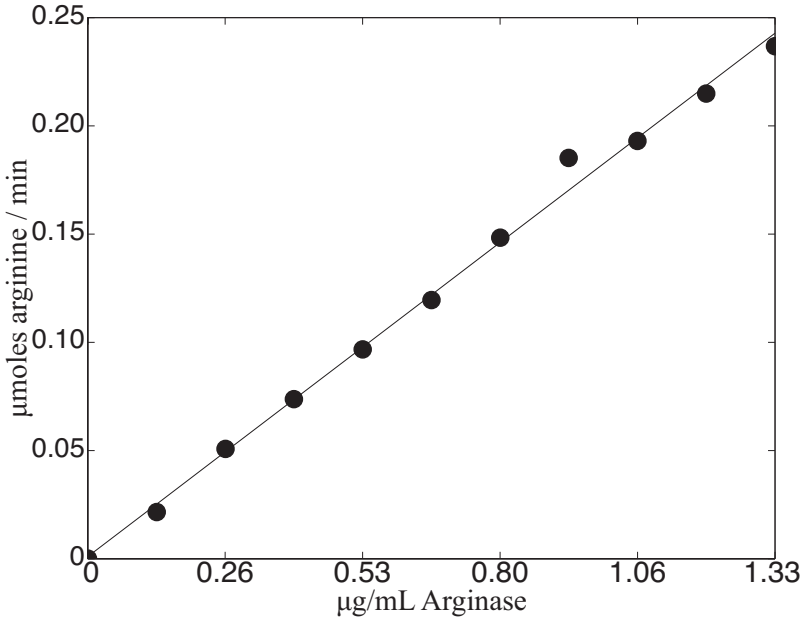

Figure 7 – Initial velocities for 11 different concentrations of arginase. Each initial velocity is determined using only a single chip, as opposed to the multiple experiments that would be required for a traditional stopped flow reaction. These results are similar to that found by Garganta and Bond[29], and well within the range of reported values in the literature, with the exception that this assay measures arginine concentration instead of ornithine concentration.

Figures of Merit

Dynamic range for this system is primarily dependent on the equipment and settings used for the mass spectrometry. Sensitivity in the attomolar range is not uncommon for DIOS-MS measurements. However, attainable sensitivity will vary widely dependent on the ionization characteristics of the molecule of interest. Particular care must be taken to avoid detector saturation. Typical mass spectra are shown in Figure 8, as an indication of the background noise present after microfabrication and device use.

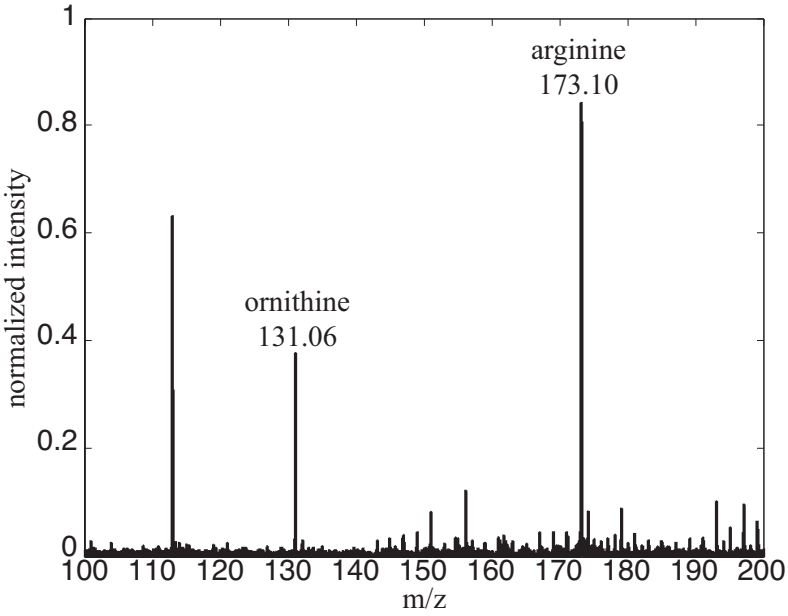

Figure 8 – Example mass spectra from microreactor channel. An approximate indication of the noise levels present can be obtained from this image. Noise is an important parameter to consider in this system, especially if one wishes to measure an increase in product concentration, as opposed to a decrease in substrate concentration, as it will influence the baseline (zero concentration point).

Control Experiments

Porous silicon has been demonstrated as an effective enzyme support for biosensor purposes.[30-32] However, since our assay assumes both minimal adsorption of enzyme onto the porous silicon surface and low activity of bound enzyme, it was important to determine that the porous silicon in our reactor did not possess the characteristics that, in other cases, have served as a useful enzyme support. The first significant difference in our design versus those that use porous silicon for an enzyme support is that previous devices have tended to use methods to stabilize the enzyme on the porous silicon surface. Bengtsson *et al.* coupled their enzyme of interest to a

porous silicon surface by an initial silanization step followed by glutaraldehyde activation and coupling of the enzyme to the aldehyde group.[30] Our device fabrication protocol involves no analogous steps. Further, the pores of our device are deliberately tuned to be smaller than the size of the enzyme itself, as detailed in the Materials and Methods section.

To determine the effects of nonspecific enzyme absorption, we first established a baseline level of substrate loss in the device due only to substrate diffusion into the porous layer, i.e., the decrease in signal as a function of time that is not due to enzymatic conversion. By passing a droplet containing only substrate through the system, this was determined to be approximately 1% over the length of the reactor.

To verify that an insignificant amount of enzyme was adsorbing on the surface, we passed a droplet containing only enzyme through the channel 10 times, and then passed a droplet containing only substrate through the channel. The only decrease in substrate concentration in this case, above the baseline level of substrate loss described in the previous paragraph, would be due to substrate coming into contact with active enzyme adsorbed on the channel walls. The decrease in signal intensity in this case was approximately 2%, though the 95% confidence intervals for this experiment and the baseline experiment overlapped. Since the decrease in signal strength for an experiment with identical enzyme and substrate concentrations that are passed through the reactor together is approximately 63%, it can be concluded that there is either insignificant enzyme adsorption to the channel floor, or that, if there is significant enzyme adsorption, the adsorbed enzyme is denatured.

To rule out the possibility that a large percentage of enzyme is in fact depositing on the channel floor, but it is simply denatured and therefore does not cause a decrease in signal intensity, we utilized a channel in which the enzyme droplet was first required to pass through a long segment of the channel (approximately 40% of the total channel length) before it was combined with the substrate droplet. If significant amounts of enzyme were being adsorbed, we would

expect to see a decrease in the enzyme initial velocity versus an equivalent measurement in a channel in which the enzyme droplet traveled a shorter distance before combining with the substrate droplet. This was not observed. That this agreement in initial velocities was due to a coincidentally identical shift in the reaction due to an equivalent loss of substrate can be ruled out by our initial control experiment, in which the baseline substrate loss was determined.

We therefore conclude that there is insignificant nonspecific enzyme adsorption to the porous silicon, and that, while diffusion of trace amounts of substrate into the porous silicon is high enough to be detected by DIOS-MS, it is low enough (~1%) that it can be ignored during kinetic modeling. Details are shown in Table 2.

Table 2 – Control experiments demonstrating that there is insignificant nonspecific enzyme adsorption to the porous silicon, and that diffusion of trace amounts of substrate into the porous silicon is high enough to be detected by DIOS-MS. P1 and P2 refer to linear regression parameters y = P1 * x + P2.

Description	**% Signal Loss**	**P1**	**P2**	**R^2**	**SSE**
10 x, Enzyme only droplets 1 x, substrate only droplet	2.04%	-7.05E-4	1.001	0.987	1.36E-5
1 x, substrate only	1.03%	-3.57E-4	1.001	0.969	8.19E-6
1 x, combined substrate and enzyme droplet	63.3%	-2.26E-2	1.039	0.979	2.18E-2

Conclusions

We have demonstrated a microreactor with broad applicability to time-resolved kinetic assays, as long as at least one substrate or product of the reaction is ionizable by DIOS-MS. Further, we have demonstrated that, as long as the experimental conditions are sufficiently well controlled, as is possible in a microfluidic system, relative quantitation of substrate concentration can be used to determine kinetic parameters.

Detailed Process Flow

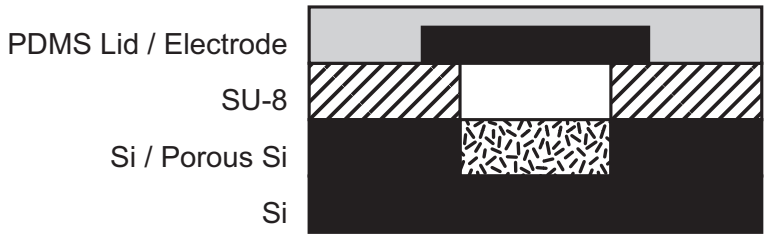

Figure 9 – Cross-section of completed device.

Process Steps

All steps refer to machinery available at the MESA+ Institute for Nanotechnology cleanroom as of 2008. In general however, these steps should be broadly applicable to other equipment with only slight modifications.

Substrate Preparation

Step Name	Details	Comments
P++ doped silicon	0.025 Ohm cm	Wafers were used without RCA cleaning, directly from the supplier as SEMI-clean.

Microchannel Walls

Step Name	Details	Comments
Dehydration bake	200º C, 10 Minutes	
Adhesion layer	Omnicoat • Spin at 2000 RPM • Bake 200 C o 2 Min	
SU-8 processing	SU-8 50 Dispensing • Spin at 2000 RPM Soft Bake • 65º C - 6 min • 95º C - 20 min Exposure • 35 sec, EVG 20 Post Exposure Bake • 65º C - 1 min • 95º C - 5 min	
Remove adhesion layer	OPD4262 (positive	For proper anodization.

from channel floor	photoresist developer) • 30 sec O_2 plasma • Tepla 300 E • 30 sec	Will vary. Verify by optical inspection.

Anodization

Step Name	Details	Comments
Anodization in custom cell (Figure 10)	In custom cell (Figure 10) • 3 mA / cm^2 • 5% HF • 5 min	

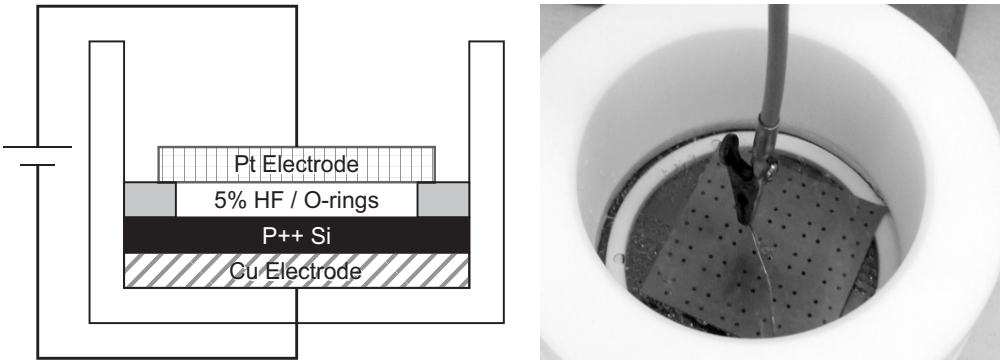

Figure 10 – Cross-section and photograph of anodization cell. Not shown in the cross section is a secondary piece which screws down into the outside holder, producing downward force that seals the top of the cell (the HF side) from the bottom of the cell.

Top Electrode (In device, to be embedded in PDMS, see Figure 9)

Step Name	Details	Comments
Substrate Selection	P++ Silicon • 0.025 Ohm cm • DSP preferred • SSP acceptable	
Cleaning P++ Si	CR112B / Wet-Bench 3-4 HNO_3 (100%) Selectipur: MERCK 100453 • Beaker 1: HNO_3 (100%) 5 min. • Beaker 2: HNO_3 (100%) 5 min. • Quick Dump	

	Rinse <0.1 µS • Spin drying	
PECVD of SiO-SiN-SiO layer (Oxford)	CR102A / OXFORD Plasmalab 80 + • Electrode temp. = 300°C o SiO	50 nm

PDMS Lid

Step Name	**Details**	**Comments**
SU-8 processing	SU-8 50 Dispensing • Spin at 2000 RPM Soft Bake • 65º C - 6 min • 95º C - 20 min Exposure • 35 sec, EVG 20 Post Exposure Bake • 65º C - 1 min • 95º C - 5 min	SU-8 posts hold the electrode above the base (the "ceiling" of the microchannel) while the PDMS is curing.
PDMS Curing	Dow Sylgard 170 • 7:1 elastomer to curing agent • 60º C, 55 min	Mold constructed from 3D printed in Objet TangoBlack, available from Materialise, BE.

Acknowledgements

The technology program of the Ministry of Economic Affairs of The Netherlands (project 6626) and the Technology Foundation STW, the applied science division of the NWO, financially supported this research. Vincent Verdoold and Roald Tiggelaar provided the parameters used to tune the porous silicon.

References

(1) Nichols, K. P.; Gardeniers, H. J. G. E., A digital microfluidic system for the investigation of pre-steady-state enzyme kinetics using rapid quenching with MALDI-TOF mass spectrometry, *Anal. Chem.* **2007**, *79*, 8699-8704.

(2) Deegan, R. D.; Bakajin, O.; Dupont, T. F.; Huber, G.; Nagel, S. R.; Witten, T. A., Capillary flow as the cause of ring stains from dried liquid drops, *Nature* **1997**, *389*, 827-829.

(3) Smalyukh, I. I.; Zribi, O. V.; Butler, J. C.; Lavrentovich, O. D.; Wong, G. C. L., Structure and dynamics of liquid crystalline pattern formation in drying droplets of DNA, *Phys. Rev. Lett.* **2006**, *96*, -.

(4) Hu, H.; Larson, R. G., Analysis of the microfluid flow in an evaporating sessile droplet, *Langmuir* **2005**, *21*, 3963-3971.

(5) Deegan, R. D.; Bakajin, O.; Dupont, T. F.; Huber, G.; Nagel, S. R.; Witten, T. A., Contact line deposits in an evaporating drop, *Physical Review E* **2000**, *62*, 756-765.

(6) Hu, H.; Larson, R. G., Evaporation of a sessile droplet on a substrate, *J. Phys. Chem. B* **2002**, *106*, 1334-1344.

(7) Shen, Z. X.; Thomas, J. J.; Averbuj, C.; Broo, K. M.; Engelhard, M.; Crowell, J. E.; Finn, M. G.; Siuzdak, G., Porous silicon as a versatile platform for laser desorption/ionization mass spectrometry, *Anal. Chem.* **2001**, *73*, 612-619.

(8) Lewis, W. G.; Shen, Z. X.; Finn, M. G.; Siuzdak, G., Desorption/ionization on silicon (DIOS) mass spectrometry: background and applications, *Int. J. Mass Spectrom.* **2003**, *226*, 107-116.

(9) Tsao, C. W.; Kumar, P.; Liu, J.; DeVoe, D. L., Dynamic Electrowetting on Nanofilament Silicon for Matrix-Free Laser Desorption/Ionization Mass Spectrometry, *Anal. Chem.* **2008**, *80*, 2973-2981.

(10) Cornett, D. S.; Reyzer, M. L.; Chaurand, P.; Caprioli, R. M., MALDI imaging mass spectrometry: molecular snapshots of biochemical systems, *Nat. Methods* **2007**, *4*, 828-833.

(11) Tice, J. D.; Song, H.; Lyon, A. D.; Ismagilov, R. F., Formation of droplets and mixing in multiphase microfluidics at low values of the Reynolds and the capillary numbers, *Langmuir* **2003**, *19*, 9127-9133.

(12) Bringer, M. R.; Gerdts, C. J.; Song, H.; Tice, J. D.; Ismagilov, R. F., Microfluidic systems for chemical kinetics that rely on chaotic mixing in droplets, *Philosophical Transactions of the Royal Society of London Series a-Mathematical Physical and Engineering Sciences* **2004**, *362*, 1087-1104.

(13) Song, H.; Ismagilov, R. F., Millisecond kinetics on a microfluidic chip using nanoliters of reagents, *J. Am. Chem. Soc.* **2003**, *125*, 14613-14619.

(14) Thorsen, T.; Roberts, R. W.; Arnold, F. H.; Quake, S. R., Dynamic pattern formation in a vesicle-generating microfluidic device, *Phys. Rev. Lett.* **2001**, *86*, 4163-4166.

(15) Song, H.; Chen, D. L.; Ismagilov, R. F., Reactions in droplets in microflulidic channels, *Angew. Chem., Int. Ed.* **2006**, *45*, 7336-7356.

(16) Zheng, B.; Roach, L. S.; Ismagilov, R. F., Screening of protein crystallization conditions on a microfluidic chip using nanoliter-size droplets, *J. Am. Chem. Soc.* **2003**, *125*, 11170-11171.

(17) Tan, Y. C.; Hettiarachchi, K.; Siu, M.; Pan, Y. P., Controlled microfluidic encapsulation of cells, proteins, and microbeads in lipid vesicles, *J. Am. Chem. Soc.* **2006**, *128*, 5656-5658.

(18) Canela, E. I.; Franco, R., Enzyme Kinetic-Studies from Progress Curves, *Biochem. J.* **1986**, *233*, 599-605.

(19) Goudar, C. T.; Harris, S. K.; McInerney, M. J.; Suflita, J. M., Progress curve analysis for enzyme and microbial kinetic reactions using explicit solutions based on the Lambert W function, *J. Microbiol. Methods* **2004**, *59*, 317-326.

(20) Duggleby, R. G., Analysis of Enzyme Progress Curves by Nonlinear-Regression, *Methods Enzymol.* **1995**, *249*, 61-90.

(21) Tiggelaar, R. M.; Verdoold, V.; Eghbali, H.; Desmet, G.; Gardeniers, J. G. E., Characterization of porous silicon integrated in liquid chromatography chips *Lab Chip* **2009**, *DOI: 10.1039/b812301b*.

(22) Groen, J. C.; Peffer, L. A. A.; Perez-Ramirez, J., Pore size determination in modified micro- and mesoporous materials. Pitfalls and limitations in gas adsorption data analysis, *Microporous Mesoporous Mater.* **2003**, *60*, 1-17.

(23) Cristini, V.; Tan, Y. C., Theory and numerical simulation of droplet dynamics in complex flows - a review, *Lab Chip* **2004**, *4*, 257-264.

(24) Castro-Perez, J.; Shockcor, J. P.; Yu, K.; Goshawk, J.; Bateman, K. P. In *56th ASMS Conference on Mass Spectrometry*: Denver, CO, USA, 2008, pp WPRR 391.

(25) Kreutzer, M. T.; Kapteijn, F.; Moulijn, J. A.; Heiszwolf, J. J., Multiphase monolith reactors: Chemical reaction engineering of segmented flow in microchannels, *Chem. Eng. Sci.* **2005**, *60*, 5895-5916.

(26) Garstecki, P.; Fuerstman, M. J.; Fischbach, M. A.; Sia, S. K.; Whitesides, G. M., Mixing with bubbles: a practical technology for use with portable microfluidic devices, *Lab Chip* **2006**, *6*, 207-212.

(27) Frenz, L.; El Harrak, A.; Pauly, M.; BØgin-Colin, S.; Griffiths, A. D.; Baret, J., Droplet-Based Microreactors for the Synthesis of Magnetic Iron Oxide Nanoparticles, *Angew. Chem.* **2008**, *47*, 6817-6820.

(28) Malloggi, F.; Vanapalli, S. A.; Gu, H.; van den Ende, D.; Mugele, F., Electrowetting-controlled droplet generation in a microfluidic flow-focusing device, *J. Phys.: Condens. Matter* **2007**, *19*, 462101.

(29) Garganta, C. L.; Bond, J. S., Assay and Kinetics of Arginase, *Anal. Biochem.* **1986**, *154*, 388-394.

(30) Bengtsson, M.; Ekstrom, S.; Drott, J.; Collins, A.; Csoregi, E.; Marko-Varga, G.; Laurell, T., Applications of microstructured porous silicon as a biocatalytic surface, *Phys. Status Solidi A* **2000**, *182*, 495-504.

(31) Letant, S. E.; Hart, B. R.; Kane, S. R.; Hadi, M. Z.; Shields, S. J.; Reynolds, J. G., Enzyme immobilization on porous silicon surfaces, *Adv. Mater. (Weinheim, Ger.)* 2004, 16, 689-693.

(32) Libertino, S.; Fichera, M.; Aiello, V.; Statello, G.; Fiorenza, P.; Sinatra, F., Experimental characterization of proteins immobilized on Si-based materials, Microelectron. Eng. 2007, 84, 468-473.

Appendix 1

Process Flow for Large Area Interdigitated Microelectrode Array

An Interdigitated Ultramicroelectrode Array (IDUA), or interdigitated ultramicroelectrodes (UME) array, with a large surface area (1.75 cm2) is presented. The IDUA is patterned on glass (Pyrex) using a Ta adhesion layer, and an Au conductive layer. Photoresist is used as an etch mask, and the pattern is defined using Ion Beam Etching (IBE). The IDUA can be used as an element in an electrochemical sensor. With the addition of a dielectric layer such as SU-8 or oxide, it has been used to analyze electrowetting effects.

Portions of this appendix were published in:
Banpurkar, A. G.; Nichols, K. P.; Mugele, F. *Langmuir*, 2008, 24(19), 10549-10551.

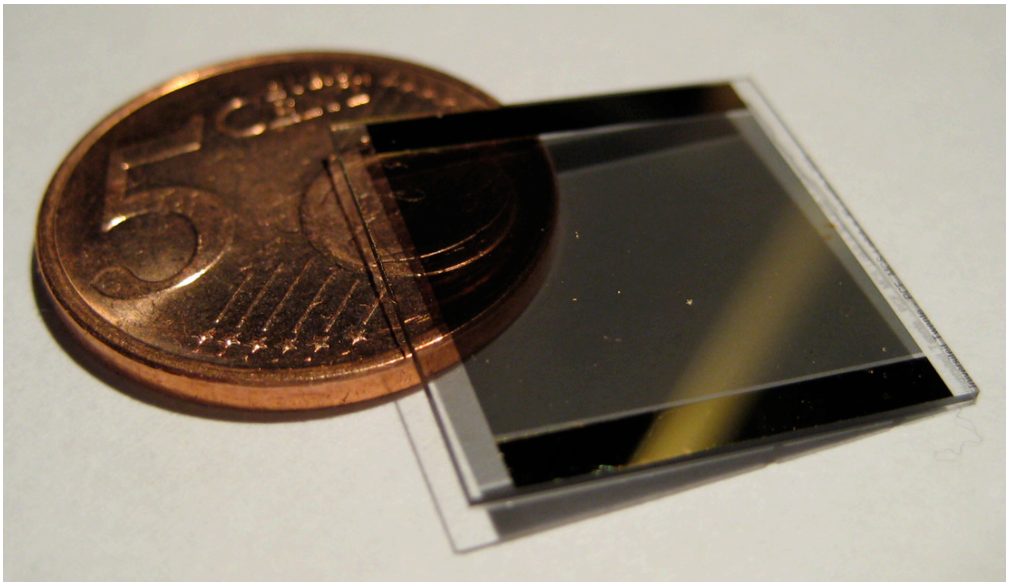

Figure 1 – Photograph of diced chip.

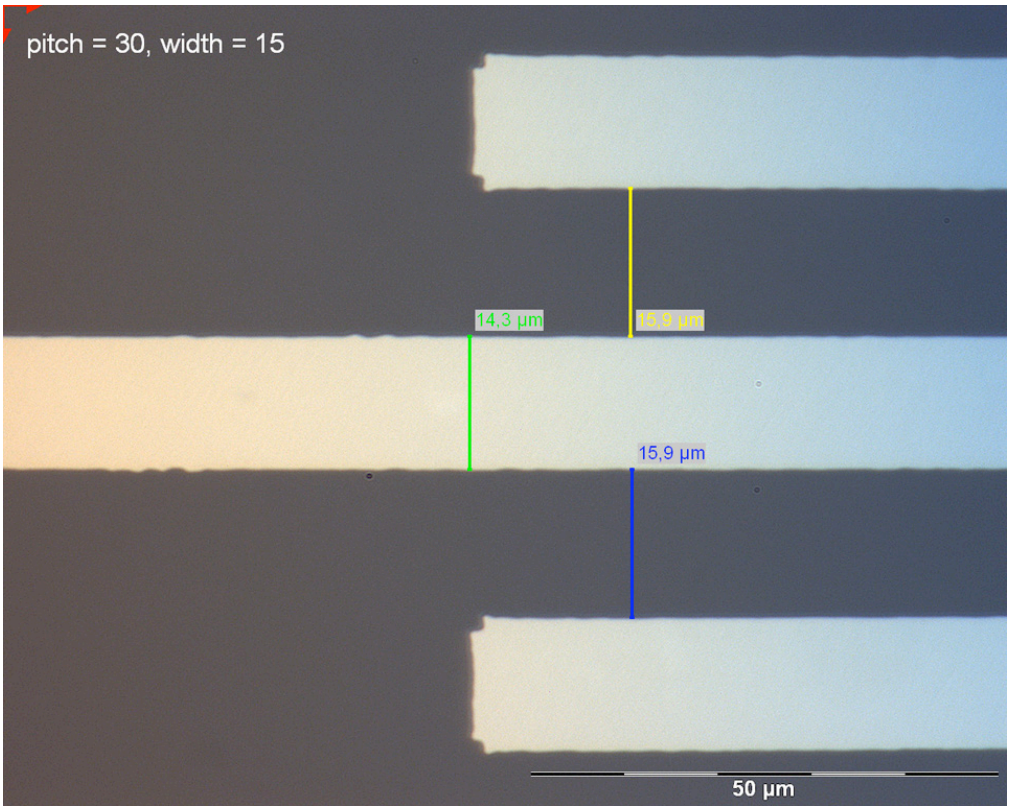

Figure 2 – Micrograph of electrodes

Detailed Process Flow

All steps refer to machinery available at the MESA+ Institute for Nanotechnology cleanroom as of 2008. In general however, these steps should be broadly applicable to other equipment with only slight modifications.

Substrate Preparation

Step Name	Details	Comments
Glass wafer	Pyrex • Polished, optically smooth	
Cleaning of glass wafer	HNO3 (100%) • Selectipur: MERCK 100453 • 10 min • Quick Dump Rinse • <0.1µS (or, rinse in two separate DI beakers) • Spin drying (or, blow dry with N2 gun)	

Patterning of Electrodes

Step Name	Details	Comments
Sputtering of Ta	Ta • Time = 1 min Au • Time = 1 min Pressure = 6.6E-3 mBar Power = 200 W	Estimated thickness Ta = 20 nm Au = 150 nm
Patterning of etch mask	Spin Photoresist • OiR 907-17 • 4000 RPM Soft bake 1 min @ 95C Expose • 4 sec @ 12 W/cm^2 Develop • 1 min OPD 4262	HMDS on Au forms a layer that can be difficult to remove. Since adhesion is not critical in IBE, an adhesion layer is not recommended.

Ion Beam Etching	Time = 25 min Accelerator • Voltage = 500 V • Current = 2 mA Beam • Voltage = 500 V • Current = 20 mA Pressure • Base = 7E-7 mT • Process = 3E-4 mT Angle = 20º Rotation = ~0.1 Hz	

Dielectric Coating

Step Name	**Details**	**Comments**
PECVD of SiO-SiN-SiO layer (Oxford)	CR102A / OXFORD Plasmalab 80 + • Electrode temp. = 300°C o SiO o SiN o SiO	
Lithography - Coating Olin907-35 (Headway)	CR112B / Headway Spinner Olin 907-35 • Spinning speed: 4000 rpm • Spinning time: 20 sec. • Prebake (95°C): 90 sec.	
Lithography - Alignment & Exposure Olin 907-35 (EV)	CR117B / EVG 20 Electronic Vision Group 20 Mask Aligner • Exposure Time: 8 sec.	
Lithography - Development Olin Resist	CR112B / Wet-Bench 11 Developer: OPD4262 Hotplate 120°C (CR112B or CR117B)) • After Exposure Bake (120°C): 60	Mask 2

	sec. Development: • Time: 30 sec. in Beaker 1 • Time: 15-30 sec. in Beaker 2 • Quick Dump Rinse <0.1µS • Spin drying	
Lithography - Post bake standard	CR112B / Hotplate 120°C • Time: 30 min.	
Plasma etching SiN (Etske)	CR102A / Elektrotech PF310/340 Dirty chamber Styros electrode • Electrode temp.: 10°C • CHF3 flow: 25sccm • O2 flow: 5sccm • pressure: 10mTorr • power: 75W Etch rate SiN = 50nm/min (for VDC=-460V) Etch rate SiN = 75 nm/min (for VDC = -580V) Etch rate Olin resist = 95nm/min If DC-Bias < 375V apply chamber clean	Time >10min Check electrical contact with MultiMate

Final Cleaning

Step Name	Details	Comments
Strip Etch Mask	Microstrip® 5010 • 80º C • 5 hours	Hard baking in vacuum (as is done in Ion Beam Etching) produces a very difficult to remove mask. Oxygen plasma may also be used, though not if a Cr adhesion layer is used instead of Ta. Optical inspection should always be performed to ensure complete removal. An additional (short) IBE step can be used to remove Microstrip residue.

Summary and Outlook

In this thesis, we described devices intended to analyze enzyme kinetics through mass spectrometry. Three miniaturized systems were fully developed towards this end: a digital microfluidic system, a digital nanofluidic system, and a non-digital, droplet-based microfluidic system. In chapters two and three we described a digital microfluidic system that electrically combined substrate and enzyme droplets and quenched an array of such droplets at varying time intervals. This produced droplets locked at points along an enzyme progress curve, from which kinetic information is easily obtainable. In chapter four, a nanochannel system, similar in principle to the microscale digital microfluidic system described in chapters two and three, except for the scale, was constructed in an attempt to overcome the internal standard requirement of our digital microfluidic system. Finally, in chapter five, we described a non-digital, droplet-based system, that manipulated nanoliter droplets in microchannels as opposed to microliter droplets on a planar electrode surface. After combining an enzyme and a substrate droplet together, this device sampled a trace amount of the reaction products and substrates, and locked them away from the enzyme on the other side of a membrane as the droplet traveled down a microchannel. The membrane could subsequently be analyzed using mass spectrometry, and since a point in space on the membrane corresponds to a point in time in the reaction, kinetic information was easily obtainable from this system as well.

Enzyme kinetics has numerous applications, including the optimization of process conditions, the study of disease progression, the understanding of drug interactions, mechanisms, and metabolism, and determining the stability of various enzyme containing commercial products.

We utilized mass spectrometry specifically because it allows the study of enzyme kinetics without the incorporation of a chromophore, which many biologically relevant substrates do not contain. The majority of previously reported microfluidic systems require the use of a chromophore, such as a fluorescent substrate

or product, to facilitate detection. The ability to interrogate non-fluorescent molecules using mass spectrometry alone means that we are able to study the enzyme in its natural conformation.

It is our view that the general strategy of utilizing droplets allows superior methods of probing enzyme kinetics, due to the lack of dispersion, faster mixing, and discrete nature of the sampling in droplet-based microfluidic systems. Where appropriate, using mass spectrometry coupled to droplet-based microfluidics allows kinetic interrogation without enzyme modification.

Samenvatting

Het doel van de in dit proefschrift beschreven apparaten is het analyseren van enzymkinetiek door middel van massaspectrometrie. Het begrijpen van enzymkinetiek is niet alleen nuttig voor de basiswetenschap maar ook voor het bestuderen van het ziekteverloop en de wisselwerking met medicijnen. Er werd hier massaspectrometrie gebruikt omdat dit het bestuderen van enzymkinetiek mogelijk maakt zonder dat er een in vele biologisch relevante moleculen niet aanwezige chromofoor vereist is. De meerderheid van microfluidische systemen vereist het gebruik van een chromofoor, zoals een fluorescent substraat of een ander product om detectie te vergemakkelijken. De mogelijkheid om non-fluorescente moleculen alleen met massaspectrometrie op te sporen heeft belangrijke voordelen. Alle beschreven apparaten werden vervaardigd met behulp van miniaturiseringstechnieken omwille van de schaalvoordelen die verbonden zijn met laboratorium-op-een-chip systemen. Voor dit doel werden drie geminiaturiseerde systemen ontwikkeld: een digitaal microfluidisch systeem, een digitaal nanofluidisch systeem en een niet-digitaal, druppelgebaseerd microfluidisch systeem.

Eerst beschrijven we een digitaal microfluidisch systeem waarmee substraat- en enzymdruppels elektrisch werden gecombineerd en een reeks van deze druppels op verschillende tijdsintervallen werden afgekoeld. Dit produceerde druppels die op progressieve punten langs een enzymreactievoortgangscurve zaten. Deze druppels werden daarna gedroogd en overgebracht naar een massaspectrometer waar ze geïoniseerd werden met behulp van matrix assisted laser desorption/ionization time-of-flight massaspectrometrie (MALDI-TOF MS) om de relatieve concentratie van de tijdens de reactie gevormde tussenproducten te bepalen. Met dit systeem was het mogelijk om op een schaal van een milliseconde pre-steady-state kinetiek te analyseren en verkreeg men resultaten evenwaardig aan die welke op een meer

tijdrovende manier werden verkregen en zonder de noodzaak om een chromofoor te gebruiken.

Om dit te kunnen doen was het echter noodzakelijk om een interne standaard te gebruiken, een molecuul dat in gelijke verhouding met het betreffende molecuul ioniseert. Zonder een interne standaard verhinderde de niet-uniforme distributie van opgeloste stoffen tijdens het drogen van de druppels zelfs al een relatieve kwantificering. Om deze beperking te verhelpen, werden twee nieuwe systemen ontwikkeld.

Er werd een nanokanaal gebouwd, waarbij er, in het kort, werd aangenomen dat een verdere miniaturisering sneller mengen en een meer uniforme oplossing mogelijk zou maken. Terwijl we ons systeem met succes uitbouwden zoals gepland, kregen we te maken met een reagensverhitting die veel hoger lag dan wat de simulaties hadden voorspeld. Daarom zijn we van dit systeem afgestapt en werd er een alternatieve oplossing gezocht.

Als alternatief voor het nanokanaalsysteem, was het laatste apparaat dat we ontwikkelden een niet-digitaal, druppelgebaseerd systeem. Hoewel dit systeem druppels manipuleerde was het naar de letter geen digitaal microfluidisch system, omdat het nanoliterdruppels manipuleert in microkanalen in tegenstelling tot wat meestal onder digitaal wordt verstaan, microliterdruppels op een plat elektrodeoppervlak. Na het combineren van een enzym- en een substraatdruppel toonde dit apparaat werkelijk een kleine hoeveelheid van de reactieproducten en substraten en zette ze los van het enzym vast aan de andere kant van een membraan, terwijl de druppel haar weg aflegde door een microkanaal. Daarom komt een punt in de ruimte op het microkanaal overeen met een punt in de tijd in de reactie en kan de concentratieverandering over de lengte van het microkanaal worden gebruikt om een enzymreactievoortgangscurve te produceren. Het membraan dat we gebruikten was poreus silicium, een geleidend, hydrofoob materiaal waarvan de poriën gemakkelijk

op de nanometerschaal instelbaar zijn en dat, wanneer het wordt gebruikt in een configuratie waarnaar wordt verwezen als desorption/ionization massa spectrometrie (DIOS MS), eveneens een geschikte vervanging is van de matrix in MALDI-TOF MS.

Acknowledgements

This thesis was developed between June, 2005 and April, 2008 in the Mesoscale Chemical Systems group, the BIOS lab-on-a-chip group and the MESA+ Institute for Nanotechnology at the University of Twente in the Netherlands. I'd like to express my sincere gratitude to everyone who helped me along the way, personally and professionally, and made this possible.

First of all, I'd like to thank my advisor, Prof. Han Gardeniers, for giving me the opportunity to work in your group, the freedom to follow my own ideas, and the guidance necessary to make those ideas come to fruition. You've been a fantastic advisor, and have helped me grow intellectually and professionally in more ways than I can possibly enumerate here.

I would of course like to thank my office mates, for an always gezellige kamer: Erik, Sebastian, Monica, Iris, Edwin, Roald, Vincent, Jacob, Anil, Liza, Manon, and Sertan. I am especially grateful to Roald for teaching me to always remain alert, and to never assume that it's safe to pick up the innocent looking box on my desk; it's probably not. Vincent, thanks for the musical inspiration and for agreeing to be my paranymph. As for the other MCS members: Wojciech, thanks for the poetic inspiration and for also agreeing to be my paranymph. David, thanks for all of our fascinating conversations. Hopefully someday the world will be less complicated. Stefan, thanks for all the technical assistance you provided, and your extensive knowledge of Dutch schlager music. Maciek, thanks for only breaking other people's stuff. And, to everyone else, thanks for all of the little things that make doing the collaborative research we're all involved in possible.

In SMCT, thank you to Francesca, for teaching me some organic chemistry, and for being the first good friend I had here in Enschede.

I would also like to thank all the members of CPM for welcoming us into their group during and after our merger; I will never forget to balance my carbon, regardless of the situation, thanks you guys.

At MESA+, I am extremely grateful to all the staff members, who run a fantastic, state of the art facility. I'm especially indebted to Hans Mertens, whose thin film knowledge and expertise was invaluable to me at many points throughout my PhD.

In the BIOS group, where I spent the first year or so of my Ph.D. before the Mesoscale Chemical Systems group was formed, thank you to Albert and Edwin for serving on my committee, to Jan Eijkel, for technical and conceptual assistance with our nanochannel work, and to Johan and Jan van Nieuwkastelle for many useful technical discussions, and assistance designing my chip holders. I would also like to thank Séverine for offering to include our work in her wonderfully edited, and recently published, book. And, of course, thank you to all the other BIOS people who I got to know during my brief time there.

In the Physics of Complex Fluids group I'd first like to thank Prof. Mugele for serving on my committee. Adrian, thank you for a number of helpful discussion on electrowetting theory. A special thank you is also reserved for Hao, for sticking with our SU-8 project long after it would have been reasonable to give up. It never worked, but we gave it a good shot.

Additionally, thank you to my outside committee members, Prof. Laurel, from Lund University in Sweden, Prof. van Hest, from Radboud University in Nijmegen, the Netherlands, and Prof. Lammertyn, from the University of Leuven, in Belgium.

To my parents: thank you for giving me the courage to do whatever I wanted to do.

Finally, and most importantly, I'd like to thank Vicky for sticking with me and supporting me through all our time together. Your love and support mean more to me than anything else.

Publications Related to This Thesis

Book Chapters

K.P. Nichols and J.G.E. Gardeniers, in *Miniaturization and Mass Spectrometry*, eds. A. van den Berg and S. le Gac, Royal Society of Chemistry, Cambridge, UK, 2008, pp. 277-288.

Peer Reviewed Publications

K.P. Nichols and J.G.E. Gardeniers. "A Digital Microfluidic System for the Investigation of Pre-Steady-State Enzyme Kinetics Using Rapid Quenching with MALDI-TOF Mass Spectrometry." *Analytical Chemistry,* vol. 79 (21), pp. 8699-8704 Nov (2007).

K.P. Nichols, J.C.T. Eijkel, and J.G.E. Gardeniers. "Nanochannels in SU-8 with Floor and Ceiling Metal Electrodes and Integrated Microchannels." *Lab on a Chip*, vol. 8 (1), pp. 173-175 (2008).

A.G. Banpurkar, K.P. Nichols, and F. Mugele. "Electrowetting-based Micro Drop Tensiometer." *Langmuir,* vol. 24 (19), 10549-10551 (2008).

K.P. Nichols, S. Azoz, and J.G.E. Gardeniers. "Enzyme Kinetics by Directly Imaging a Porous Silicon Microreactor using DIOS Mass Spectrometry" *Analytical Chemistry*, vol. 80 (21), pp. 8314-8319 (2008).

B. Matas Güell, I. Babich, K.P. Nichols, J.G.E. Gardeniers, L. Lefferts and K. Seshan. "Design of a stable steam reforming catalyst - A promising route to sustainable hydrogen from biomass oxygenates" *Applied Catalysis B: Environmental,* submitted (2009).

Conference Proceedings

K.P. Nichols and A.J. Baeumner. "A Metallically Doped DNA Based Biosensor" *Fifth Workshop on Biosensors and Biological Techniques in Environmental Analysis*, Ithaca, NY, 2002.

K.P. Nichols and J.G.E. Gardeniers. "Ultrarapid Droplet Mixer for Digital Microfluidics" Proc. of MicroTAS 2006, Tokyo, Japan, pp. 582-584, 5-9 Nov 2006.

K.P. Nichols and J.G.E. Gardeniers. "A Digital Microfluidic System To Facilitate Pre-Steady-State Kinetic Studies Using MALDI-TOF MS" Proc. of MicroTAS 2006, Tokyo, Japan, pp. 564-566, 5-9 Nov 2006.

K.P. Nichols, J.C.T. Eijkel, and J.G.E. Gardeniers. "Nanofluidic Channels in SU-8 with Integrated Floor and Ceiling Electrodes" Proc. of MicroTAS 2007, Paris, France, pp. 982-984, 7-11 Oct 2007.

K.P. Nichols, and J.G.E. Gardeniers. "A Zero Dead Time Microfluidic System for Pre-steady-state Kinetics by DIOS-TOF MS" 56th American Society of Mass Spectrometry Conference on Mass Spectrometry, Denver, U.S.A., June 1-5, 2008.

K.P. Nichols and J.G.E. Gardeniers. "Enzyme Kinetics by Directly Imaging a Porous Silicon Microreactor Using DIOS Mass Spectrometry" Proc. of MicroTAS 2008, San Diego, U.S.A., pp. 1943-1945, October 12-16, 2008.